Electrospun Composite Nanofibres with Magnetic Carbon Nanotubes

by

Nedine van Deventer

Thesis presented in partial fulfilment of the requirements for the

degree Master of Science in Polymer Science

at Stellenbosch University

Supervisor: Prof. Peter E. Mallon

March 2016

Declaration

By submitting this thesis/dissertation electronically, I declare that the entirety of the work contained therein is my own, original work, that I am the sole author thereof (save to the extent explicitly otherwise stated), that reproduction and publication thereof by Stellenbosch University will not infringe any third party rights and that I have not previously in its entirety or in part submitted it for obtaining any qualification.

March 2016

Abstract

Functional composite nanofibres incorporated with magnetic carbon nanotubes (CNTs) were successfully synthesized using the electrospinning technique. This is the first example of the preparation of such composite nanofibres. In this study, a nanofibrous mat of electrospun nanofibres constitutes the polymer matrix, with the addition of various CNTs as reinforcing nanomaterials in order to form polymer/CNT nanocomposites (PCNs). Poly(methyl methacrylate) homopolymer, possessing a sufficiently high molar mass for electrospinning, was synthesized for use as polymer matrix. The effect that the polymer solution parameters, processing parameters and ambient parameters have on the fibre morphology are discussed.

In a parallel study, multi-wall carbon nanotubes (MWCNTs) and magnetic CNTs (with controlled amounts of magnetic nanoparticles embedded in the walls) were chemically modified by means of oxidation and subsequent polymer grafting. Chemical modification was carried out in order to compatibilize the reinforcing nanomaterials with the polymer matrix for production of PCNs with a well dispersed and exfoliated structure.

As a comparison to the magnetic CNTs mentioned above, magnetic CNTs were synthesized by decorating the surface of oxidized MWCNTs with magnetic nanoparticles. Decoration was made possible by carboxylic acid moieties present on the oxidized MWCNT backbone, which acted as anchoring sites through which chemical functionalities could be attached. Successful synthesis of MWCNT-Fe_3O_4 was achieved using an *ex-situ* and simpler single-step *in-situ* approach. Compatibilization with the polymer matrix for production of PCNs is achieved via the remaining carboxylic acid functionalities present as a result of initial oxidation.

The various CNTs were incorporated into electrospun nanofibres as reinforcing nanomaterials and PCNs were thus formed. Increasing amounts of the various CNTs were added to the electrospinning polymer solution. By the addition of CNTs, the viscosity of the electrospinning solution increased, which prevented efficient electrospinning. The polymer concentration was, therefore, varied in specific ratios depending on the amount of CNTs incorporated. The effect the addition of CNTs has on the fibre morphology is discussed. After electrospinning, fibres in the nanometer range were obtained. Successful incorporation, and thus interaction of the CNTs with the electrospun polymer matrix, was confirmed by scanning transmission electron microscopy (STEM) images which verified the presence of well distributed CNTs which align along the electrospun polymer nanofibres due to the stretching of the fibres during electrospinning.

The magnetic response of nanofibres reinforced with *ex-situ* and *in-situ* MWCNT-Fe_3O_4 exhibited superparamagnetic behaviour; as was proved with superconducting quantum interference device

magnetometry where curves with the characteristic sigmoidal shape showing zero coercivity, zero remanence and no hysteresis loops were obtained.

In summation, property enhancement of electrospun polymer nanofibres was achieved by the incorporation of two different types of reinforcing nanomaterials – CNTs and magnetic nanoparticles. The magnetic properties induced by the reinforcing materials can potentially be used for SMART polymer applications; where SMART polymer materials (also referred to as stimuli-responsive polymer materials) are materials which behave in predictable and measurable ways when exposed to various external stresses. Electrospun composite nanofibres containing *ex-situ* synthesized MWCNT-Fe_3O_4 possessed the highest magnetization value of all the composites; and is proposed for use in SMART polymer applications such as magnetic filters or tissue scaffolds.

Samevatting

Suksesvolle sintese van funksionele saamgestelde nanovesels is bereik deur gebruik te maak van die elektrospin-tegniek. Magnetiese koolstof nanobuisies (CNTs) is inkorporeer in die nanovesels – dit is die eerste voorbeeld van die samevoeging van sulke saamgestelde nanovesels. In die studie bestaan die polimeer matriks uit ‘n mat van elektro-gespinde nanovesels. As versterking word verskillende CNTs bygevoeg om polimeer/CNT nanosamestellings (PCNs) te vorm. Poli(metiel metakrilaat) polimeer, wat ‘n hoë molêre massa voldoende vir elektrospin besit, is sintetiseer om as polimeer matriks te dien. Die uitwerking van die verskillende polimeer-oplossings, prosesse en omgewings parameters op die morfologie van die vesels, word bespreek.

In ‘n vergelykbare studie, is multi-wand koolstof nanobuisies (MWCNTs) en magnetiese CNTs (waar ‘n beheerde aantal magnetiese nanopartikels ingebed is in die wande) chemies verander om PCNs met eweredig verspreide CNTs te produseer. Chemiese modifikasie, deur middel van oksidasie en daaropeenvolgende polimeer-enting, sorg dat die nanomateriaal wat ter versterking by die polimeer matriks gevoeg word PCNs met ‘n eweredige samestelling produseer.

In aansluiting by bogenoemde magnetiese CNTs, is magnetiese CNTs ook sintetiseer deur die oppervlak van geoksideerde MWCNTs met magnetiese nanopartikels te versier. Die teenwoordigheid van karboksielsuur op die geoksideerde MWCNT oppervlak het as ankerpunte gedien waaraan paslike chemiese nanopartikels kon bind. Suksesvolle sintese van MWCNT-Fe_3O_4 is bereik deur ‘n *ex-situ*, sowel as eenvoudiger enkel stap *in-situ* metode. Die orige karboksielsuur, as resultaat van vroeëre oksidasie, sorg vir PCNs met ‘n eweredige samestelling wat waargeneem is deur MWCNT-Fe_3O_4 wat in verhouding versprei in die polimeer matriks.

Verskillende CNTs is as vullers by die elektro-gespinde nanovesels inkorporeer om PCNs te vorm. Toenemende hoeveelhede van die verskillende CNTs is by die elektrospin-polimeer-oplossing gevoeg. Die byvoeging van CNTs het die viskositeit van die elektrospin-oplossing verhoog, en dit het tot ‘n oneffektiewe elektrospin-proses gelei. Gevolglik is die polimeer-oplossing konsentrasie proporsioneel aangepas, afhangende van die hoeveelheid CNTs wat inkorporeer is. Die effek van die toevoeging van die CNTs op die morfologie van die vesels, word bespreek. Vesels van nanometer grootte is verkry as resultaat van die elektrospin-proses. Suksesvolle inkorporasie is bevestig deur STEM beelde wat dui op die interaksie van die CNTs met die elektro-gespinde polimeer matriks. Die beelde toon eweredig verspreide CNTs wat in lyn is met die lengte van die vesels as gevolg van die rekking van die vesels gedurende die elektrospin-proses.

Nanovesels met *ex-situ* en *in-situ* MWCNT-Fe_3O_4 as vuller het superparamagnetiese eienskappe getoon. Resultate verwerk in grafieke toon S-vormige kurwes wat die 0-0-as kruis, wat kenmerkend is van superparamagnetisme.

In opsomming, waarde is toegevoeg tot die eienskappe van elektro-gespinde polimeer-nanovesels deur die inkorporasie van twee soorte nanomateriale as vullers – CNTs en magnetise nanopartikels. Die magnetiese eienskappe toegevoeg deur die gebruik van magnetiese CNTs as vuller besit groot potensiaal vir gebruik in “SMART” polimeer-materiale. “SMART”-materiale reageer op ‘n voorspelbare en meetbare wyse wanneer dit blootgestel word aan eksterne stimuli. Elektro-gespinde saamgestelde nanovesels met MWCNT-Fe_3O_4 wat *ex-situ* produseer is, is die mees magneties van al die samestellings. Die nanovesels kan potensieel gebruik word in “SMART” polimeer toepassings soos magnetiese filters of as raamwerk vir ‘n menslike weefsel-mat.

Acknowledgements

Firstly, I would like to thank my supervisor, Prof. Peter Mallon. Whenever I had a question I could just knock on your door and you would help me, regardless of your busy schedule. Thank you for your guidance and support throughout the course of this thesis.

I thank the following people for their great and constant help in analysing my samples: Mohamed Jaffer from UCT for TEM analysis as well as Angelique Laurie and Madelaine Frazenburg at CAF for SEM and STEM analysis.

I would like to give a special thanks to the academic staff, personnel and students at the Department of Chemistry and Polymer Science of Stellenbosch University for always helping when possible. Also, I would like to thank my research group from the Physical lab (Chantelle, Piere, Hussein, Neil and Stefan) for always helping me when advice or assistance was needed.

A special thanks to my coffee crew (Chantelle, Piere, Carlo and Lisa) for always being willing to go for a break and chat in both the good and stressful times. You kept me sane.

Last but not least I would like to thank my family, especially my parents, for their constant love and support. Thank you for affording me the opportunity to study at Stellenbosch University and for always showing interest in my studies. Thank you especially for your help and words of wisdom throughout this thesis – I really appreciate it. I am also very grateful to Christiaan for all his love, support and encouragement. Thank you for always motivating me and sitting with me in the late hours of work – without you this thesis would not have been possible.

Table of Contents

List of Figures

Appendix

List of Schemes

List of Tables

Glossary

Notations

θ_P	Pyramidalization angle
φ	π-orbital misalignment angle
°C	Degree Celsius
cm	Centimetres
Đ	Dispersity
emu	Electromagnetic unit
g	Grams
$K = k_a/k_d$	Equilibrium constant
k_a	Addition reaction rate
k_d	Polymerization deactivation rate
k_p	Polymer chain propagation rate
k_t	Polymerization termination rate
kV	Kilovolts
L	Complexing ligand
M	Mole
mg	Milligrams
mL	Millilitres
M_n	Molar mass
M_t^n	Transition metal that has an oxidation state which can increase
nm	Nanometres
Oe	Oersted

P•	Radical
P_n, P_m and P_{n+m}	Terminated polymer chains with a degree of polymerization of *n*, *m* and *n+m* respectively
P_n• and P_m•	Polymer chain with an active propagating radical at the chain end and a degree of polymerization of *n* and *m* respectively
P-X	Alkyl halide compound
R	Free-radical leaving group which requires the ability to reinitiate polymerization
μm	Micrometres
X-M_t^{n+1}/L	Metal halide complex with an increased oxidation state
Z	Group which regulates the reactivity of the C-S double bond of a RAFT agent

Abbreviations

1D	One-dimensional
2D	Two-dimensional
ATR	Attenuated total reflectance
ATRP	Atom transfer radical polymerization
b.p.	Boiling point
CNT	Carbon nanotube
CRP	Controlled/living free-radical polymerization
Ex-situ MWCNT-Fe_3O_4	*Ex-situ* synthesized magnetic multi-wall carbon nanotube decorated with iron oxide nanoparticles
FEG	Field emission gun
FRP	Conventional free-radical polymerization
FTIR	Fourier transform infrared spectroscopy

In-situ MWCNT-$CoFe_2O_4$	*In-situ* synthesized magnetic multi-wall carbon nanotube decorated with iron/cobalt oxide nanoparticles
In-situ MWCNT-Fe_3O_4	*In-situ* synthesized magnetic multi-wall carbon nanotube decorated with iron oxide nanoparticles
Magnetic CNT-COOH	Oxidized magnetic carbon nanotube
Magnetic CNT-PMMA	Poly(methyl methacrylate) grafted magnetic carbon nanotube
MWCNT	Multi-wall carbon nanotube
MWCNT-COOH	Oxidized carbon nanotube
MWCNT-PMMA	Poly(methyl methacrylate) grafted carbon nanotube
NMP	Nitroxide-mediated polymerization
NMR	Nuclear magnetic resonance spectroscopy
PCN	Polymer/carbon nanotube nanocomposites
PMMA	Poly(methyl methacrylate)
PMAA	Poly(methacrylic acid)
PMMA-co-PMAA	Poly(methyl methacrylate)/poly(methacrylamide) copolymer
PN	Polymer nanocomposite
PS	Polystyrene
RAFT	Reversible addition fragmentation chain transfer
RPM	Revolutions per minute
SEC	Size exclusion chromatography
SEM	Scanning electron microscopy
STEM	Scanning transmission electron microscopy
SPM	Superparamagnetism
SQUID	Superconducting quantum interference device
SWCNT	Single-wall carbon nanotube
TEM	Transmission electron microscopy

TGA	Thermogravimetric analysis
wt. %	Weight percentage
XRD	X-ray powder diffraction

Chapter 1: Introduction and Objectives

1.1 Introduction

Interest in the nanotechnology field has increased significantly over the past few years; where the development of polymer nanocomposites (PNs) is an area of nanotechnology research which has shown great promise. The inclusion of reinforcing nanomaterials in a polymer matrix results in the formation of PNs.

Electrospinning is an uncomplicated yet versatile method used to produce nanoscale continuous polymer fibres (nanofibres). The process was discovered and patented by Formhals in 1934;[1] and numerous articles and reviews on the electrospinning of various polymers and composites have been published since.[2-5] A mat of electrospun polymer nanofibres has a highly porous structure; thus resulting in products which possess exceptionally high surface area to volume ratios.[2-7] This makes it suitable for use in a wide variety of applications including: filtration media, tissue scaffolds, drug delivery systems, biomedical textiles, sensors, protective clothing and more.[2,5-13] The versatility of electrospun polymer nanofibres can be enhanced by the addition of reinforcing materials; which impart new properties and functionality to the nanofibres. Effectively, the inclusion of reinforcing nanomaterials in polymer nanofibres results in the formation of PNs; where the fibres constitute the polymer matrix.

Carbon nanotubes (CNTs), which sparked interest due to an article by Iijima in 1991,[14] are popular for use as reinforcing nanomaterials in order to produce polymer/carbon nanotube nanocomposites (PCNs). This is owing to their outstanding mechanical, electrical and thermal properties.[15-18] These nanomaterials are, however, chemically inert; and challenges associated with the uniform distribution of the nanomaterials in the polymer matrix to ensure efficient utilization are apparent. This obstacle can be overcome by chemical modification of the CNT surface; where various covalent and non-covalent modification approaches have been reported to reduce CNT agglomeration in order to form a true nanocomposite.[19-21] This study will look at different methods in which the CNT surface can be chemically modified. The modified CNTs will then be incorporated into electrospun nanofibres in order to generate PCN nanofibres; where the effect the incorporation has on the fibre diameter and morphology will also be investigated.

It has recently been demonstrated that there are major potential advantages to the inclusion of two different types of nanomaterials into a polymer matrix; through which greater property enhancement can be achieved. An interesting aspect which has not yet received attention is the incorporation of magnetic CNTs (and thus magnetic nanoparticles and CNTs) as reinforcing nanomaterials, in order to produce magnetic PCN nanofibres. Recent studies by Mattia *et al.*,[22] Galland *et al.*[23] and He *et al.*[24] have shown the successful synthesis of carbon nanomaterials incorporated or decorated with magnetic nanoparticles; which renders the carbon nanomaterials magnetic. The magnetic properties induced by the filler materials can potentially be used for

SMART polymer applications; where SMART polymer materials (also referred to as stimuli-responsive polymer materials) are materials which behave in predictable and measurable ways when exposed to various external stresses. The synthesis of magnetic CNTs and the effect of their incorporation on the morphology and magnetic properties of electrospun polymer nanofibres will be investigated. The research done in this project will be the first example of the preparation of electrospun composite nanofibres containing magnetic CNTs.

A major problem which occurs during filtration is fouling, which causes damage to the filter and also prevents sufficient filtration. If magnetic CNTs are incorporated into the filter, it will provide the filter with magnetic properties. Effectively, if fouling occurs the filter can simply be oscillated by means of a magnetic field in order to 'shake' it clean. In the case of using similar nanofibre matrices as tissue scaffolds, the constant movement of the scaffold by means of a magnetic field may promote cell growth.[25,26] By the selection of different polymer matrix materials, various end-applications for the PCN nanofibres are possible.

1.2 Objectives

The main objective of this study is to synthesize electrospun composite nanofibres containing magnetic CNTs. The various sub-objectives that have to be reached in order to fulfil the main objective can be summarized as follows:

- Synthesis of the polymer matrix homopolymer PMMA.
- Processing of the polymer into nanofibres by means of electrospinning and investigation on the effect of process parameters on the fibre morphology.
- Chemical modification of the surface of CNTs by means of oxidation and polymer grafting in order to compatibilize the nanofiller with the polymer matrix for production of PCNs with a well dispersed and exfoliated structure.
- Inclusion of CNTs into electrospun nanofibres as reinforcing nanomaterials and investigation on the effect this may have on the fibre morphology.
- Investigation on the synthesis of magnetic CNTs by decoration of the CNT surface with magnetic nanoparticles.
- Inclusion of magnetic CNTs into electrospun nanofibres as reinforcing nanomaterials in order to produce SMART polymer materials, and investigation on the effect this may have on fibre morphology.
- Analysis of the magnetic properties imparted on the nanofibrous mat of electrospun nanofibres by the magnetic CNT nanofillers.

1.3 References

1. US Pat., US1975504, 1934.
2. L. Cronje and B. Klumperman, *Eur. Polym. J.,* 2013, **49**, 3814-3824.
3. Y. Qian, Y. Su, X. Li, H. Wang and C. He, *Iran. Polym. J.,* 2010, **19**, 23-129.
4. J. Vonch, A. Yarin and C. Megaridis, *Am. J. Undergrad. Res.,* 2007, **1**, 1-6.
5. S. Sarabi-Maneji, J. Scott and D. J. Pagé, *Proceedings of the International Conference on New Trends in Transport Phenomena,* Avestia Publishing, Ottawa, 2014, pp. 1-8.
6. G. M. Bayley and P. E. Mallon, *Polymer,* 2012, **53**, 5523-5539.
7. X. Wang, Y. Kim, C. Drew, B. Ku, J. Kumar and L. A. Samuelson, *Nano Lett.,* 2004, **4**, 331-334.
8. P. P. Tsai, H. Schreuder-Gibson and P. Gibson, *J. Electrostat.,* 2002, **54**, 333-341.
9. T. Subbiah, G. Bhat, R. Tock, S. Parameswaran and S. Ramkumar, *J. Appl. Polym. Sci.,* 2005, **96**, 557-569.
10. E. Kenawy, G. L. Bowlin, K. Mansfield, J. Layman, D. G. Simpson, E. H. Sanders and G. E. Wnek, *J. Controlled Release,* 2002, **81**, 57-64.
11. D. Yu, L. Zhu, K. White and C. Branford-White, *Health,* 2009, **1**, 67-75.
12. P. Bhattarai, K. B. Thapa, R. B. Basnet and S. Sharma, *IJBAR,* 2014, **5**, 401-405.
13. H. M. Khanlou, A. Sadollah, B. C. Ang, J. H. Kim, S. Talebian and A. Ghadimi, *Neural Comput. Appl.,* 2014, **25**, 767-777.
14. S. Iijima, *Nature,* 1991, **354**, 56-58.
15. S. Anandhan and S. Bandyopadhyay, *Nanocomposites and Polymers with Analytical Methods,* ed. J. Cuppoletti, InTech, Croatia, 2011, ch. 1, pp. 3-28.

16. V. N. Popov, *Mater. Sci. Eng.,R,* 2004, **43**, 61-102.

17. H. Hou, J. J. Ge, J. Zeng, Q. Li, D. H. Reneker, A. Greiner and S. Z. D. Cheng, *Chem. Mater.,* 2005, **17**, 967-973.

18. V. Choudhary and A. Gupta, *Carbon Nanotubes - Polymer Nanocomposites*, ed. S. Yellampalli, InTech, Croatia, 2011, ch. 4, pp. 65-90.

19. O. Breuer and U. Sundararaj, *Polym. Compos.,* 2004, **25**, 630-645.

20. L. Meng, C. Fu and Q. Lu, *Prog. Nat. Sci.,* 2009, **19**, 801-810.

21. D. Tasis, N. Tagmatarchis, A. Bianco and M. Prato, *Chem. Rev.,* 2006, **106**, 1105-1136.

22. D. Mattia, G. Korneva, A. Sabur, G. Friedman and Y. Gogotsi, *Nanotechnology,* 2007, **18**, DOI: 10.1088/0957-4484/18/15/155305.

23. S. Galland, R. L. Andersson, M. Salajková, V. Ström, R. T. Olsson and L. A. Berglund, *J. Mater. Chem. C,* 2013, **1**, 7963-7972.

24. H. He and C. Gao, *J. Nanomater.,* 2011, **2011**, DOI: 10.1155/2011/193510.

25. B. E. Sumpio, A. J. Banes, L. G. Levin and G. Johnson, *J. Vasc. Surg.,* 1987, **6**, 252-256.

26. C. Schild and B. Trueb, *Exp. Cell Res.,* 2002, **274**, 83-91.

Chapter 2: Historical and Theoretical Background

2.1 Polymer/carbon nanotube nanocomposites (PCNs)

Nanotechnology in general has received a considerable amount of attention over the last few years. One important area of nanotechnology research has been the development and use of so-called polymer nanocomposites (PNs). The combination of a polymeric material and reinforcing nanomaterials make up PNs, where nanomaterials have minimum one dimension in the nanometer range. There are numerous types of nanomaterials commercially available which can be introduced into a polymer matrix in order to form PNs. These reinforcing nanomaterials possess certain properties which are carried over to the PNs, and the properties of the polymer matrix are thus enhanced. In addition, the nanometer dimensions of the reinforcing material allow for a bigger interfacial area between the reinforcing material and polymer matrix when compared to reinforcing materials of conventional size; which improves the property enhancement.[1-3]

Reports have shown increasing interest in the use of carbon nanotubes (CNTs) as reinforcing nanomaterial, and thus the formation of polymer/carbon nanotube nanocomposites (PCNs). The first PCNs were reported in 1994 by Ajayan *et al.*,[3-5] where the inclusion of CNTs into a polymer matrix (more on CNT incorporation in section 2.2) leads to increased tensile strength and modulus.[1,6,7] Promising end-uses arise where CNTs incorporated with magnetic nanoparticles (refer to magnetic CNTs in section 2.5) are introduced as reinforcing nanomaterial in order to form magnetic PCNs; where this topic of interest has not yet been reported on.

PNs can be synthesized using three different methods, which include solution blending, melt blending and *in-situ* polymerization.[1,3,8] In this study PCNs are produced by solution blending, which comprises the intensive mixing of a polymer solution (polymer and solvent) and CNTs by means of sonication. The solvent is then evaporated, resulting in the formation of PCNs commonly in the form of a thin film or an electrospun nanofibrous mat (refer to electrospinning in section 2.4).[3,8]

2.2 Carbon nanotube (CNT) incorporation

Graphitic carbon sheets are made up of carbon atoms linked in hexagonal shapes, where each carbon atom is bonded in the sp^2-hybridization state. In the case of CNTs, these graphitic carbon sheets take on a tubular configuration with diameters in the nanometer range.[9] CNTs can be classified according to their structure, and are categorized as either single-wall carbon nanotubes (SWCNTs) or multi-wall carbon nanotubes (MWCNTs).[6,10] In this study MWCNTs are used, where multiple coaxial graphitic carbon sheets in tubular configuration make up the end product as depicted in figure 2.1.

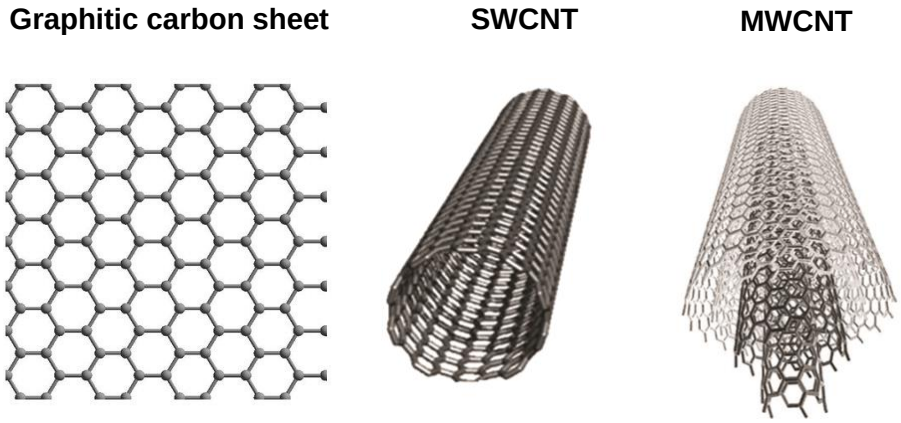

Figure 2.1: *Schematic representation of a graphitic carbon sheet, a SWCNT and a MWCNT.*[10]

CNTs are ideal for use as composite reinforcing nanomaterials due to their exceptional mechanical, electrical and thermal properties.[3,6,7,10-13] When referring to PCNs, it is very crucial for the CNTs to disperse uniformly and individually in the polymer matrix to ensure efficient utilization. The CNT incorporation is, however, a more stringent task than may be anticipated. This is due to the CNTs' surface characteristics which lead to strong Van der Waals forces being present between CNTs, which in turn cause them to agglomerate and form bundles. This problem can be overcome by the chemical modification of the CNT surface, which will allow for interactions between CNTs and the polymer solution used for distribution to increase. Consequently agglomeration will be reduced, resulting in successful CNT incorporation.[14,15]

Applicable ways in which chemical modification of the CNT surface can be achieved include: (a) covalent attachment of chemical functionalities to CNT surfaces and (b) non-covalent attachment by means of adsorption forces between functional groups and CNT surfaces.[15,16]

(a) Covalent attachments

Covalent attachments require a covalent bond to form between chemical functionalities and carbon atoms on CNT surfaces. Covalent attachments are encouraged by CNTs – graphitic carbon sheets adopt tubular configuration when forming CNTs (as depicted in figure 2.1), which leads to local strain induced by pyramidalization and π-orbital misalignment; which again leads to higher reactivity.

The pyramidalization angle (θ_P) is the angle present between the σ- and π-orbitals, minus 90 degrees ($\theta_P = \theta_{\sigma\pi} - 90°$). When looking at a sp^2-hybridized (trigonal) carbon atom as present in graphitic carbon sheets, $\theta_P = 0°$; whereas in the case of a sp^3-hybridized (tetrahedral) carbon atom $\theta_P = 19.47°$ (refer to figure 2.2). For carbon atoms in tubular configuration as present in CNTs, $\theta_P = 11.6°$ (when specifically referring to (5,5) SWCNTs, where values for other CNTs are in the close proximity); which is close to the value for sp^3-hybridized (tetrahedral) carbon atoms. The carbon atoms in CNTs thus have a geometry which prefer to be in a state of sp^3-hybridization rather than the sp^2-hybridization state it is predominantly in. In order for the change in hybridization state to occur, covalent bonding can take place. The pyramidalization angle present in CNTs thus renders the carbon atoms more reactive towards covalent bonding.[17]

On the other hand; π-orbital misalignment causes a local strain which can be relieved by addition reactions. This misalignment is apparent at the two different C-C bonds found in CNTs and can be explained in terms of the π-orbital misalignment angle (φ); where a larger value for φ is associated with a larger strain. When specifically referring to (5,5) SWCNTs the first C-C bond is perpendicular to the central axis of the nanotube and brings about a π-orbital misalignment angle value of $\varphi = 0°$, while the second C-C bond has a π-orbital misalignment angle value of $\varphi = 21.3°$ relative to the central axis of the nanotube (refer to figure 2.3). The second C-C bond possesses a higher φ value and is more likely to undergo addition reactions in order to relieve the strain. The π-orbital misalignment angle present in CNTs thus leads to carbon atoms which are more susceptible towards covalent bonding.[17-19]

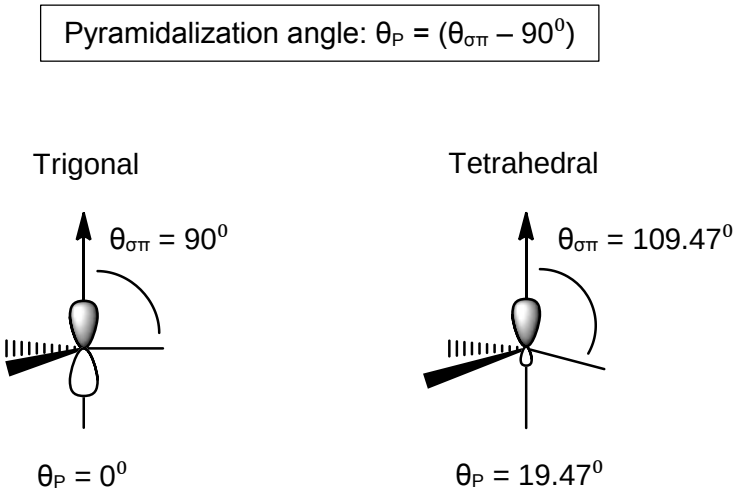

Figure 2.2: *Schematic representation of pyramidalization angle (θ_P).*[17, 18]

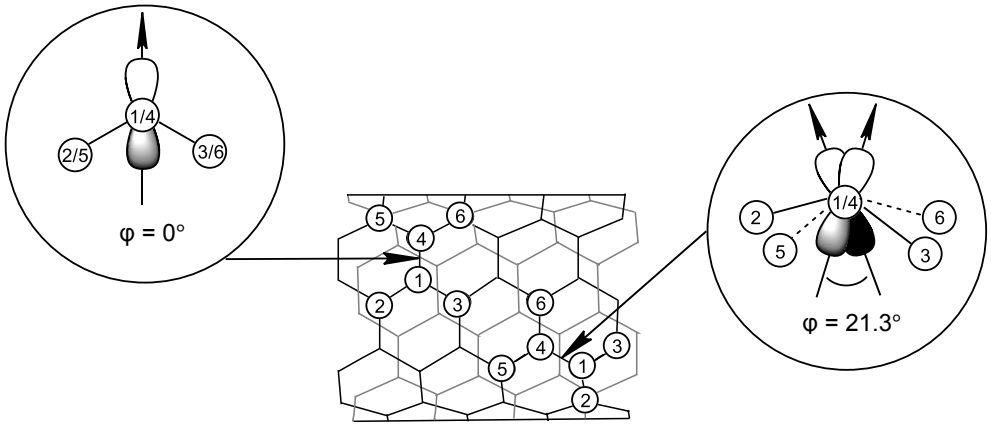

Figure 2.3: *Schematic representation of π-orbital misalignment angle (φ) for a (5,5) SWCNT.*[17, 18]

The covalent attachment of chemical functionalities to CNT surfaces can be divided into direct and indirect covalent functionalization. Direct covalent functionalization correlates to a change in the hybridization state from sp^2 to sp^3 for the carbon atoms present in CNTs.[15] Examples of this include fluorination, hydrogenation by means of Birch reduction, cycloaddition and radical addition.[16] Indirect covalent functionalization is associated with carboxylic acid functionalities which arise on the CNT surface due to oxidation using severe acidic conditions. The oxidized CNTs can then be directly incorporated into a polymer matrix, or chemical functionalities can be further attached through the carboxylic groups present.[15]

(b) Non-covalent attachments

Non-covalent attachments to CNT surfaces are achieved using different adsorption forces, which allow supramolecular complexes to form. These adsorption forces include Van der Waals forces, electrostatic forces and π-stacking interactions.[15] Non-covalent attachments mostly do not require harsh reaction conditions, as opposed to covalent attachments. The mild reaction conditions prevent damage of the CNTs' chemical structure and result in their mechanical, electrical and thermal properties being fully maintained.[15,20,21] The adsorption forces present for non-covalent attachments are, however, weak in comparison with the bonds present for covalent attachments. During stringent reaction conditions it cannot be certain that these weak forces will stay intact, which makes the use of covalent attachments advantageous in such circumstances.

In this study stringent conditions are induced by electrospinning due to the high shearing force involved in this process, which makes the use of covalent functionalization a more viable approach.

2.3 Grafting onto solid surfaces

Grafting allows for the formation of strong chemical bonds between solid surfaces and chemical functionalities; and is thus a way in which covalent functionalization of solid surfaces can be attained.[22,23]

As previously mentioned; it is very crucial for CNTs to disperse uniformly and individually in a polymer solution to ensure efficient utilization in PCNs.[14,15] By increasing the interactions between CNTs and the polymer solution, uniform and individual dispersion can be achieved. This increase in interactions can be achieved by covalently grafting polymer chains (specifically the polymer used as polymer matrix) onto solid CNT surfaces in order to form tethered polymer chains which are connected to the surface at one chain end. Advantages of this technique include control over the type of polymer and the polymer chain lengths to be grafted onto the surface. Grafting of polymer chains onto the CNT surface can be carried out using either the “grafting to” or “grafting from” method (depicted in scheme 2.1).[22,23]

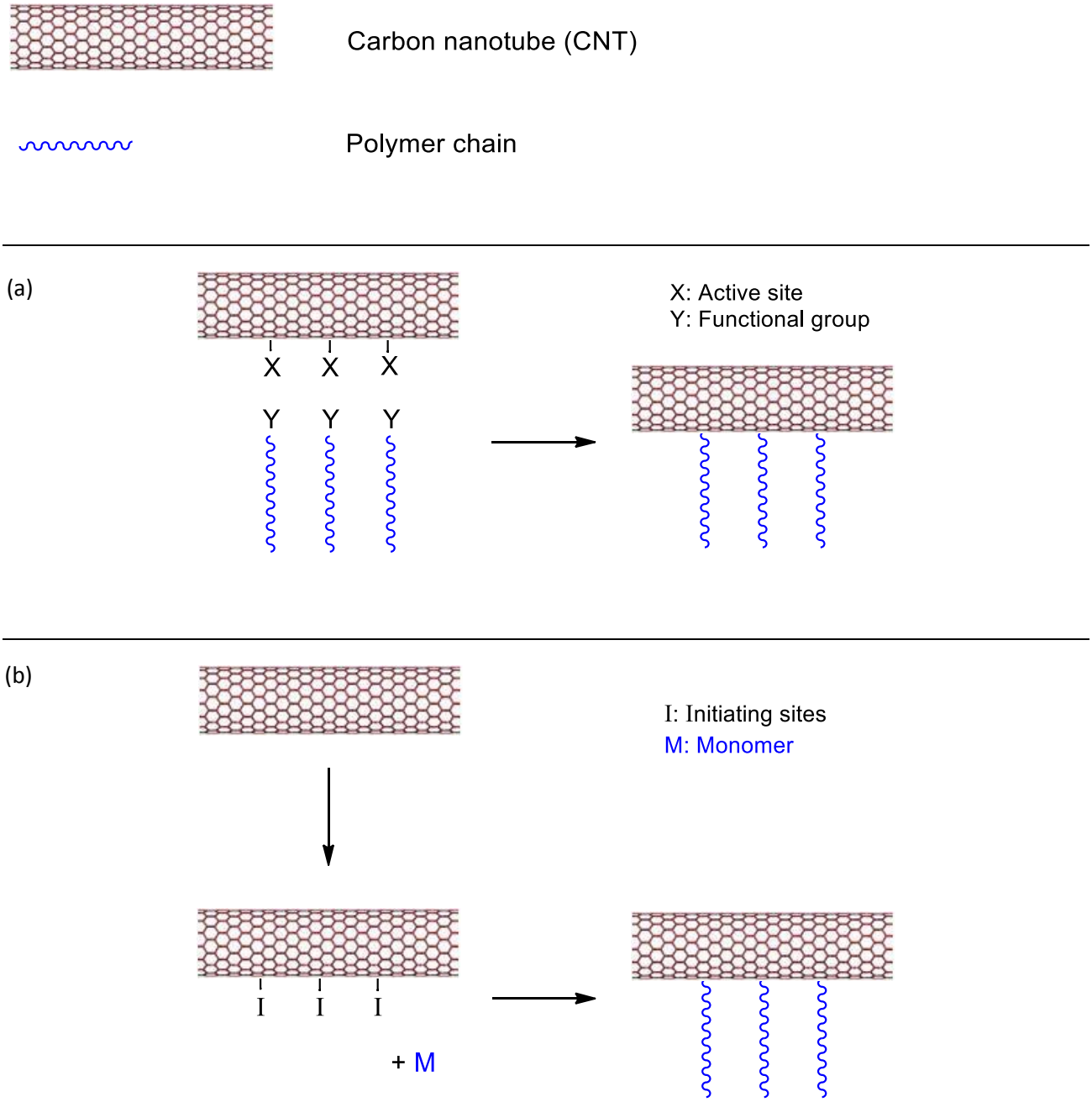

Scheme 2.1: *Schematic representation of the grafting of polymers onto the CNT surface by means of the (a) "grafting to" and (b) "grafting from" method.*

In the "grafting to" approach, the polymer chain branches are polymerized independently. The CNT surface contains appropriate functional groups (active sites) which can react with the functional groups present on the polymer chain branches, and when the two components are combined a coupling reaction occurs. The amount of polymer chains in the final product can be controlled by regulating the amount of functional groups initially present on the CNT surface.[22,24,25]

The “grafting from” approach involves the attachment of a macro-initiator to the CNT surface, and thus the formation of initiating sites along the surface. Once monomer is added, polymerization takes place from the CNT surface due to the initiating sites capable of initiating polymerization. The amount of polymer chains in the final product can, in theory, be controlled by regulating the amount of initiating sites formed on the CNT surface.[22,24-27]

A problem with steric hindrance may be encountered when using the “grafting to” approach due to the presence of the independently polymerized polymer chains; leading to poor surface coverage. Consequently the “grafting from” method, which results in greater surface coverage, is preferred in this study.[28,29]

2.3.1 Methods for grafting polymer chains

2.3.1.1 Conventional free-radical polymerization (FRP)

Conventional free-radical polymerization (FRP) is one of the most widely used polymerization techniques, particularly to synthesize polymers of high molar mass (M_n) .[30-32] A simplified mechanism is depicted in scheme 2.2; where M represents a vinyl monomer unit, P_n• represents a polymer chain with an active propagating radical at the chain end and a degree of polymerization of *n, and* k_p represents the polymer chain propagation rate. Propagation takes place by the consecutive addition of monomer units to the active propagating radical at the chain end.[30,32,33]

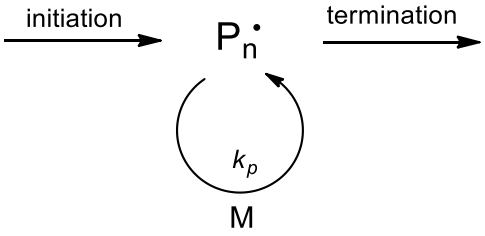

Scheme 2.2: *Simplified conventional FRP mechanism.*

Due to the lack of control over chain transfer and termination associated with the FRP mechanism, certain limitations arise. These include insufficient control over the M_n and dispersity (Đ), and a problem with synthesizing polymers with specific end-group functionality. All these limitations are apparent when grafting of polymer chains onto solid surfaces is done by the “grafting from” method via FRP. In addition, the disadvantage of the formation of free polymer chains is always

encountered. In some instances the amount of free polymer chains present even exceeds the amount of tethered polymer chains; generating the need for expensive washing and recovery processes.[28] To overcome the limitations associated with FRP, techniques like controlled/living free-radical polymerization (CRP) (elaborated on below) are used.[30-32,34,35]

2.3.1.2 Controlled/living free-radical polymerization (CRP)

Irreversible termination in FRP is overcome by CRP. CRP involves the activation and deactivation of the propagating radicals at chain ends by means of compounds which can reversibly react with these radicals; thus rendering the termination reversible. CRP relies on the establishment of a rapid equilibrium between these propagating radicals and dormant species, where the rapid equilibrium results in a linear increase of the polymer chains' M_n as time increases.[30,33,36] The reversible termination and linear increase in M_n associated with the CRP technique allow for good control over functionality as well as final M_n and Đ. In order to ensure reversible termination is achieved, CRP reaction vessels have to be entirely pure to prevent termination caused by impurities.[30,37]

All radicals are initiated at the beginning of CRP, where macro-initiators suitable for grafting of polymer chains by the "grafting from" approach can effectively be formed by attaching CRP initiators onto solid surfaces (such as the CNT surface).[34] This makes CRP an ideal method for use where grafting onto solid surfaces is demanded.

The different methods of CRP available include: (a) nitroxide-mediated polymerization (NMP), (b) reversible addition fragmentation chain transfer (RAFT) polymerization and (c) atom transfer radical polymerization (ATRP).[30,31,33]

(a) NMP

The equilibrium reaction between an active propogating radical at chain end and a dormant polymer chain end-capped with a nitroxide species is governed by the NMP approach (refer to scheme 2.3).[38-40] The disadvantage of NMP is that high temperatures are required to establish the equilibrium; which restricts the range of monomers which can be used.[38,39] Fan *et al.*[41] synthesized polystyrene (PS) grafted MWCNTs by *in-situ* NMP. This method resulted in polymerization which wasn't highly controlled, and alternatively RAFT polymerization and ATRP were investigated for the purpose of this study.

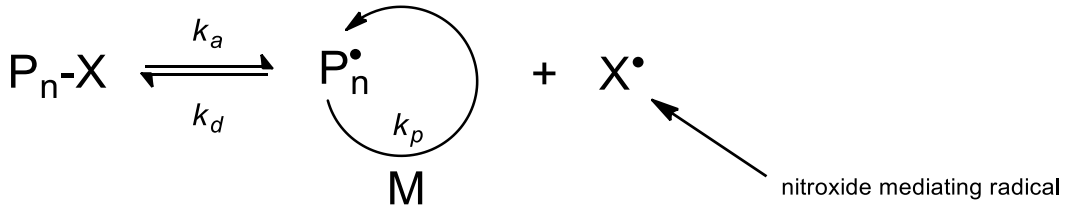

Scheme 2.3: *General NMP mechanism.*

(b) RAFT polymerization

During RAFT polymerization control over the M_n and Đ is afforded by use of a chain transfer agent (RAFT agent). The RAFT polymerization process entails the addition of monomer units to the reactive C-S double bond of the RAFT agent; where RAFT agents are thiocarbonyl-thio compounds (refer to figure 2.4).[42,43] The RAFT agents' performance is influenced by the type of R- and Z-groups present; where R is a free-radical leaving group which requires the ability to reinitiate polymerization, and Z is a group which regulates the reactivity of the C-S double bond of the RAFT agent.[30,37,44-46]

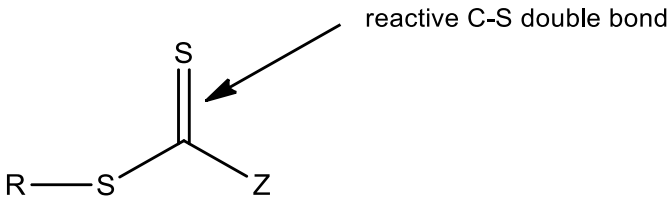

Figure 2.4: *General thiocarbonyl-thio chain transfer agent (RAFT agent).*[30,43]

Arslan[36] and Spitalsky *et al.*[23] report on the grafting of polymer chains from the CNT backbone by means of RAFT polymerization; where polymerization takes place from the RAFT agents initially immobilized on the CNT surface. The polymer chains produced by the RAFT polymerization technique contain thiocarbonyl-thio end-groups.[30,33,37,43,45] Published work by Hernández-Guerrero *et al.*[47] states that the immobilization of RAFT agents onto solid surfaces can be approached in two ways – the R-group approach and the Z-group approach. In the R-group approach, the RAFT agent is fragmented from the CNT surface leading to the presence of a free radical capable of acting as a macro-RAFT agent on the CNT backbone. Termination where the R-group approach is implemented can, however, result in coupling; where this may consequently lead to the broadening of the Đ and effective crosslinking of the

polymer chains via the CNTs (refer to scheme 2.4 (i)). This coupling can, in theory, be avoided by implementing the Z-group approach. Fragmentation of the RAFT agent does not occur during the Z-group approach, and free radicals capable of coupling are thus never present on the CNT backbone. A disadvantage associated with the Z-group approach is the fact that the RAFT agent remains attached to the CNT backbone, which may potentially cause steric hindrance and limit the access of growing polymer chains to the RAFT moiety (refer to scheme 2.4 (ii)).[47]

(i) *R-group approach:*

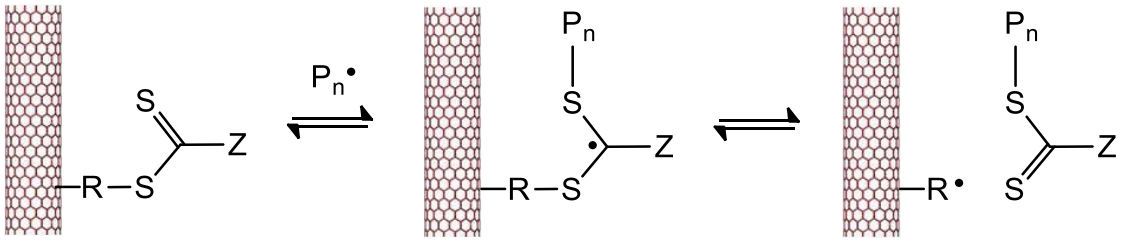

Termination:

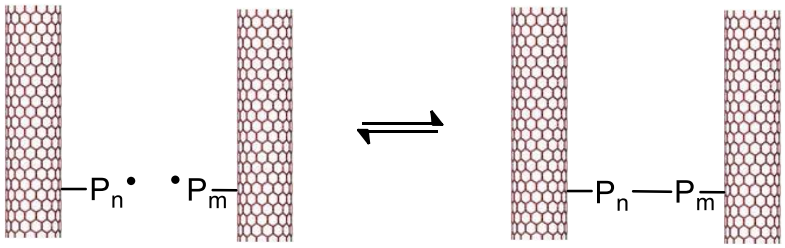

(ii) *Z-group approach:*

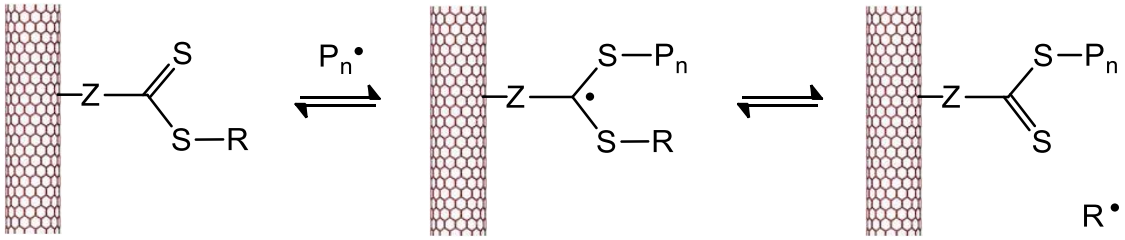

Termination:

Scheme 2.4: *Schematic representation of the grafting of polymers onto CNTs by means of the immobilization of RAFT agents onto the CNT surface via the (i) R-group approach and (ii) Z-group approach.*[47]

R- and Z-groups have to be carefully considered to ensure the right approach is being followed in order to produce predicted products.[48] By studying these different approaches it is noted that the grafting of polymers onto solid surfaces using the RAFT polymerization technique is a more complex task than may be expected. Consequently; ATRP was reviewed for the grafting of polymer chains from solid surfaces for the purpose of this study.

(c) ATRP

In ATRP, transition metal based complexes are used as catalysts; where these complexes consist of a complexing ligand (L) and a transition metal (M_t^n) that has an oxidation state which can increase. These transition metal based compounds are used to extract a halogen from the initiator, which is an alkyl halide compound (P-X), at a reaction rate of k_a. This leads to the formation of a radical ($P^{\bullet}$) and a metal halide complex with an increased oxidation state ($X\text{-}M_t^{n+1}/L$). Polymer chain propagation takes place at a rate of k_p as monomer (M) is added to the propagating radicals at the chain ends. The polymerization reaction can then again deactivate at a reaction rate of k_d, which leads to capped/dormant polymer chains and thus deactivated propagating radicals at the chain end. Equilibrium is established in ATRP between the activation and deactivation reactions, and due to this equilibrium a linear increase in M_n at a polymerization rate of k_a/k_d is achieved. Termination is overcome by this equilibrium, but intentional reaction termination (which takes place at a reaction rate of k_t) can be implemented.[30,31,49-54] The general ATRP mechanism is depicted below:

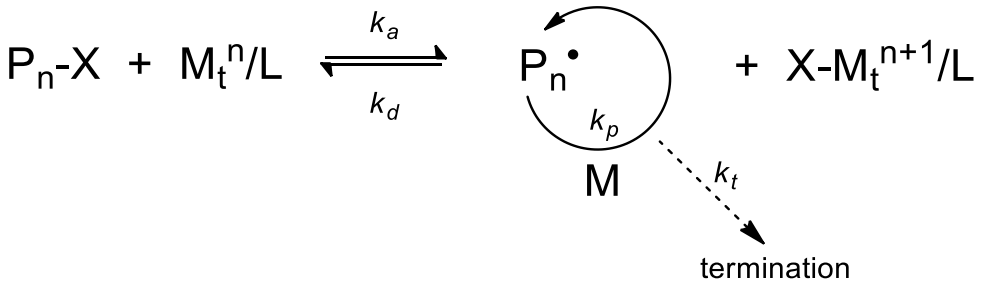

Scheme 2.5: *General ATRP mechanism.*

ATRP is a well regulated reaction, which accounts for advantages including: (1) the degree of polymerization, and thus the M_n of the polymer, can be targeted while a narrow M_n distribution ($1.0 < Đ < 1.5$) will be achieved and (2) polymer chains with specific end-functionalities, as well as block and graft copolymers, can be synthesized.[50,51]

Work published by Kong *et al.*[55,56] shows the grafting of poly(methyl methacrylate) (PMMA) and PS polymer onto the surface of CNTs by means of the "grafting from" method in conjunction with *in-situ* ATRP. Their strategy involves the introduction of hydroxyl functional groups on the CNT surfaces, from which multifunctional ATRP macro-initiator sites (bromide functional groups) for grafting are formed. The strategy allows for good control over the thickness of the polymer layer on the CNTs; where the wt. % of bromide functionalized CNTs relative to polymer can be adjusted in order to obtain a different thickness.

When grafting polymer chains onto solid CNT surfaces, ATRP holds advantages over RAFT polymerization by reason of there only being one pathway through which polymerization can occur – in ATRP polymerization will take place from the macro-initiator sites formed on the CNT surface, while RAFT polymerization can be approached via either the R- or Z-group.[57] Hence, ATRP is a simpler and more accurate method, and is accordingly used in this study to graft PMMA from the CNT backbone.

2.4 Electrospinning

Electrospinning is an uncomplicated yet versatile method in which continuous polymer fibres with diameters in the nanometer range (nanofibres) are produced.[58-62] The large range of polymers which can be used to produce nanofibres adds to the versatility of the process. Furthermore, the product can be enhanced by the addition of nanoscale reinforcing/filler materials. The versatility of this process allows one to produce products suitable for various end-uses.[58-70] In this study, a nanofibrous mat of electrospun nanofibres constitutes the polymer matrix, with the addition of various CNTs as reinforcing nanomaterial.

2.4.1 Electrospinning set-up

A schematic representation of a basic single needle electrospinning set-up is shown in figure 2.5.[70-73]

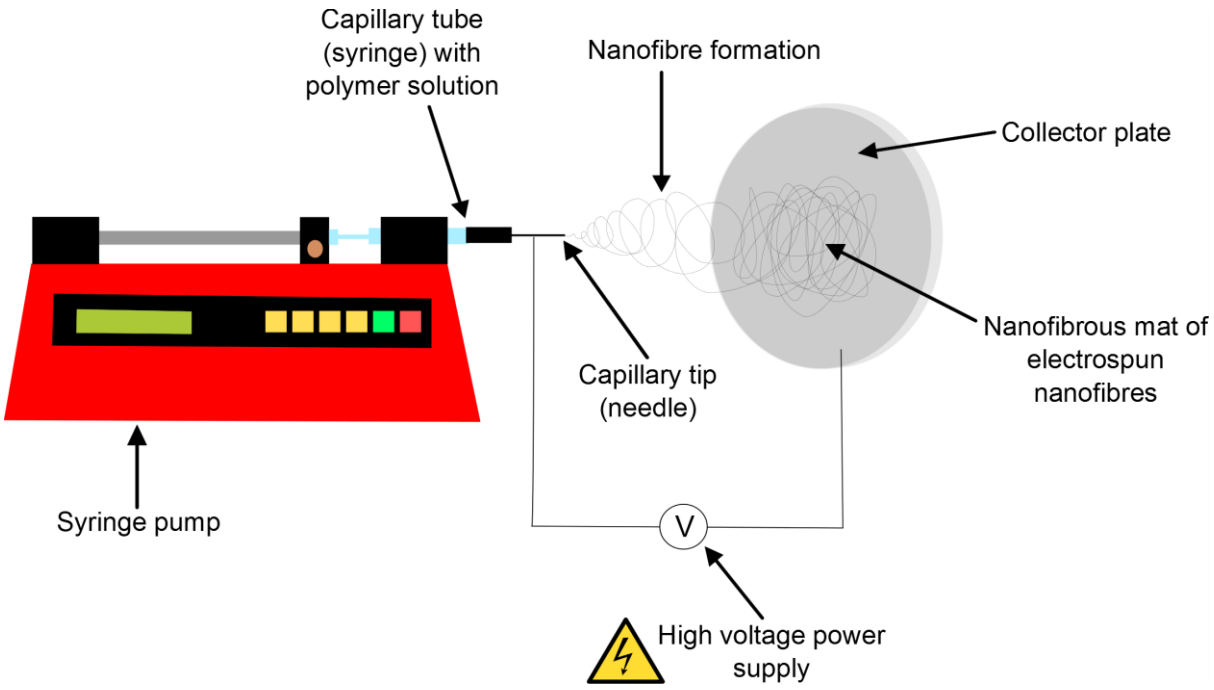

Figure 2.5: *Basic single needle electrospinning set-up.*

2.4.2 Electrospinning process

The three main components used in the basic single needle electrospinning process include: a capillary tube (syringe) with a capillary tip of small diameter (needle) and a collector plate, connected with a high voltage power supply. The capillary tube is filled with a polymer solution of a certain surface tension. A syringe pump is then connected to the capillary tube, and feeds polymer solution to the capillary tip at a constant rate in order to generate polymer droplets at the tip of the capillary. The surface of a polymer droplet is induced with electrical charges by means of a high voltage, where the high voltage is applied to the capillary through an electrode. The induced charges cause mutual charge repulsion on the surface of the polymer droplet, which leads to the deformation of the polymer droplet into a so-called Taylor cone. When the applied voltage reaches a certain critical value, a jet of charged polymer solution emerges from the tip of the Taylor cone due to the electrostatic repulsive forces overcoming the surface tension of the solution (refer to figure 2.6). A grounded collector plate is placed at a certain distance from the tip of the capillary, and acts as a counter electrode. The electrostatic repulsive forces within the jet cause the jet to undergo a whipping action as it accelerates towards the collector plate, which allows the solvent to

evaporate and fibres to form on the collector plate surface. The whipping action also allows the jet to stretch, thus decreasing the fibre diameter from micrometres to nanometres. When the electrospinning process is complete, a nanofibrous mat of electrospun nanofibres is obtained on the collector plate.[66-69,74,75]

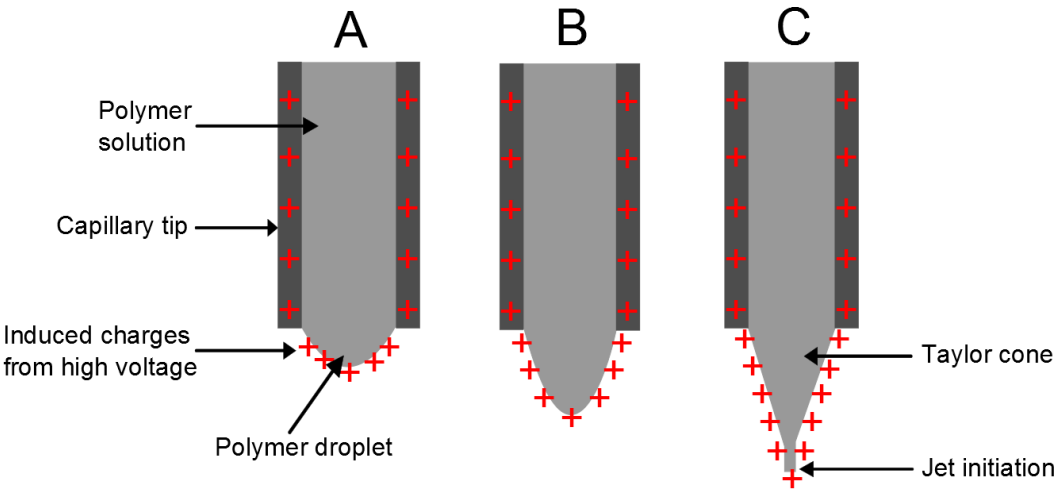

Figure 2.6: *Schematic representation of the Taylor cone formation: (A) surface of a polymer droplet induced with electrical charges, (B) elongation of the polymer droplet and (C) deformation of the pendant droplet to a Taylor cone due to the mutual charge repulsion on the surface of the droplet. A jet emerges from the tip of the Taylor cone.*

2.4.3 Parameters affecting the fibre diameter

There are mainly three factors that influence the electrospinning process and may, in turn, affect the fibre diameter: polymer solution parameters, processing parameters and ambient parameters. The three parameters are elaborated on below, while a summary of the effect the parameters have on the fibre diameter is tabulated in table 2.1.

2.4.3.1 Polymer solution parameters

(a) Viscosity

The viscosity of a polymer solution depends on the polymer M_n as well as the polymer solution concentration. A higher M_n and solution concentration give rise to a higher polymer solution viscosity. The fibre morphology and size are greatly influenced by the polymer solution viscosity. If a set M_n is assumed – a lower solution viscosity correlates to a lower solution

concentration.[58,66] Consequently a lower amount of polymer chain entanglements will be present, leading to more stretching and decreased fibre diameters; as shown by Teo *et al.*[74] In addition, if the viscosity of a solution is too low it may give rise to beaded fibres or electrospraying due to the amount of polymer chain entanglements being inadequate in stabilizing the jet.[58,69,75] On the other hand, it is shown by Khanlou *et al.*[70] that a higher solution viscosity will cause a greater amount of polymer chain entanglements, which in turn will lead to less stretching and increased fibre diameters. The flow of polymer solution through the capillary tube to the capillary tip may also be disrupted.[58,66,75]

(b) Electrical conductivity

A polymer solution possesses higher electrical conductivity potential as the amount of charges in the solution increase. Thus, as the electrical conductivity of a solution increases, more mutual charges will be present. These mutual charges repel one another and increase the electrostatic repulsive forces within the solution. As previously stated, the whipping action of the electrospinning jet is caused by electrostatic repulsive forces within the jet; where a higher force induces more whipping. An increased whipping action leads to more stretching of the jet; therefore a polymer solution with a higher electrical conductivity will have decreased fibre diameters. The opposite occurs as the electrical conductivity of a polymer solution decreases.[58,66,75] In a polymer solution the solvent is one of the leading solution conductivity contributors; where dimethylformamide (DMF), with a conductivity value of 10.9μS/cm, is a good example of a highly conductive solvent. This was proved in a study by Jarusuwannapoom *et al.*,[76] where the effect of eighteen different solvents for the electrospinning of polystyrene solutions were investigated.

2.4.3.2 Processing parameters

(a) Flow rate of polymer solution

Flow rate refers to the constant speed at which the syringe pump feeds the polymer solution to the capillary tip. A higher flow rate will result in the formation of larger polymer droplets with small surface tensions at the tip of the capillary. Smaller electrostatic repulsive forces are thus required to overcome the droplet surface tension in order to initiate an electrospinning jet; where the smaller electrostatic repulsive forces will induce less whipping and stretching, leading to fibres with increased diameters. This will occur up to a point where the polymer solution will simply start dripping from the capillary tip, because there is not enough electrical charge to carry it towards the collector plate. On the contrary, if the flow rate is lower fibre diameters will

decrease. Even lower flow rates will not allow a Taylor cone to form at the tip of the capillary, which will give rise to a discontinuous electrospinning jet.[58,75]

(b) Tip-to-collector distance

As the tip-to-collector distance increases the electric field strength decreases, while flight time of the electrospinning jet is lengthened. This allows for more whipping and stretching of the jet to occur, which results in decreased fibre diameters. The opposite occurs as the tip-to-collector distance is decreased.[58,66,69,75]

(c) Voltage

The surface of a polymer droplet is induced with electrical charges by means of a high voltage, where a higher voltage induces more charge. When the applied voltage reaches a certain critical value, a jet of charged polymer solution emerges from the tip of the Taylor cone. If the applied voltage exceeds the critical value, the electrostatic repulsive forces caused by the induced charges will increase, allowing for more whipping and stretching of the jet in order to form fibres with decreased diameters. The higher voltage may also affect the shape and stability of the Taylor cone, which may influence the fibre morphology and lead to beaded fibres. If a lower voltage is applied, less whipping and stretching of the jet will take place, resulting in fibres with increased diameters.[58,66,69,75]

(d) Diameter of capillary tip

The smaller the capillary tip diameter, the smaller the size of the polymer droplet at the tip of the capillary and the higher the surface tension of the droplet will be. Greater electrostatic repulsive forces are thus required to overcome the droplet surface tension in order to initiate an electrospinning jet; where the greater electrostatic repulsive forces will induce more whipping and stretching, leading to fibres with decreased diameters. The opposite will occur if the capillary tip diameter is increased.[75]

2.4.3.3 Ambient parameters

(a) Humidity

Lower humidity encourages solvent evaporation during electrospinning, while a very high humidity may hinder solvent evaporation and result in entangled fibres which are not properly dried.[66,75]

Table 2.1: *Summary of parameters affecting the fibre diameter during electrospinning.*

	Parameter increase	Influence on diameter
Polymer solution parameters	Viscosity ↑	↑
	Electrical conductivity ↑	↓
Processing parameters	Flow rate of polymer solution ↑	↑
	Tip-to-collector distance ↑	↓
	Voltage ↑	↓
	Diameter of capillary tip ↑	↑
Ambient parameters	Humidity ↑	↑

.

2.4.4 Effect of CNTs on the fibre diameter

In the case of PCNs, CNTs are added to the polymer solution as reinforcing material. The addition of CNTs will thus directly influence the polymer solution parameters.

(a) Viscosity

As shown by Bayley *et al.*[63] during the electrospinning of MWCNT PAN-*g*-PDMS solutions; the viscosity of a polymer solution increases as the concentration of CNTs incorporated increase. When the concentration of incorporated CNTs was too high, the polymer solution became unspinnable. The optimal concentration for electrospinning of the copolymer was decreased in order to compensate for the viscosity added by the incorporated CNTs. Since the viscosity of a polymer solution has a great effect on the fibre morphology and size, the concentration of polymer and CNTs incorporated has to be carefully adjusted; where ratios of polymer to CNTs similar to that of Bayley *et al.*[63] were used during this study.

(b) Electrical conductivity

Bayley *et al.*[63] reported that the incorporation of the electrically conductive CNTs into a polymer solution increases the solution conductivity. Consequently, the electrostatic repulsive forces within the solution increases which results in more stretching and thus decreased fibre diameters (as explained in section 2.4.3.1 (b) above).

2.5 Magnetic carbon nanotubes

Nanoparticles varying in configuration and size can be incorporated with CNTs. Depending on the type of nanoparticles incorporated; the nanoparticles allow functionality to be added to the properties already known for CNTs.[77] When magnetic nanoparticles and CNTs are incorporated, magnetic CNTs are formed. Two types of magnetic CNTs are possible: (2.5.1) magnetic CNTs with embedded magnetic nanoparticles and (2.5.2) magnetic CNTs decorated with magnetic nanoparticles.

2.5.1 Magnetic CNTs with embedded magnetic nanoparticles

When looking at magnetic CNTs as synthesized by Mattia *et al.*,[77] controlled amounts of magnetic nanoparticles (iron oxide nanoparticles) are embedded in the walls of the CNTs during synthesis. This results in CNTs with added magnetic properties due to the remaining metallic iron.

The incorporation of nanoparticles leads to nanostructures embedded in the walls of CNTs, without the surface chemistry of the CNTs being changed.[77] This is verified using scanning electron microscopy (SEM) and transmission electron microscopy (TEM) – the unchanged surface chemistry is confirmed by the smooth external surface of the fractured magnetic CNTs in SEM images (refer to figure 2.7 (a)); while the embedding of nanoparticles in the wall of the CNTs are confirmed by 'bumps' seen in SEM images, as well as TEM images where iron (Fe) nanoparticles completely surrounded by carbon can be observed (refer to figure 2.7 (a) and (b)).[77] This allows one to successfully modify magnetic CNTs with embedded nanoparticles using the same strategy as explained for MWCNTs in section 2.2 above – as was done in this study.

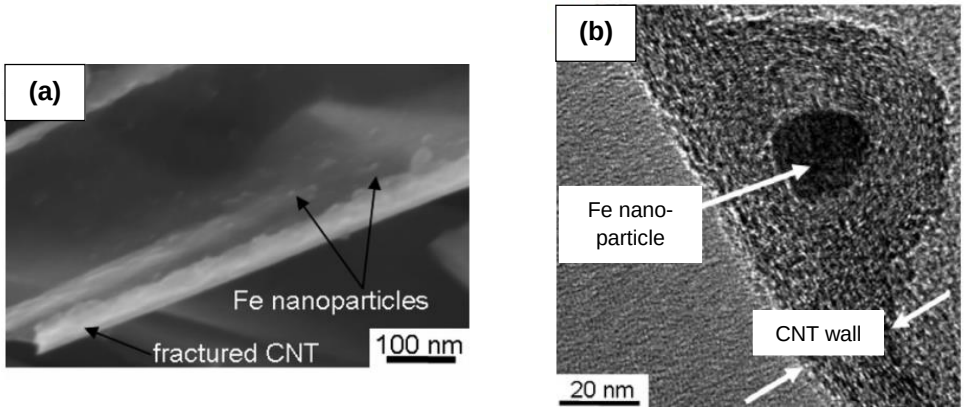

Figure 2.7: *(a) SEM image of fractured magnetic CNTs with a smooth external surface containing 'bumps', thus embedded Fe nanoparticles and (b) TEM image of magnetic CNTs with Fe nanoparticles embedded in the CNT walls (reproduced from ref. 77).*

2.5.2 Magnetic CNTs decorated with magnetic nanoparticles

CNTs can be decorated with magnetic nanoparticles using either an *in-situ* or *ex-situ* approach; however, only a few studies on this topic of interest have been reported on. In the *in-situ* approach a simpler single-step method is followed which entails the synthesis of magnetic nanoparticles directly onto the CNT surface, while in the *ex-situ* approach magnetic nanoparticles are synthesized separately and only then attached to the CNT surface.[78]

An example where cellulose nanofibres are decorated with iron/cobalt oxide ($CoFe_2O_4$) nanoparticles (magnetic ferrite nanoparticles) using an *in-situ* approach was reported by Galland *et al.*[79] and Olsson *et al.*[80] Firstly, an aqueous metal-salt solution containing cellulose nanofibrils is heated to 90 °C, which results in hydrolysis of the metal precursor. This leads to the precipitation of metal-ion complexes onto the surface of the cellulose nanofibrils. Rapid addition of an alkaline medium at 90 °C permits a metal-ion condensation of the precipitated precursors as magnetic ferrite crystal nanoparticles on the fibrils. The precipitation and condensation of these magnetic ferrite crystal nanoparticles are confined by the hydroxyl groups present on the nanofibril surface.[79,80] By using oxidized CNTs with carboxylic-rich surfaces the same *in-situ* decoration is believed to be possible, and was investigated in the present study.

Another *in-situ* approach for CNT decoration with iron oxide (Fe_3O_4) nanoparticles is reported by He *et al.*[78] Nanoparticles are immobilized on the carboxylic acid functionalized CNT backbone by the hydrolysis of a coordinating metal precursor ($FeCl_3$) at high temperatures. This approach is in agreement with green chemistry standards, and is attempted in this study.

When considering the *ex-situ* approach, the problem of magnetic ferrite nanoparticle agglomeration arises due to interparticle dipolar forces.[80] This can be overcome by capping of the magnetic ferrite nanoparticles. The capping agent allows monodisperse nanoparticles to form, prevents nanoparticle agglomeration by improving its solubility in organic solvents, and also imparts reactivity to the nanoparticle depending on the chemical functionality used as capping agent.[81-84] An example of capped iron oxide (Fe_3O_4) nanoparticles is reported on by Georgakilas *et al.*,[84] where oleic acid is used as capping agent (refer to figure 2.8). By the covalent reaction of chemical functionalities present on the oxidized CNTs with the capping agent functionalities on the iron oxide surface, magnetic CNTs are predicted to be formed.

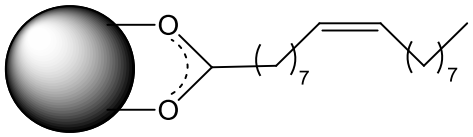

Figure 2.8: *Illustration of an oleic acid capped iron oxide nanoparticle (for clarity, only one oleic acid molecule is shown on the iron oxide nanoparticle surface).*[81-86]

2.6 Analysis Techniques

Analysis techniques used to confirm and characterize polymer synthesis include nuclear magnetic resonance (NMR) and size exclusion chromatography (SEC). NMR is a spectroscopic method in which nuclei (mostly hydrogen nuclei) are studied. It allows one to determine the amount of distinct types of nuclei present in the molecule, as well as to obtain data about the nature of each type of nuclei's immediate environment. NMR results obtained assist one in determining/confirming the structure of an unknown molecule.[87] SEC (also referred to as gel permeation chromatography) is a technique which separates molecules according to size, and allows for the determination of the M_n and Đ of polymers. These values are important when electrospinning, where a M_n that is too low will not lead to a polymer solution viscosity high enough for electrospinning.[75,88,89]

Thermogravimetric analysis (TGA) measures the weight change over a specific temperature range in a controlled atmosphere, and is used to characterize covalently functionalized CNTs.[90] The degree of CNT functionalization can be deduced from the weight change data, since CNTs have distinct thermal properties. These thermal properties allow CNTs to remain stable at high temperatures under nitrogen atmosphere; however combustion of the CNTs will take place at the same temperature where an oxygen cycle is implemented.[91] TEM can also be used to observe if the covalent functionalization of CNTs, as well as synthesis of magnetic nanoparticles, is successful. TEM images extremely small objects by transmitting a beam of electrons through it and thus allows one to observe the internal composition of the sample. In this way CNTs' internal composition as well as 'coating' (covalent attachments) can be observed in conjunction in order to evaluate the products synthesized. The sample must be thin enough in order to enable the electrons to pass through.[92] Fourier transform infrared spectroscopy (FTIR) is used to characterize the structure of a molecule and can thus be used to determine if the synthesis of magnetic nanoparticles are successful. FTIR generates an infrared absorption pattern which is different for every molecule, since the absorption of various frequencies of infrared radiation is distinctive of the bonds in a molecule.[87] Analysis of covalently functionalized CNTs can, however, not be done using FTIR. This is due to the nature of CNTs which leads to the absorption of too many frequencies of infrared radiation, thus causing a pattern with excessive noise which makes the spectrum

impossible to interpret. FTIR may, nonetheless, be efficient for use when only a change in one specific peak has to be observed.

During X-ray diffraction (XRD) a diffraction pattern is produced as X-rays are scattered from atoms of a crystalline sample. The X-ray diffraction pattern obtained is characteristic of the crystalline structure, and thus the arrangement of the atoms, of a sample. In this study XRD can be used to confirm the synthesis of covalently functionalized CNTs where magnetic ferrite nanoparticles are attached.[93] As opposed to FTIR, XRD will deliver a characteristic peak for CNTs at a 2θ value of 10 degrees and just above 20 degrees.

SEM can be used to observe electrospun nanofibres for fibre morphology and size analysis. SEM reflects a beam of electrons off the surface of an object, thereby producing a 2D image of the surface of the object.[94] TEM can also be used to confirm successful incorporation of CNTs in electrospun polymer nanofibres due to internal composition being visible when using TEM. SEM equipped with a scanning transmission electron microscopy (STEM) detector can also be used to acquire TEM comparable images.

A magnetometer (such as a superconducting quantum interference device (SQUID)) measures the magnetic response of a magnetic material, and is thus ideal for use where CNTs covalently functionalized with magnetic nanoparticles are incorporated in order to determine the effect that the magnetic nanoparticles have on the final product.[95]

2.7 References

1. J. H. Koo, *Polymer nanocomposites*, McGraw-Hill, New York, 2006, 9.

2. R. Roy, R. A. Roy and D. M. Roy, *Mater. Lett.,* 1986, **4**, 323-328.

3. S. Anandhan and S. Bandyopadhyay, *Nanocomposites and Polymers with Analytical Methods,* ed. J. Cuppoletti, InTech, Croatia, 2011, ch. 1, pp. 3-28.

4. P. M. Ajayan, O. Stephan, C. Colliex and D. Trauth, *Science,* 1994, **265**, 1212-1214.

5. P. Ajayan and L. Schadler, *Polym. Prepr.,* 2001, **42**, 35.

6. V. N. Popov, *Mater. Sci. Eng.,R,* 2004, **43**, 61-102.

7. H. Hou, J. J. Ge, J. Zeng, Q. Li, D. H. Reneker, A. Greiner and S. Z. D. Cheng, *Chem. Mater.,* 2005, **17**, 967-973.

8. M. T. Byrne and Y. K. Gun'ko, *Adv. Mater.,* 2010, **22**, 1672-1688.

9. S. Iijima, *Nature,* 1991, **354**, 56-58.

10. V. Choudhary and A. Gupta, *Carbon Nanotubes - Polymer Nanocomposites*, ed. S. Yellampalli, InTech, Croatia, 2011, ch. 4, pp. 65-90.

11. M. Biercuk, M. C. Llaguno, M. Radosavljevic, J. Hyun, A. T. Johnson and J. E. Fischer, *Appl. Phys. Lett.,* 2002, **80**, 2767-2769.

12. Z. Ounaies, C. Park, K. Wise, E. Siochi and J. Harrison, *Compos. Sci. Technol.,* 2003, **63**, 1637-1646.

13. M. Weisenberger, E. Grulke, D. Jacques, A. T. Rantell and R. Andrewsa, *J.Nanosci. Nanotechno.,* 2003, **3**, 535-539.

14. O. Breuer and U. Sundararaj, *Polym. Compos.,* 2004, **25**, 630-645.

15. L. Meng, C. Fu and Q. Lu, *Prog. Nat. Sci.,* 2009, **19**, 801-810.

16. D. Tasis, N. Tagmatarchis, A. Bianco and M. Prato, *Chem. Rev.,* 2006, **106**, 1105-1136.

17. S. Niyogi, M. Hamon, H. Hu, B. Zhao, P. Bhowmik, R. Sen, M. Itkis and R. Haddon, *Acc. Chem. Res.,* 2002, **35**, 1105-1113.

18. S. Banerjee, T. Hemraj-Benny and S. S. Wong, *Adv. Mater.,* 2005, **17**, 17-29.

19. F. Tournus and J. Charlier, *Phys. Rev. B,* 2005, **71**, 165421.

20. P. Bilalis, D. Katsigiannopoulos, A. Avgeropoulos and G. Sakellariou, *R. Soc. Chem. Adv.,* 2014, **4**, 3060-3083.

21. A. Mandal and A. K. Nandi, *J. Phys. Chem. C,* 2012, **116**, 9360-9371.

22. C. Li and B. C. Benicewicz, *Macromolecules,* 2005, **38**, 5929-5936.

23. Z. Spitalsky, D. Tasis, K. Papagelis and C. Galiotis, *Prog. Polym. Sci.,* 2010, **35**, 357-401.

24. N. Hadjichristidis, M. Pitsikalis, S. Pispas and H. Iatrou, *Chem. Rev.,* 2001, **101**, 3747-3792.

25. N. Hadjichristidis, M. Pitsikalis and H. Iatrou, *Block Copolymers I*, ed. V. Abetz, Springer, Berlin, 2005, ch. 1, pp. 1-124.

26. Y. Liu, V. Klep, B. Zdyrko and I. Luzinov, *Langmuir,* 2004, **20**, 6710-6718.

27. J. Parvole, J. Montfort and L. Billon, *Macromol. Chem. Phys.,* 2004, **205**, 1369-1378.

28. E. Malmström and A. Carlmark, *Polym. Chem.,* 2012, **3**, 1702-1713.

29. Y. Li, L. S. Schadler and B. C. Benicewicz, *Handbook of RAFT polymerization,* ed. C. Barner-Kowollik, Wiley, Weinheim, 2008, vol. 423, ch. 11, pp. 423-454.

30. V. Mishra and R. Kumar, *J. Sci. Res.*, 2012, **56**, 141-176.

31. J. Qiu, B. Charleux and K. Matyjaszewski, *Prog. Polym. Sci.,* 2001, **26**, 2083-2134.

32. K. Matyjaszewski, *Handbook of Radical Polymerization,* ed. K. Matyjaszewski and T. P. Davis, Wiley, Hoboken, 2002, ch. 8, pp. 361-406.

33. G. Moad, E. Rizzardo and S. H. Thang, *Aust. J. Chem.,* 2005, **58**, 379-410.

34. K. Matyjaszewski and J. Spanswick, *Mater. Today,* 2005, **8**, 26-33.

35. C. J. Hawker, *Acc. Chem. Res.,* 1997, **30**, 373-382.

36. H. Arslan, *Polymerization*, ed. A. De Souza Gomes, InTech, Croatia, 2012, ch. 13, pp. 279-320.

37. J. Chiefari, Y. Chong, F. Ercole, J. Krstina, J. Jeffery, T. P. Le, R. T. Mayadunne, G. F. Meijs, C. L. Moad and G. Moad, *Macromolecules,* 1998, **31**, 5559-5562.

38. J. Nicolas, Y. Guillaneuf, C. Lefay, D. Bertin, D. Gigmes and B. Charleux, *Prog. Polym. Sci.,* 2013, **38**, 63-235.

39. F. Chauvin, P. Dufils, D. Gigmes, Y. Guillaneuf, S. R. Marque, P. Tordo and D. Bertin, *Macromolecules,* 2006, **39**, 5238-5250.

40. C. J. Hawker, A. W. Bosman and E. Harth, *Chem. Rev.,* 2001, **101**, 3661-3688.

41. D. Fan, J. He, W. Tang, J. Xu and Y. Yang, *Eur. Polym. J.,* 2007, **43**, 26-34.

42. Y. K. Chong, G. Moad, E. Rizzardo and S. H. Thang, *Macromolecules,* 2007, **40**, 4446-4455.

43. G. Moad, E. Rizzardo and S. H. Thang, *Polym. Int.,* 2011, **60**, 9-25.

44. Y. Chong, J. Krstina, T. P. Le, G. Moad, A. Postma, E. Rizzardo and S. H. Thang, *Macromolecules,* 2003, **36**, 2256-2272.

45. G. Moad, J. Chiefari, J. Krstina, R. T. A. Mayadunne, A. Postma, E. Rizzardo and S. H. Thang, *Polym. Int.,* 2000, **49**, 993-1001.

46. R. T. Mayadunne, E. Rizzardo, J. Chiefari, Y. K. Chong, G. Moad and S. H. Thang, *Macromolecules,* 1999, **32**, 6977-6980.

47. M. Hernández-Guerrero, T. P. Davis, C. Barner-Kowollik and M. H. Stenzel, *Eur. Polym. J.,* 2005, **41**, 2264-2277.

48. A. M. Bivigou Koumba, MSc Thesis, University of Stellenbosch, 2005.

49. W. A. Braunecker and K. Matyjaszewski, *Prog. Polym. Sci.,* 2007, **32**, 93-146.

50. K. Matyjaszewski and J. Xia, *Chem. Rev.,* 2001, **101**, 2921-2990.

51. K. Matyjaszewski, *Macromolecules,* 2012, **45**, 4015-4039.

52. J. Wang and K. Matyjaszewski, *Macromolecules,* 1995, **28**, 7901-7910.

53. J. Wang and K. Matyjaszewski, *J. Am. Chem. Soc.,* 1995, **117**, 5614-5615.

54. K. Matyjaszewski, T. E. Patten and J. Xia, *J. Am. Chem. Soc.,* 1997, **119**, 674-680.

55. H. Kong, C. Gao and D. Yan, *J. Am. Chem. Soc.,* 2004, **126**, 412-413.

56. H. Kong, C. Gao and D. Yan, *Macromolecules,* 2004, **37**, 4022-4030.

57. R. Chen, W. Feng, S. Zhu, G. Botton, B. Ong and Y. Wu, *J. Polym. Sci. A Polym. Chem.,* 2006, **44**, 1252-1262.

58. L. Cronje and B. Klumperman, *Eur. Polym. J.,* 2013, **49**, 3814-3824.

59. Y. Qian, Y. Su, X. Li, H. Wang and C. He, *Iran. Polym. J.,* 2010, **19**, 23-129.

60. *US Pat.*, US1975504, 1934.

61. J. Vonch, A. Yarin and C. Megaridis, *Am. J. Undergrad. Res.,* 2007, **1**, 1-6.

62. S. Sarabi-Maneji, J. Scott and D. J. Pagé, *Proceedings of the International Conference on New Trends in Transport Phenomena,* Avestia Publishing, Ottawa, 2014, pp. 1-8.

63. G. M. Bayley and P. E. Mallon, *Polymer,* 2012, **53**, 5523-5539.

64. X. Wang, Y. Kim, C. Drew, B. Ku, J. Kumar and L. A. Samuelson, *Nano Lett.,* 2004, **4**, 331-334.

65. P. P. Tsai, H. Schreuder-Gibson and P. Gibson, *J. Electrostat.,* 2002, **54**, 333-341.

66. T. Subbiah, G. Bhat, R. Tock, S. Parameswaran and S. Ramkumar, *J. Appl. Polym. Sci.,* 2005, **96**, 557-569.

67. E. Kenawy, G. L. Bowlin, K. Mansfield, J. Layman, D. G. Simpson, E. H. Sanders and G. E. Wnek, *J. Controlled Release,* 2002, **81**, 57-64.

68. D. Yu, L. Zhu, K. White and C. Branford-White, *Health,* 2009, **1**, 67-75.

69. P. Bhattarai, K. B. Thapa, R. B. Basnet and S. Sharma, *IJBAR,* 2014, **5**, 401-405.

70. H. M. Khanlou, A. Sadollah, B. C. Ang, J. H. Kim, S. Talebian and A. Ghadimi, *Neural Comput. Appl.,* 2014, **25**, 767-777.

71. Z. Huang, Y. Zhang, M. Kotaki and S. Ramakrishna, *Compos. Sci. Technol.,* 2003, **63**, 2223-2253.

72. D. H. Reneker and I. Chun, *Nanotechnology,* 1996, **7**, 216-223.

73. F. Zhou, R. Gong and I. Porat, *J. Appl. Polym. Sci.,* 2010, **115**, 2591-2598.

74. W. Teo, R. Gopal, R. Ramaseshan, K. Fujihara and S. Ramakrishna, *Polymer,* 2007, **48**, 3400-3405.

75. G. Bayley, PhD Dissertation, University of Stellenbosch, 2011.

76. T. Jarusuwannapoom, W. Hongrojjanawiwat, S. Jitjaicham, L. Wannatong, M. Nithitanakul, C. Pattamaprom, P. Koombhongse, R. Rangkupan and P. Supaphol, *Eur. Polym. J.,* 2005, **41**, 409-421.

77. D. Mattia, G. Korneva, A. Sabur, G. Friedman and Y. Gogotsi, *Nanotechnology,* 2007, **18**, DOI: 10.1088/0957-4484/18/15/155305.

78. H. He and C. Gao, *J. Nanomater.,* 2011, **2011**, DOI: 10.1155/2011/193510.

79. S. Galland, R. L. Andersson, M. Salajková, V. Ström, R. T. Olsson and L. A. Berglund, *J. Mater. Chem. C,* 2013, **1**, 7963-7972.

80. R. T. Olsson, M. A. Samir, G. Salazar-Alvarez, L. Belova, V. Ström, L. A. Berglund, O. Ikkala, J. Nogues and U. W. Gedde, *Nat. Nanotechnol.,* 2010, **5**, 584-588.

81. D. Wilson and M. Langell, *Appl. Surf. Sci.,* 2014, **303**, 6-13.

82. L. Bronstein, X. Huang, J. Retrum, A. Schmucker, M. Pink, B. Stein and B. Dragnea, *Chem. Mater.,* 2007, **19**, 3624-3632.

83. S. Lee and M. T. Harris, *J. Colloid Interface Sci.,* 2006, **293**, 401-408.

84. V. Georgakilas, V. Tzitzios, D. Gournis and D. Petridis, *Chem. Mater.,* 2005, **17**, 1613-1617.

85. G. Lamanna, A. Garofalo, G. Popa, C. Wilhelm, S. Bégin-Colin, D. Felder-Flesch, A. Bianco, F. Gazeau and C. Ménard-Moyon, *Nanoscale,* 2013, **5**, 4412-4421.

86. F. Herranz, B. Salinas, H. Groult, J. Pellico, A. V. Lechuga-Vieco, R. Bhavesh and J. Ruiz-Cabello, *Nanomaterials,* 2014, **4**, 408-438.

87. G. Lampman, D. Pavia, G. Kriz, J. Vyvyan, *Spectroscopy*, Brooks/Cole, US, 4th edn., 2010, ch. 2-3, pp. 15-176.

88. H. Barth, C. Jackson and B. Boyes, *Anal. Chem.,* 1994, **66**, 595R-620R.

89. S. Mori and H. Barth, *Size exclusion chromatography*, Springer, Berlin, 1999, ch. 1, pp. 1-5.

90. T. Ozawa, *Bull. Chem. Soc. Jpn.,* 1965, **38**, 1881-1886.

91. A. Mahajan, A. Kingon, A. Kukovecz, Z. Konya and P. M. Vilarinho, *Mater. Lett.,* 2013, **90**, 165-168.

92. D. Williams and C. Carter, *The Transmission Electron Microscopy*, Springer, US, 2nd edn., 2009, ch. 1, p. 3-22.

93. B. E. Warren, *X-ray Diffraction*, Dover Publications, US, 1969, ch. 1, p. 1-14.

94. *US Pat.*, US5872358, 1999.

95. B. Chesca, R. Kleiner and D. Koelle, *The SQUID Handbook: Fundamentals and Technology of SQUIDs and SQUID Systems*, ed. J. Clarke and A. I. Braginski, Wiley, Weinheim, 2004, ch. 2, pp. 29-92.

Chapter 3: Experimental

3.1 Chemicals for synthesis

All the chemicals were used as purchased from the supplier, except for methyl methacrylate monomer (MMA) and azobisisobutyronitrile (AIBN) which required purification by means of distillation and recrystallization. All chemicals used were of high grade.

Methyl methacrylate monomer (MMA) (99 %, stabilized with hydroquinone, Sigma-Aldrich), potassium hydroxide (KOH) (≥85 %, pellets, Merck) and magnesium sulphate ($MgSO_4$) (62-70 %, anhydrous, UniLab) were used in the MMA distillation process. AIBN (98 %, Aldrich) was purified by recrystallization from methanol (CP grade, Kimix). Toluene (CP grade, Kimix) was used as continuous phase during the polymerization of PMMA, and methanol was used to precipitate the polymer.

Multi-wall carbon nanotubes (MWCNTs) (>95 %) were obtained from Chengdu Organic Chemicals Co. Ltd., while carbon nanotubes (CNTs) with magnetic nanoparticles embedded in the walls (magnetic CNTs) were obtained from the University of Bath as synthesized by Mattia *et al.*[1] Sodium nitrate ($NaNO_3$) (99 %, NT Laboratory Supplies (Pty) Ltd.), sulfuric acid (H_2SO_4) (95-97 %, Merck), potassium permanganate ($KMnO_4$) (99 %, Scienceworld) and hydrogen peroxide (PERDROGEN®, 30 % by weight H_2O_2, Riedel-de Haën) were used to oxidize the CNTs.

Thionyl chloride ($SOCl_2$) (synthetic quality, Merck), tetrahydrofuran (THF) (anhydrous, ≥99.9 %, inhibitor free, Sigma-Aldrich), ethylene glycol ($HOCH_2CH_2OH$) (anhydrous, 99.8 %, Aldrich), chloroform ($CHCl_3$) (anhydrous, ≥99 %, contains 0.5-1.0 % ethanol as stabilizer, Sigma-Aldrich), 4-dimethylaminopyridine (DMAP) (≥98 %, Fluka), triethylamine (≥99 %, Sigma-Aldrich), α-bromoisobutyryl bromide (98 %, Aldrich), copper(I) bromide (CuBr) (98 %, Aldrich), N,N,N′,N′,N″-pentamethyldiethylenetriamine (PMDETA) (99 %, Aldrich), dimethylformamide (DMF) (CP grade, Kimix), MMA and methanol were used to graft MMA from oxidized CNTs via ATRP. Cleavage of PMMA from CNT-PMMA was achieved using THF (CP grade, Kimix), KOH and ethanol (99.9 %, Kimix). THF was used to dissolve the cleaved polymer chains while methanol was used for precipitation purposes.

Ammonium iron sulphate ($(NH_4)_2Fe(SO_4)_2$) (≥98 %, Merck), KOH, ammonium persulfate ($(NH_4)_2S_2O_8$) (98 %, Sigma-Aldrich), oleic acid (65-88 %, Riedel-de Haën), toluene and ethanol were used in the synthesis of oleic acid capped iron oxide nanoparticles. The nanoparticles were then covalently attached to oxidized MWCNTs by using chloroform ($CHCl_3$) (CP grade, Kimix), ethanol and acetone (CP grade, Kimix) (synthesis of *ex-situ* MWCNT-Fe_3O_4).

Previously oxidized MWCNTs, distilled water, cobalt(II) chloride hexahydrate ($CoCl_2.6H_2O$) (≥98 %, Labchem), iron(II) sulfate heptahydryte ($FeSO_4.7H_2O$) (≥99.5 %, Labchem), sodium hydroxide (NaOH) (≥98 %, Labchem) and potassium nitrate (KNO_3) (≥99 %, Labchem) were used to

precipitate magnetic nanoparticles *in-situ* on MWCNTs with approach 1 (synthesis of *in-situ* MWCNT-$CoFe_2O_4$).

NaOH, diethylene glycol (DEG) (99.5 %, UniLab), previously oxidized MWCNTs and iron(III) chloride hexahydrate ($FeCl_3$) (≥99.9 %, Riedel-de Haën) were used to precipitate magnetic nanoparticles *in-situ* on MWCNTs with approach 2 (synthesis of *in-situ* MWCNT-Fe_3O_4), while ethanol and distilled water were used to rinse the product.

Various CNTs and synthesized PMMA were used during the electrospinning process, where DMF was used as solvent.

3.2 Analysis techniques

Various analytical techniques were used for analysis and characterization of products. Nuclear magnetic resonance (NMR) was achieved using a Varian VXR-Unity 300 MHz spectrometer set at 25 °C. Wilmad® NMR tubes were filled with ± 50 mg of sample dissolved in 1 mL deuterated chloroform ($CDCl_3$) (deuteration degree minimum 99.96 %, Merck). The solvent ($CDCl_3$) was then used to fill the NMR tube to the 5 cm height mark. ^1H NMR was carried out; where 32 scans were done.

Size exclusion chromatography (SEC) was achieved using a Breeze V3.30 SPA software system and the following components: a Waters 1515 isocratic HPLC pump, a Waters 717 plus auto-sampler, a Waters 2487 dual wavelength absorbance detector and a Waters 2414 refractive index detector at 30 °C. Dimethylacetamide (DMAC) (HPLC grade, 0.125 % BHT and LiCl stabilized) was used as the eluent with a flow rate of 1 mL/min. An injection volume of 100µL was used to introduce the sample into two PLgel 5 µm mixed-C 300x7.5 mm (Polymer Laboratories) columns connected in series with one PLgel 5 µm guard 50x7.5 mm (Polymer Laboratories) column kept at 30 °C. Samples were dissolved in DMAc and filtered through 0.45 µm nylon filters, where a sample concentration of 1 mg/mL was used. PMMA standards (Polymer Laboratories) were used as calibration standards.

Thermogravimetric analysis (TGA) was achieved using a Perkin Elmer TGA 7. Samples of 2-5 mg were analysed under nitrogen atmosphere with a nitrogen gas flow rate of 50 mL/min. A temperature cycle ranging between 20 °C and 600 °C was used with a heating rate of 10 °C/min. In some instances an oxygen atmosphere with an oxygen gas flow rate of 50 mL/min was implemented at 600 °C, where the isothermal cycle was maintained for 20 minutes.

Fourier transform infra-red (FTIR) analysis was achieved using a Thermo Scientific Nicolet iS10 Smart iTR instrument. The absorption was measured in attenuated total reflectance (ATR) mode

over the wavenumber range of 700-4100 cm^{-1}, with a resolution of 4 and an average number of 64 scans.

A FEI Tecnai 20 transmission electron microscope (TEM) (FEI, Eindhoven, Netherlands) operating at 200 kV (Lab6 emitter) and equipped with a Gatan CCD camera and Tridem energy filter was used. Samples were sectioned using a Reichert Ultracut S ultramicrotome (Leica Microsystems, Vienna, Austria) fitted with a diamond blade in order to prepare samples with a thickness of 100-150 nm.

Average particle diameters were determined using a Zetasizer Nano ZS90 from Malvern Instruments fitted with a 633 nm laser and 90° scattering angle optics. A quartz glass cuvette filled with 1 mL of sample was used during size measurements.

X-ray powder diffraction (XRD) diffractograms were recorded with a Bruker AXS D2 PHASER equipped with a LYNXEYE^{TM} 1D detector and Ni-filtered copper Kα radiation (X-ray generator parameters: 30 kV/10 mA restricted by a 1.0 mm divergence slit and a 2.5° Soller collimator). A step width of 0.04° was used; where the instrument was coupled to DIFFRAC.SUITE^{TM} software in order to make analysis possible.

A LEO 1430VP scanning electron microscope (SEM) instrument was used with a Centaurus detector with a 133 eV resolution at 5.9 keV and a 10 mm^2 detector area. Double-sided carbon tape was used to apply the samples to the SEM stubs, and the samples were then coated with a gold sputter for 3 minutes in order for the samples to have the conductive surface necessary for SEM analysis. A voltage of 7 kV and working distance of 6-10 mm were used.

A Zeiss EVO MA 15 (or MERLIN Field Emission Gun (FEG)) SEM equipped with a scanning transmission electron microscopy (STEM) detector was used to acquire TEM comparable images. Beam conditions during the quantitative analyses on the MERLIN FEG SEM were 20 kV and 16 nA, with a working distance of 3-4 mm.

Superconducting quantum interference device (SQUID) magnetometry was achieved using a Quantum Design Magnetic Properties Measurement System or MPMS 7XL, supplied by Quantum Design in San Diego. The machine was equipped with a high field uniformity coil with a field capability of 7 Tesla and high accuracy field reset; where measurements were taken at room temperature.

3.3 Purification of chemicals

3.3.1 Distillation of MMA

A conventional distillation technique was used to purify the MMA monomer. Firstly the MMA was washed in order to remove any inhibitor present. A 1:1 ratio of MMA:KOH (0.3 M) was used and the MMA was retrieved by use of a separation funnel. The washing process was repeated three times, where the MMA constituted the top layer. The MMA was then dried for 24 hours, using $MgSO_4$, and filtered off. After the drying step was completed the MMA was transferred to a distillation setup composed of a round bottom flask containing boiling stones, a condenser, a thermometer, a fraction collector and a vacuum pump. A schematic of the setup is illustrated in figure 3.1. The MMA was distilled at 50 °C under vacuum, where the first fraction obtained (± 10 %) was not used in order to ensure that the end product was entirely pure. The pure MMA was then stored on molecular sieves of 1.7-2.4 mm in diameter until further use.

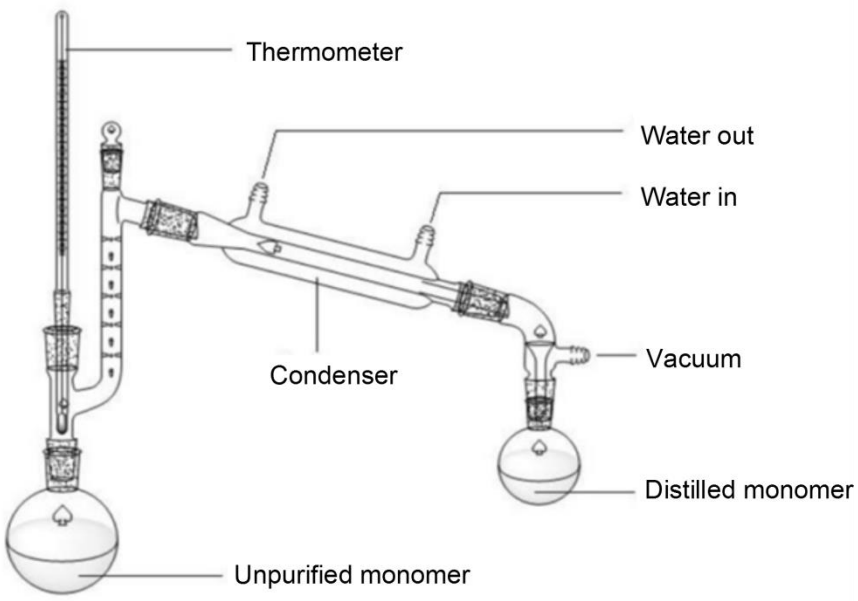

Figure 3.1: *Schematic representation of distillation setup used for MMA monomer purification (reproduced from ref. 2).*

3.3.2 Recrystallization of AIBN

The purification of AIBN initiator by means of a conventional recrystallization process consists of five steps which include: dissolution, filtration, crystallization, collection of crystals and drying of crystals. For the dissolution step AIBN was placed in excess methanol (5 g AIBN in 80 mL methanol) and stirred at 45 °C in order for the AIBN to dissolve (± 10 minutes). The solution was then filtered to remove any impurities by means of a Büchner filter using a methanol wetted filter paper. The resultant solution was placed in a freezer to allow AIBN crystals to form (± 2 hours). The resulting AIBN crystals were then filtered off by means of a Büchner filter, again using a methanol wetted filter paper, and the filter paper containing the crystals was placed in a vacuum oven for 5 hours in order for the crystals to dry. The dried crystals were placed in a sealed container and stored in a freezer until use.

3.4 Polymerization of PMMA

Poly(methyl methacrylate) (PMMA) was synthesised using a conventional free-radical polymerization (FRP) technique. A 100 mL round bottom flask was equipped with a magnetic stirrer, and AIBN as well as toluene were added to the flask. The flask was then sealed off with a rubber septum and, while stirring, the contents were degassed for 10 minutes using Argon gas. At the same time MMA monomer was degassed in a separate container, also with Argon gas for 10 minutes. MMA monomer was then added to the round bottom flask by means of a syringe, and the entire contents were again degassed under the same conditions previously stated. The reaction flask was then inserted into a temperature regulated oil bath set at 70 °C, and the polymerization reaction was allowed to take place for 42 hours. Ratios of 0.1 wt. % initiator (AIBN) relative to monomer, and 20 wt. % monomer relative to solvent (toluene) were used. After the polymerization reaction was complete the contents of the flask were slowly added to an excess of rapidly stirring cold methanol in order for precipitation to take place. The product was then filtered off by means of a Büchner filter and allowed to dry in a vacuum oven overnight at 40 °C. The reaction scheme is presented in scheme 3.1 below:

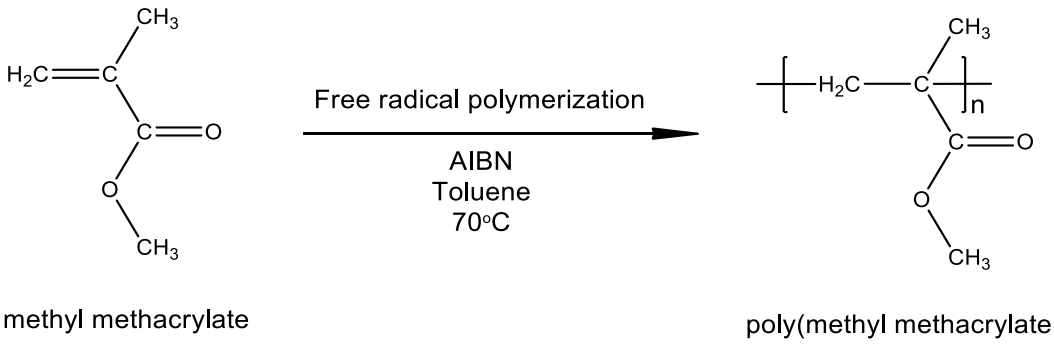

methyl methacrylate poly(methyl methacrylate)

Scheme 3.1: *Synthesis of PMMA via FRP.*

3.5 Carbon nanotube (CNT) functionalization

3.5.1 Oxidation of CNTs

Surface functionalization by means of oxidation was carried out on pristine MWCNTs and magnetic CNTs, which results in carboxylic groups being introduced on the CNT surface. The procedure was followed as set out in an article by Bayley *et al.*[3] Firstly CNTs (2 g), either pristine or magnetic, were added to a 250 mL beaker containing a magnetic stirrer and $NaNO_3$ (1 g). The beaker was placed in an ice bath and H_2SO_4 (46 mL, 95-97 wt. %) was carefully added to the mixture. The contents were allowed to stir gently for 10 minutes, after which $KMnO_4$ (6 g) was added by slow addition in order to ensure that the temperature of the reaction did not exceed 20 °C. The contents were then left to stir vigorously for another 10 minutes. Afterwards the beaker was removed from the ice bath and immersed in a temperature regulated oil bath set at 98 °C. The contents were allowed to stir for about 30 minutes, after which it had lost its effervescence and turned grey-brown in colour. Distilled H_2O (92 mL) was added and the contents were then stirred for an additional 15 minutes at 98 °C. A 3 wt. % solution H_2O_2 in distilled H_2O was then added to the beaker to increase the volume of the reaction mixture to 200 mL. The final contents in the beaker were left to stir for another 20 minutes. After the reaction was completed the CNTs were neutralized by repeated dilution with distilled H_2O and centrifugation. When a neutral pH was obtained the CNTs were freeze dried and sealed in a container until use.

3.5.2 Grafting of PMMA from CNTs via *in-situ* ATRP

The process for grafting of polymers from solid CNT surfaces was carried out as prescribed in an article by Kong *et al.*,[4,5] and consists of four steps. These include: (a) synthesis of carbonyl chloride functionalized CNTs (CNT-COCl) by reaction of oxidized CNTs (CNT-COOH) with $SOCl_2$,

(b) synthesis of hydroxyl functionalized CNTs (CNT-OH) by reaction of CNT-COCl with glycol, (c) formation of initiating sites for ATRP (CNT-Br) by reaction of CNT-OH with α-Bromoisobutyryl bromide and (d) grafting of MMA from CNT-Br by means of ATRP, which results in CNT-PMMA. The four steps are depicted in scheme 3.2 below, and were carried out on oxidized (refer to section 3.5.1) MW- as well as magnetic-CNTs.

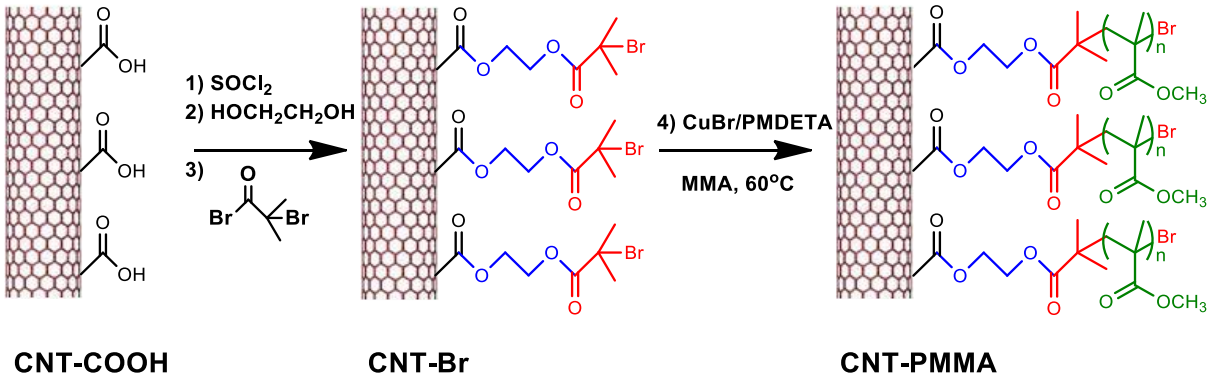

Scheme 3.2: *Schematic representation of the four steps that make up the grafting process.*[4]

(a) Synthesis of CNT-COCl

Dried CNT-COOH (0.56 g) and $SOCl_2$ (20 mL) were placed in a 100 mL round bottom flask equipped with a magnetic stirrer, and stirred in a temperature regulated oil bath at 65 °C for 24 hours. The resultant CNTs were separated by means of centrifugation and then washed three times with anhydrous THF; where separation after washing was also achieved by means of centrifugation. The product was then dried under vacuum at room temperature for 2 hours.

(b) Synthesis of CNT-OH

The resultant CNT-COCl (0.54 g) was mixed with glycol (20 mL) in a 100 mL round bottom flask equipped with a magnetic stirrer, and immersed in a temperature regulated oil bath for 48 hours at 120 °C. The solid was separated by means of centrifugation and then washed three times with anhydrous THF; where separation after washing was also achieved by means of centrifugation. The product was then dried overnight under vacuum at room temperature.

(c) Synthesis of CNT-Br

A 2-neck 100 mL round bottom flask equipped with a magnetic stirrer and a dropping funnel was filled with CNT-OH (0.40 g), anhydrous $CHCl_3$ (10 mL), DMAP (0.0292 g) and triethylamine (0.3031 g). The contents were degassed for 30 minutes using Argon gas.

α-Bromoisobutyryl bromide (0.3832 g) dissolved in anhydrous $CHCl_3$ (5 mL) was added dropwise by means of the dropping funnel for 1 hour at 0 °C, where 0 °C was reached by immersing the flask in an ice bath. After the hour was completed, the mixture was stirred at 0 °C for another 3 hours and then at room temperature for 48 hours. The resultant CNTs were separated by means of centrifugation and then washed five times with anhydrous $CHCl_3$; where separation after washing was also achieved by means of centrifugation. The product was then dried overnight under vacuum at 40 °C; resulting in a multifunctional ATRP macro-initiator.

(d) Synthesis of CNT-PMMA

A 100 mL round bottom flask equipped with a magnetic stirrer was filled with 25.2 mg CNT-Br, 7.2 mg (0.05 mmol) CuBr, 8.7 mg (0.05 mmol) PMDETA and 1.5 mL DMF. The contents were sealed with a rubber septum and degassed for 30 minutes using Argon gas. At the same time MMA monomer was degassed in a separate container, also with Argon gas for 30 minutes. After degassing was completed, 512 mg (5.10 mmol) MMA monomer was added to the round bottom flask and the entire contents were, again, degassed under the same conditions previously stated. The reaction flask was then inserted into a temperature regulated oil bath set at 60 °C, and the grafting process was allowed to take place for 30 hours. The solid was separated by means of centrifugation and then washed three times with anhydrous $CHCl_3$; where separation after washing was also achieved by means of centrifugation. The solid was then redispersed in 5 mL $CHCl_3$ and precipitated in 50 mL cold methanol; where separation after precipitation was again achieved by means of centrifugation. The product was dried overnight under vacuum at room temperature and stored in a sealed container until use.

3.5.2.1 Cleavage of PMMA from CNT-PMMA

By using SEC the molar mass (M_n) and dispersity (Đ) of polymer chains can be determined. However, to obtain these results for the PMMA which is grafted onto the CNT surface, the polymer chains first have to be cleaved. Cleavage was achieved by adapting procedures as described by Salami-Kalajahi *et al.*[6] and Rahimi-Razin *et al*;.[7] during which CNT-PMMA was dispersed in 40 mL THF and allowed to stir for 3 hours in a 100 mL round bottom flask equipped with magnetic stirrer and condenser. Thirty millilitres of a 1 M KOH/ethanol solution was then added to the flask, after which the contents were refluxed at 80 °C for 72 hours. A Büchner filter was then used to filter off the CNTs before dissolving the cleaved polymer chains in THF. The cleaved polymer was precipitated in an excess cold methanol prior to drying overnight under vacuum at room temperature.

3.6 Synthesis of CNTs decorated with magnetic nanoparticles

In this study, magnetic CNTs were synthesized by decorating CNTs with magnetic nanoparticles using an *ex-situ* and *in-situ* approach. In the *ex-situ* approach magnetic nanoparticles are synthesized separately and only then attached to the CNT surface, while the latter is a simpler single-step method which entails the synthesis of magnetic nanoparticles directly onto the CNT surface. Two different *in-situ* approaches were attempted, while the *ex-situ* approach was only carried out in one manner. In order for covalent attachments to take place, oxidized CNTs (and thus CNTs with carboxylic acid moieties present on the surface - refer to section 3.5.1), were utilized. In some instances the use of PMMA grafted CNTs was also investigated (refer to table A.1 in appendix A).

3.6.1 *Ex-situ* approach (synthesis of *ex-situ* MWCNT-Fe_3O_4)

In the *ex-situ* approach, oleic acid capped iron oxide (Fe_3O_4) nanoparticles were synthesized separately before being covalently attached to the CNT surface. The covalent attachment was governed by the reaction of chemical functionalities present on the oxidized CNT surface with the capping agent functionalities on the Fe_3O_4 surface. Synthesis procedures adapted from work by Georgakilas *et al.*[8] were followed, and can be explained in two steps:

(a) Synthesis of oleic acid capped Fe_3O_4 nanoparticles

A 250 mL round bottom flask equipped with a magnetic stirrer was filled with 2 g of $(NH_4)_2Fe(SO_4)_2$ and 50 mL distilled water. Added to the contents already in the round bottom flask were 1.14 g KOH dissolved in 20 mL distilled water, 0.38 g $(NH_4)_2S_2O_8$ in 10 mL distilled water and 1.5 mL oleic acid in 30 mL toluene. The contents were then stirred at 80 °C for 30 minutes; after which the organic phase was separated by means of a separating funnel. Oleic acid capped Fe_3O_4 nanoparticles were obtained by precipitating the organic phase in cold ethanol and removing the ethanol under direct vacuum in a Schlenk tube.

(b) Covalent attachment of nanoparticles on CNT surface

Oleic acid capped Fe_3O_4 nanoparticles (4 mg) were dispersed in 5 mL chloroform and added to a 100 mL round bottom flask containing a magnetic stirrer. Oxidized MWCNTs (2 mg) dispersed in 50 mL chloroform/ethanol (1:1) were then added to the flask and the contents were stirred for two days at room temperature. The solid was separated by means of centrifugation and then washed three times with acetone; where separation after washing was also achieved by means of centrifugation.

3.6.2 *In-situ* approach 1 (synthesis of *in-situ* MWCNT-$CoFe_2O_4$)

In the first *in-situ* approach, MWCNTs were decorated with iron/cobalt oxide ($CoFe_2O_4$) nanoparticles by the *in-situ* precipitation of aqueous iron/cobalt ion complexes onto MWCNTs. The procedure set out by Galland *et al.*[9] was adapted; and the synthesis path followed can be outlined in three steps:

(a) Mixing of metal-salts and MWCNTs

Oxidized MWCNTs (125 mg) were dispersed in 41.67 mL distilled water and added to a 100 mL round bottom flask containing a magnetic stirrer. $CoCl_2.6H_2O$ (447.05 mg) and $FeSO_4.7H_2O$ (894.10 mg) were then added to the dispersion and the contents of the flask were stirred under high-shear mixing (250 RPM) for 30 minutes at 90 °C.

(b) Mixing of alkaline medium

A 100 mL round bottom flask containing a magnetic stirrer and a dispersion of 1.44 g NaOH and 5.48 g KNO_3 in 13.89 mL distilled water was stirred under high-shear mixing (250 RPM) for 30 minutes at 90 °C.

(c) Rapid addition of the alkaline medium to the metal salt solution

The alkaline medium was rapidly (in three seconds) added to the round bottom flask containing the metal-salt solution. The contents of the flask were then stirred under high-shear mixing (500 RPM) for 6 hours at 90 °C. The product was rinsed and cleaned at least four times with distilled water by means of centrifugation and placed in an oven (heated to 50 °C) to dry overnight.

3.6.3 *In-situ* approach 2 (synthesis of *in-situ* MWCNT-Fe_3O_4)

In the second *in-situ* approach MWCNTs were decorated with Fe_3O_4 nanoparticles by loading the MWCNT-COOH surface with a coordinating metal precursor ($FeCl_3$) capable of hydrolysis. The synthesis method was followed as published by He *et al.*;[10] and can also be summarized in three steps:

(a) Mixing of alkaline medium

NaOH (100 mg) dissolved in 10 mL DEG was placed in a 100 mL round bottom flask equipped with a magnetic stirrer. The mixture was allowed to stir under nitrogen atmosphere at 120 °C for 1 hour; after which it was cooled and maintained at 70 °C for later use.

(b) Mixing of metal precursor and MWCNTs

MWCNT-COOH (30 mg) was dispersed in 10 mL DEG and the mixture was ultrasonicated (20 kHz) for 1 minute. The mixture was then placed in a 100mL 2-neck round bottom flask equipped with a magnetic stirrer and condenser. $FeCl_3$ (126 mg) was then added to the flask under nitrogen atmosphere, after which the contents of the flask was kept at 220 °C by means of an oil bath for 30 minutes.

(c) Rapid addition of alkaline medium to the metal precursor solution

Five millilitres of the alkaline medium was instantaneously injected to the round bottom flask containing the rapidly stirring metal precursor solution. The resultant contents were then stirred for 1 hour at 220 °C. The product was cooled to room temperature, redispersed (three times) in ethanol and separated by means of centrifugation in order to rinse it. Afterwards the same rinsing procedure was followed using distilled water. The washed product was then dried in an oven (heated to 60 °C) overnight.

The three approaches were analysed as set out in section 4, and different combinations and ratios were used in an attempt to optimize the end-product. The numerous reactions carried out are noted in table A.1 in appendix A. Ultimately the reactions resulting in the best products were identified for further use as reinforcing nanomaterial in electrospun composite nanofibres (refer to section 3.7 below).

3.7 Electrospinning

The electrospinning set-up was done as set out in an article by Khanlou *et al.*;[11] where the set-up is also depicted in the historical and theoretical background section in part 2.4.1. A picture of the actual in-house-built electrospinning set-up can be seen in figure 3.2. The apparatus used in the electrospinning set-up was a variable high voltage supply capable of a voltage of up to 50 kV and a Kent Scientific (Genie Plus) syringe pump. Humidity was controlled at 30-40 %.

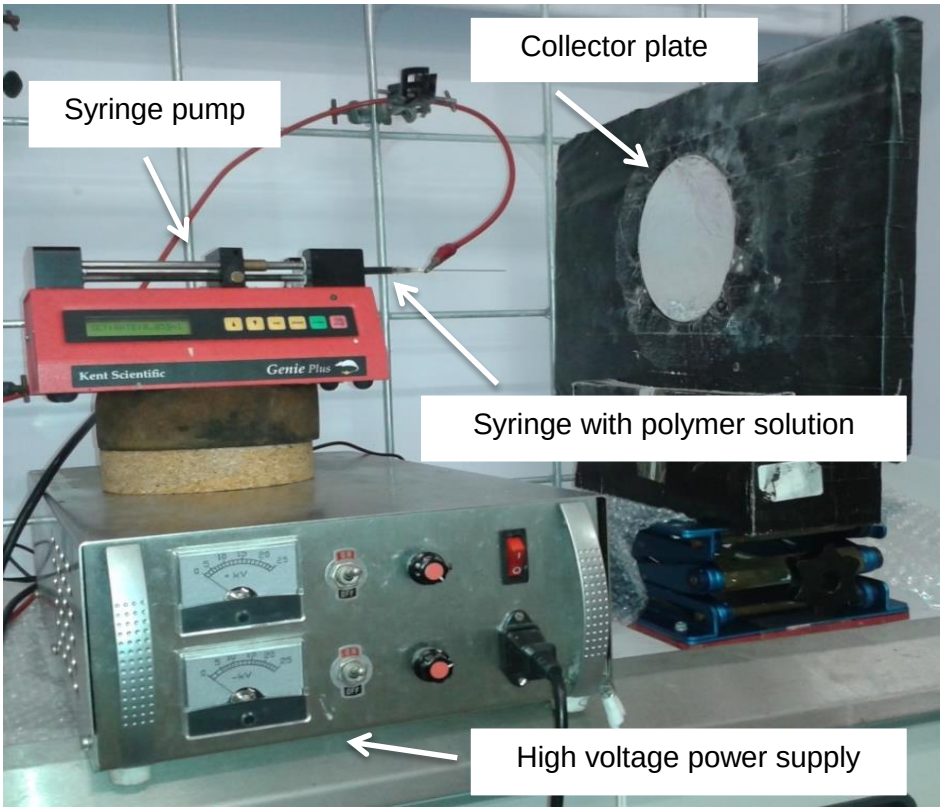

Figure 3.2: *In-house-built electrospinning set-up.*

The optimal electrospinning parameters were found to be 15 wt. % PMMA with an applied voltage of 15 kV, a distance between the capillary and target of 15 cm as well as a flow rate of 0.039 mL/min. Needles used had a blunt tip and an outside diameter of 0.90 mm and a length of 70 mm, with a gauge of 20. The amounts of CNTs as well as the type of CNTs (MWCNT-COOH, magnetic CNT-COOH, MWCNT-PMMA, magnetic CNT-PMMA, *ex-situ* MWCNT-Fe_3O_4, *in-situ* MWCNT-$CoFe_2O_4$ and *in-situ* MWCNT-Fe_3O_4) were varied; where 0.5 wt. %, 1.5 wt. % and 3.0 wt. % of every type of CNTs were added to the polymer solution. Polymer solutions were prepared at room temperature and stirred by means of a magnetic stirrer until the polymer had completely dissolved. Polymer solutions were then sonicated for 20 minutes prior to electrospinning.

The concentration of the polymer was varied depending on the amount of CNTs incorporated in order for the viscosity of the polymer solution to remain spinnable, because the viscosity increases as the concentration of incorporated CNTs increase (more on the effect of CNT on the solution viscosity in section 2.4.4). Ratios were adjusted according to an article by Bayley *et al.*[3] Adjustments resulted in 15 wt. % PMMA being used in the presence of 0.5 wt. % CNTs, 14 wt. % PMMA being used in the presence of 1.5 wt. % CNTs, and 12.75 wt. % PMMA being used in the presence of 3.0 wt. % CNTs. In the case of PMMA grafted CNTs the weight of the

PMMA present was calculated by using TGA results and was also accounted for when making up the various polymer solutions. The following polymer solutions were thus made up for electrospinning:

Table 3.1: *Various polymer solution ratios for electrospinning.*

Polymer solution	wt. % CNT	wt. % PMMA
a	0.5 MWCNT-COOH	15
b	1.5 MWCNT-COOH	14
c	3.0 MWCNT-COOH	12.75
d	0.5 magnetic CNT-COOH	15
e	1.5 magnetic CNT-COOH	14
f	3.0 magnetic CNT-COOH	12.75
g	0.5 MWCNT-PMMA	15
h	1.5 MWCNT-PMMA	14
i	3.0 MWCNT-PMMA	12.75
j	0.5 magnetic CNT-PMMA	15
k	1.5 magnetic CNT-PMMA	14
l	3.0 magnetic CNT-PMMA	12.75
m	*ex-situ* 0.5 MWCNT-Fe_3O_4	15
n	*ex-situ* 1.5 MWCNT-Fe_3O_4	14
o	*ex-situ* 3.0 MWCNT-Fe_3O_4	12.75
p	*in-situ* 0.5 MWCNT-$CoFe_2O_4$	15
q	*in-situ* 1.5 MWCNT-$CoFe_2O_4$	14
r	*in-situ* 3.0 MWCNT-$CoFe_2O_4$	12.75
s	*in-situ* 0.5 MWCNT-Fe_3O_4	15
t	*in-situ* 1.5 MWCNT-Fe_3O_4	14
u	*in-situ* 3.0 MWCNT-Fe_3O_4	12.75

3.8 References

1. D. Mattia, G. Korneva, A. Sabur, G. Friedman and Y. Gogotsi, *Nanotechnology,* 2007, **18**, DOI: 10.1088/0957-4484/18/15/155305.

2. B. Haseeb, MSc Thesis, KTH Chemical Science and Engineering, 2011.

3. G. M. Bayley and P. E. Mallon, *Polymer,* 2012, **53**, 5523-5539.

4. H. Kong, C. Gao and D. Yan, *J. Am. Chem. Soc.,* 2004, **126**, 412-413.

5. H. Kong, C. Gao and D. Yan, *Macromolecules,* 2004, **37**, 4022-4030.

6. M. Salami-Kalajahi, V. Haddadi-Asl, F. Behboodi-Sadabad, S. Rahimi-Razin and H. Roghani-Mamaqani, *Polym. Compos.,* 2012, **33**, 215-224.

7. S. Rahimi-Razin, V. Haddadi-Asl, M. Salami-Kalajahi, F. Behboodi-Sadabad and H. Roghani-Mamaqani, *Int. J. Chem. Kinet.,* 2012, **44**, 555-569.

8. V. Georgakilas, V. Tzitzios, D. Gournis and D. Petridis, *Chem. Mater.,* 2005, **17**, 1613-1617.

9. S. Galland, R. L. Andersson, M. Salajková, V. Ström, R. T. Olsson and L. A. Berglund, *J. Mater. Chem. C,* 2013, **1**, 7963-7972.

10. H. He and C. Gao, *J. Nanomater.,* 2011, **2011**, DOI: 10.1155/2011/193510.

11. H. M. Khanlou, A. Sadollah, B. C. Ang, J. H. Kim, S. Talebian and A. Ghadimi, *Neural Comput. Appl.,* 2014, **25**, 767-777.

Chapter 4: Results and Discussion

4.1 Polymer synthesis

Poly(methyl methacrylate) (PMMA), used as the polymer matrix in this study, was synthesised using a conventional free-radical chain growth polymerization (FRP) technique with toluene as solvent and AIBN as initiator. During the polymerization the reaction mixture remained clear; however, an increase in the viscosity was observed. Upon precipitation a white polymer was obtained. The reaction scheme is presented in scheme 4.1, where the consequent addition of methyl methacrylate (MMA) monomer units result in the formation of a PMMA polymer chain consisting out of *n* monomer units.

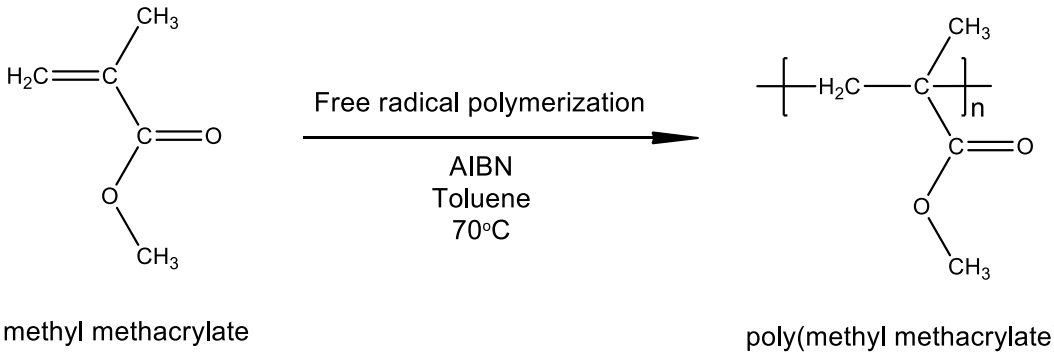

methyl methacrylate

poly(methyl methacrylate)

Scheme 4.1: *Synthesis of PMMA by means of FRP.*

The monomer was distilled before use and ^{1}H-NMR, using deuterated chloroform ($CDCl_3$) as solvent, was used to confirm that pure MMA was obtained. ^{1}H-NMR with $CDCl_3$ as solvent was also used to confirm the synthesis of the PMMA homopolymer. NMR results with allocated peaks can be seen in figure 4.1 and 4.2.

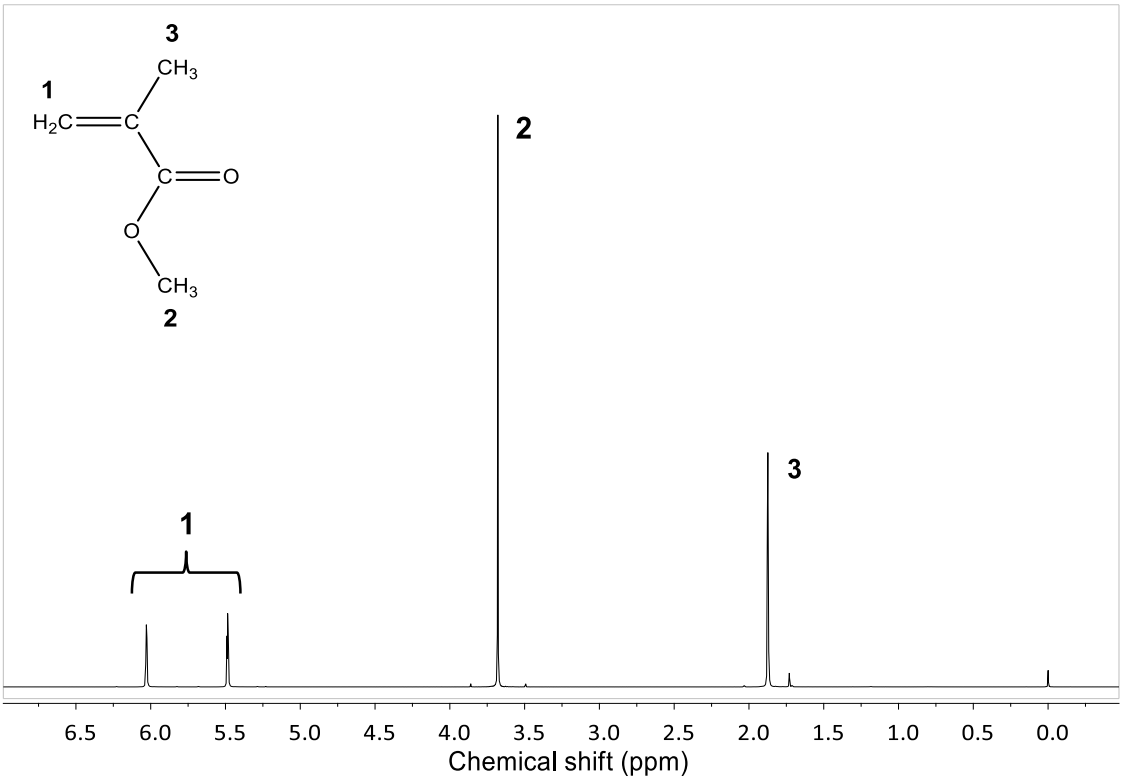

Figure 4.1: *^{1}H-NMR spectrum obtained for pure MMA.*

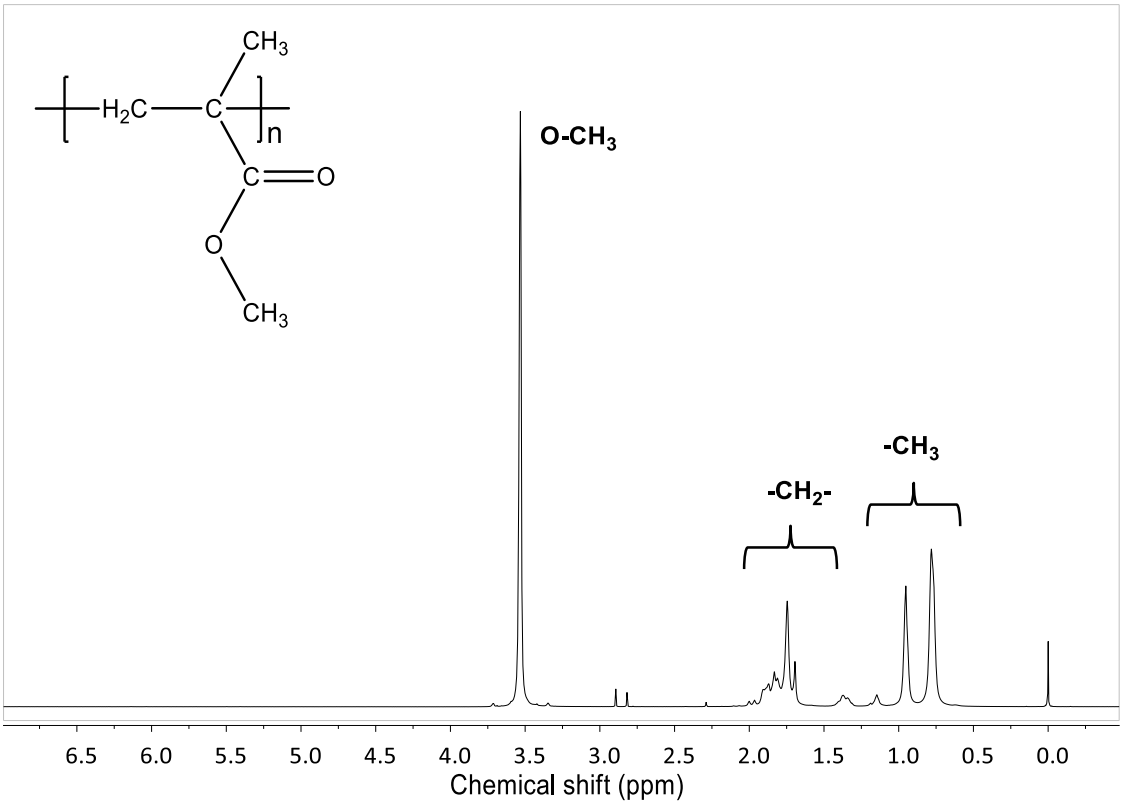

Figure 4.2: *^{1}H-NMR spectrum obtained for PMMA homopolymer.*

As explained in chapter 2; the molar mass (M_n in g.mol^{-1}) of the polymer used has to be adequately high in order to reach a polymer solution viscosity suitable for electrospinning.[1] SEC with a DMAC mobile phase was used to analyse the M_n of PMMA, which was found to be a sufficiently high value for electrospinning at 10.28x10^4 g.mol^{-1}. A dispersity (Đ) of 1.55 was achieved, which is a narrow value considering a conventional FRP technique was used.[2]

4.2 Carbon nanotube (CNT) functionalization

As mentioned in chapter 2, electrospinning is an uncomplicated yet versatile method in which nanofibres can be produced.[1,3-7] With the addition of nanoscale reinforcing/filler materials, the properties of these nanofibres can be enhanced.[8-10] By the addition of MWCNTs and magnetic CNTs specifically; nanofibres with increased mechanical, electrical, thermal and magnetic properties will be produced.[10-16] In this study electrospun nanofibres constitutes the polymer matrix, with the addition of MWCNTs and magnetic CNTs as reinforcing nanomaterials in order to produce PCNs.

It is, however, very crucial for CNTs to disperse uniformly and individually in a solution or matrix in order to ensure efficient utilization. In the pristine form, CNTs tend to agglomerate and form bundles due to the Van der Waals forces present (as elaborated on in section 2.2). Uniform dispersion can be obtained by surface functionalization of the CNTs, where functionalization allows interactions between the matrix or solution and CNTs to increase.[17,18] In this study, covalent functionalization of the various CNT surfaces was achieved by oxidation as well as grafting of polymer chains.

4.2.1 Oxidiation of CNTs

Surface functionalization by means of oxidation was carried out on the pristine MWCNTs and magnetic CNTs as explained in the experimental section. This results in carboxylic acid functionalities being introduced along the CNT surface. A wide variety of chemical reactions can be carried out with this functional group, making oxidation a very convenient and favourable functionalization method.[19,20]

TGA, under a nitrogen atmosphere, was used to confirm the presence of these carboxylic groups; where the weight percentage of carboxylic groups present is directly proportional to the percentage weight loss seen between the curves for before and after oxidation. This is due to the nature of CNTs, which allow them to remain stable and well intact without major physical damage up to high temperatures under nitrogen atmosphere.[21] At 600 °C the pristine MWCNTs were seen to retain

close to 100 % of its original weight (refer to figure 4.3 (a)), while a weight loss of 25 % was observed for the oxidized MWCNTs (refer to figure 4.3 (b)). This indicates that 25 wt. % carboxylic groups were present on the MWCNT surface after oxidation. When looking at the magnetic CNTs, the pristine magnetic CNTs were also seen to retain close to 100 % of its original weight at 600 °C (refer to figure 4.4 (a)), while a weight loss of 41 % was observed for the oxidized magnetic CNTs (refer to figure 4.4 (b)).

4.2.2 Grafting of PMMA from CNTs via *in-situ* ATRP

The increase in interactions between CNTs and the polymer solution can also be achieved by covalently grafting polymer chains (specifically the polymer used as polymer matrix) onto solid CNT surfaces, in order to form tethered polymer chains which are connected to the surface at one chain end. Before polymer chains can be grafted from the CNT surfaces via *in-situ* ATRP, multifunctional ATRP macro-initiator sites (bromide functional groups) first have to be formed. Depicted in scheme 4.2 steps 1-3 is the formation of the macro-initiator sites on the CNT surface by the reaction of oxidized CNTs (CNT-COOH) with $SOCl_2$, glycol and bromoisobutyryl bromide. These macro-initiator sites (CNT-Br) were subsequently used to graft PMMA from the CNTs via *in-situ* ATRP in order to form CNT-PMMA, as observed in step 4 of scheme 4.2. Controlled/living free-radical polymerization (CRP) such as ATRP allows one to target a specific polymer chain M_n.[22,23] It is, however, hard to determine the initiator efficiency and the amount of initiating sites (CNT-Br) present on the surface when grafting onto solid surfaces. This makes M_n targeting a challenging task under such circumstances. For this reason, a certain polymer weight percentage which can be associated with an average thickness of enwrapped grafted polymer layer (as reported by Kong *et al.*[24]) was rather attempted in the current study. Specifically a weight percentage of 30 % PMMA, which can be associated with an average thickness of 3.8 nm enwrapped PMMA layer, was attempted.

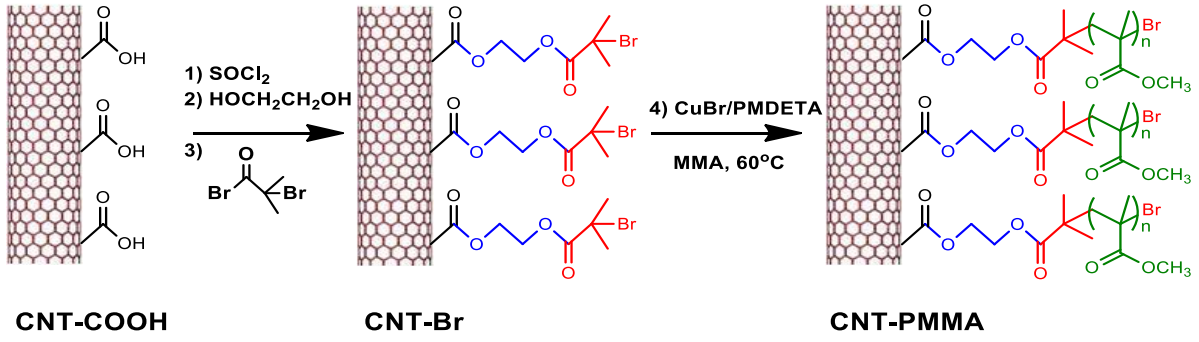

Scheme 4.2: *Schematic representation of the steps that make up the grafting process.*[24]

In order to obtain the weight percentage of PMMA present on the CNT surface, the percentage weight loss between the oxidized CNT (CNT-COOH) and PMMA grafted CNT (CNT-PMMA) curves have to be noted. This is due to the carboxylic groups present along the oxidized CNT surface being used as anchoring sites by other functionalities (in this case PMMA) during grafting via *in-situ* ATRP; as depicted in scheme 4.2 above. At 600 °C, a weight loss of 58 % was observed for the PMMA grafted MWCNTs. This correlates to a weight percentage of 33 % PMMA present on the MWCNT surface (refer to figure 4.3 (c)). When looking at the magnetic CNT a weight loss of 53 % was observed for the PMMA grafted magnetic CNTs at 600 °C, which correlates to a weight percentage of 12 % PMMA present on the CNT surface (refer to figure 4.4 (c)). Table 4.1 displays a summary of the weight percentage results obtained with TGA for the various functionalized CNTs.

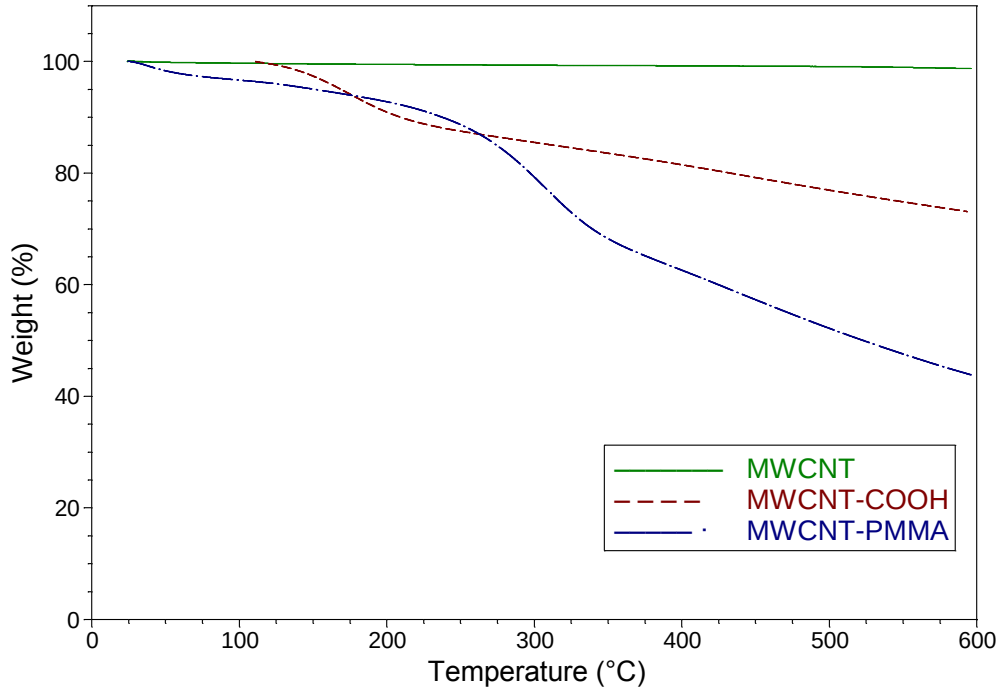

Figure 4.3: *TGA curves of (a) pristine MWCNTs (MWCNT), (b) oxidized MWCNTs (MWCNT-COOH) and (c) PMMA grafted MWCNTs (MWCNT-PMMA) under nitrogen atmosphere.*

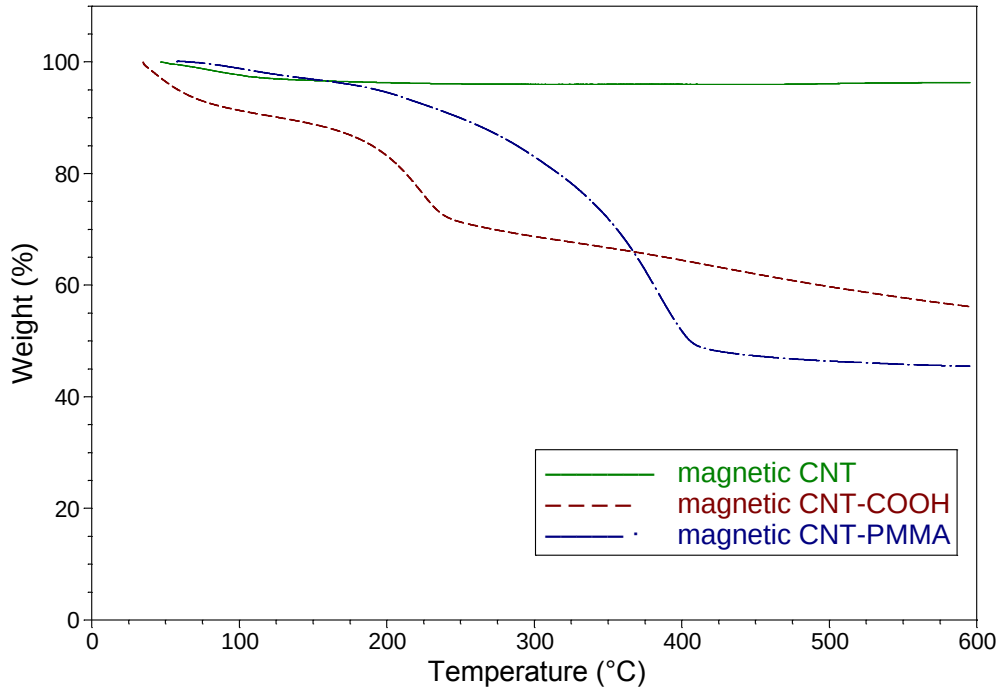

Figure 4.4: *TGA curves of (a) pristine magnetic CNTs (magnetic CNT), (b) oxidized magnetic CNTs (magnetic CNT-COOH) and (c) PMMA grafted magnetic CNTs (magnetic CNT-PMMA) under nitrogen atmosphere.*

Table 4.1: *Summary of weight percentage results obtained at 600 ℃ with TGA for oxidized and PMMA grafted CNTs.*

	MWCNTs	**Magnetic CNTs**
Retained wt. % for pristine CNTs	100 wt. %	100 wt. %
Retained wt. % for oxidized CNTs	75 wt. %	59 wt. %
wt. % Carboxylic acid moieties present (retained wt. % for pristine CNTs - retained wt. % for oxidized CNTs)	100 wt. % - 75 wt. % = 25 wt. %	100 wt. % - 59 wt. % = 41 wt. %
Retained wt. % for PMMA grafted CNTs	42 wt. %	47 wt. %
wt. % PMMA moieties present (retained wt. % for oxidized CNTs - retained wt. % for PMMA grafted CNTs)	75 wt. % - 42 wt. % = 33 wt. %	59 wt. % - 47 wt. % = 12 wt. %

Further proof of successful PMMA grafting was achieved using ATR-FTIR and TEM, while information regarding the grafted PMMA polymer chains was obtained by cleaving the polymer chains from the CNT backbone:

4.2.2.1 ATR-FTIR

CNTs are very difficult to analyse with ATR-FTIR due to their nature which leads to the absorption of too many frequencies of infrared radiation. This causes a pattern with excessive noise, which makes spectrum interpretation impossible. Regardless of the poor quality of the spectrums obtained, ATR-FTIR may still be efficient for use when only a change in one specific peak needs to be observed. For the pristine MWCNT and magnetic CNT samples the absorption signal of the carbonyl bond at around 1730 cm^{-1} could not be observed, while in the case of the PMMA grafted MWCNTs and magnetic CNTs a strong signal for the carbonyl bond was found (refer to figure 4.5).[24] Samples were washed repeatedly in order to remove any excess ungrafted PMMA before ATR-FTIR analysis; and the presence of the grafted PMMA was thus again confirmed in both cases.

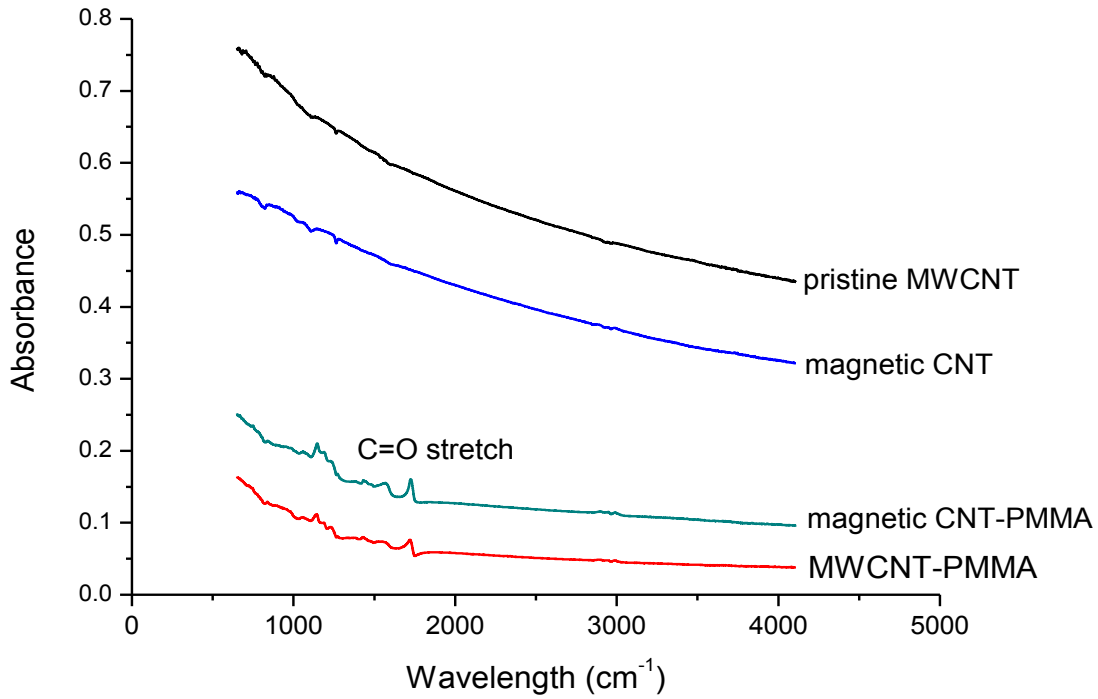

Figure 4.5: *ATR-FTIR spectrum of PMMA grafted CNTs as proved by the C=O (carbonyl) stretch.*

4.2.2.2 TEM

Figure 4.6 shows the TEM images of unfunctionalized (*a* and *c*) and PMMA grafted (*b* and *d*) CNTs. An indication of a layer of PMMA grafted onto the CNT surface was observed in the TEM images of PMMA grafted CNTs, which confirmed that successful surface modification by means of grafting of PMMA from the CNT backbone was accomplished. When looking at the PMMA grafted MWCNTs (refer to figure 4.6 (b)) and PMMA grafted magnetic CNTs (refer to figure 4.6 (d)), an average thickness of 4 nm enwrapped PMMA polymer was observed for both samples.

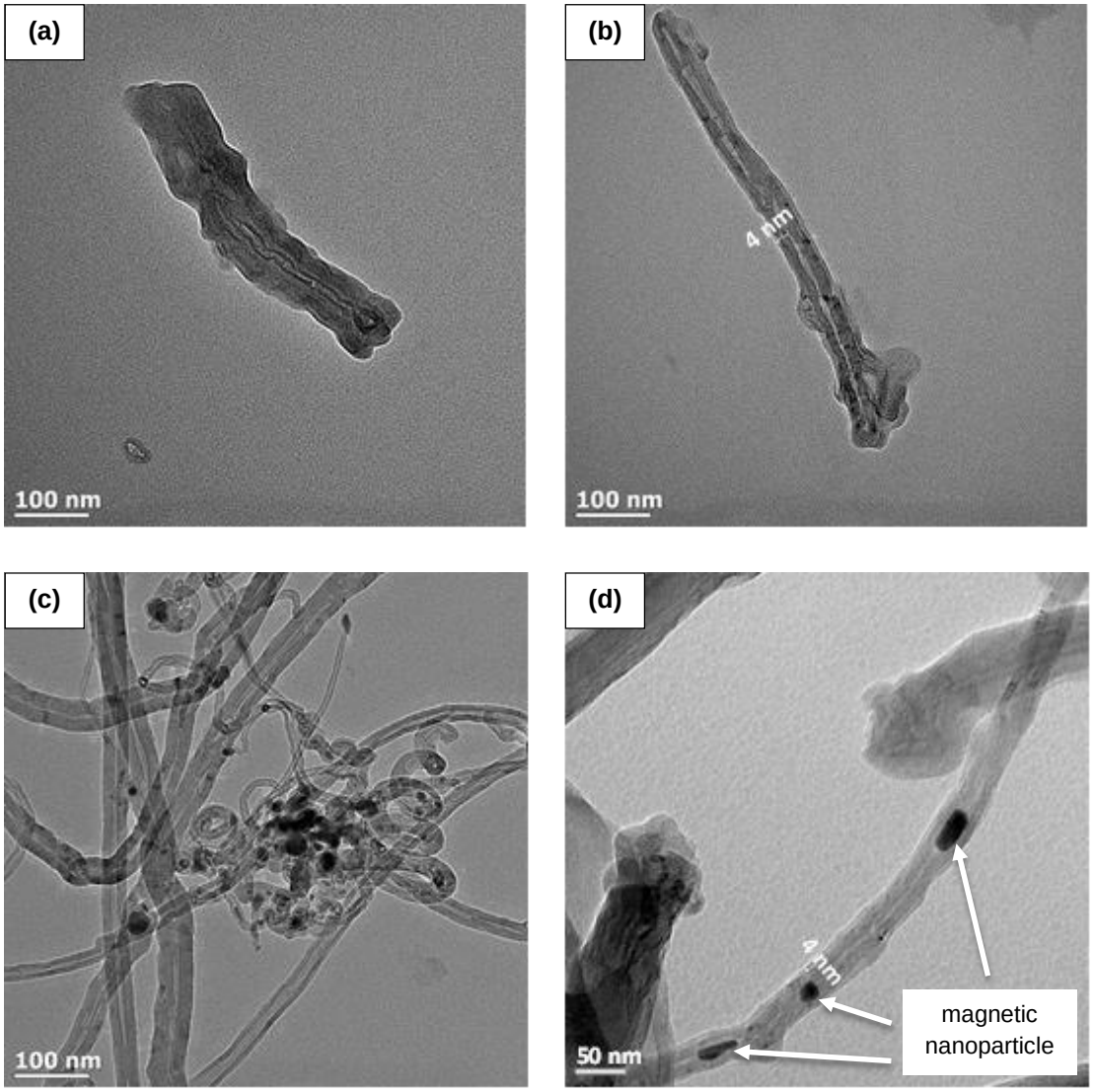

Figure 4.6: *TEM images of (a) pristine MWCNT, (b) MWCNT-PMMA, (c) magnetic CNT and (d) magnetic CNT-PMMA for grafted PMMA thickness observation.*

4.2.2.3 Cleavage

As previously mentioned, it is difficult to accurately control the graft chain length due to the difficulty of determining the initiator efficiency and amount of initiating sites present on the CNT surface. In order to investigate the length of the grafted polymer chains, the chains were cleaved off the CNT surface using a strong base (KOH) and ethanol. During cleavage the ester linkages present between PMMA polymer chains and their surface grafted CNT backbones are hydrolized, resulting in the removal of the polymer chains from the CNT backbone. The polymer chains were then investigated by SEC in order to obtain values for the M_n and Đ achieved, while ^{1}H NMR was used to confirm that PMMA was in fact successfully cleaved. For the PMMA cleaved from the MWCNT-PMMA, a M_n of 2361 g.mol^{-1} and Đ of 1.02 were achieved. For the PMMA cleaved from the magnetic CNT-PMMA surface, on the other hand, a M_n of 2193 g.mol^{-1} and Đ of 1.13 were achieved. Narrow M_n distributions were confirmed by the Đ values obtained; where these values fall well within the range expected for ATRP ($1.00 < Đ < 1.50$).[22,23]

Successful grafting of PMMA from the CNTs via *in-situ* ATRP was thus confirmed using TGA, ATR-FTIR, TEM and cleavage. TGA and TEM data of the PMMA grafted MWCNTs showed a weight percentage of 33 % PMMA and an average thickness of 4 nm enwrapped grafted polymer layer, which correlate well to the attempted values. For the PMMA grafted magnetic CNTs an average thickness of 4 nm enwrapped grafted polymer layer was also observed, however, a weight percentage of only 12 % PMMA was found to be present. In figure 4.6 (c) it can be noticed that the magnetic CNTs are fundamentally fused and also vary substantially in size and regularity. This is recognized as the reason for the wt. % grafted PMMA being much less when compared to MWCNTs, where the entire surface of the magnetic CNTs cannot be accessed for grafting due to the clumping and knotting of the CNTs.

4.2.3 Dispersion tests

In figure 4.7 the dispersion test observations obtained for both the oxidized and PMMA grafted CNTs are presented. For these tests 3 mg of sample was dispersed in 1 mL of solvent (DMF) (or 1.5 mg sample in 0.5 mL solvent where the amount of sample available was limited). The mixture was sonicated for 20 minutes prior to dispersion observations at room temperature. The tests indicated that the oxidation of the CNTs improved interactions between the CNTs and polar solvents (such as DMF) significantly, since CNTs which are well dispersed in the solvent were observed (refer to columns *b* and *e* as opposed to *a* and *d*). The interactions were also greatly enhanced where CNTs were grafted with PMMA (refer to columns *c* and *f*). In columns *c* and *f* it was, however, observed that the interaction with the solvent decreased as time progressed. This

was noticed where CNTs grafted with PMMA started to accumulate at the bottom of the vial as time increased. In figure 4.8 it can be observed that the interaction of the respective oxidized CNTs with the solvent was stable even after one month.

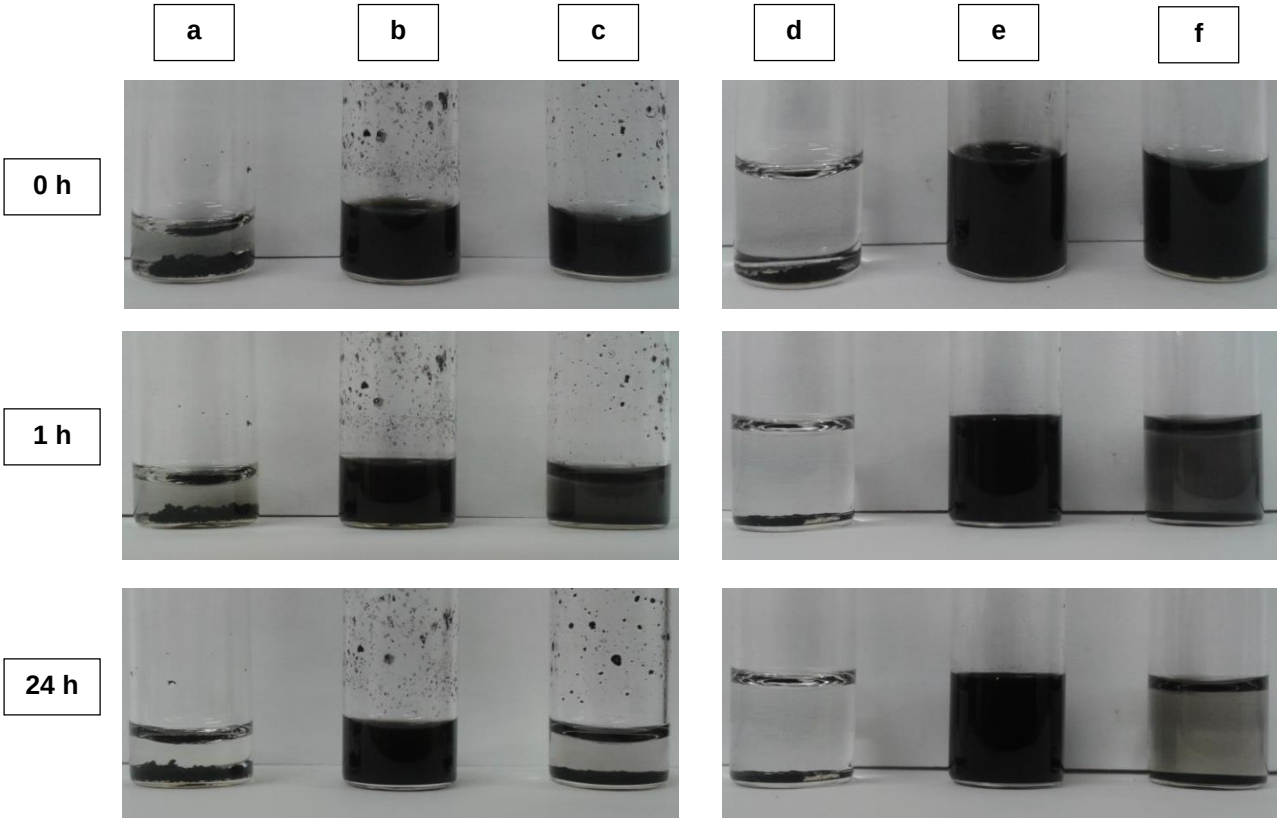

Figure 4.7: *Dispersion test observations, in DMF after 20 minutes of sonication, of (a) pristine MWCNTs, (b) MWCNT-COOH, (c) MWCNT-PMMA, (d) magnetic CNTs, (e) magnetic CNT-COOH and (f) magnetic CNT-PMMA.*

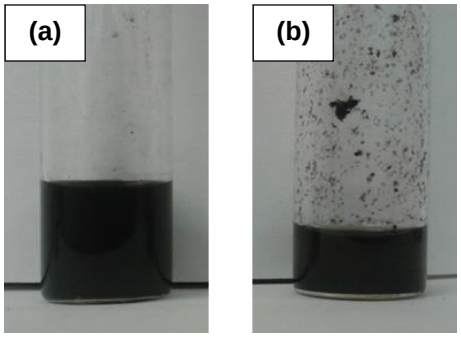

Figure 4.8: *Dispersion test observations, in DMF after 20 minutes of sonication and standing for one month, of (a) MWCNT-COOH and (b) magnetic CNT-COOH.*

Good dispersion can be attributed to the polar groups arising on the CNT surface due to oxidation and grafting of PMMA, thus rendering the functionalized CNTs more polar, which fascilitates dissolution in polar solvents. For electrospinning, interactions between the solvent molecules and the carboxylic acid moieties (as present for oxidized CNTs) or PMMA moieties (as present for PMMA surface functionalized CNTs) were replaced with interactions between the functional groups of the PMMA homopolymer used as matrix and carboxylic acid or PMMA moieties. This interaction allowed for good dispersion of the various CNTs in the PMMA polymer matrix.

It should be noted that the dispersion test observations were only carried out in DMF and not in the actual electrospinning solutions containing PMMA homopolymer. When the electrospinning solutions were made-up, dispersion stability results of samples containing PMMA grafted CNTs were comparable to that of samples containing oxidized CNTs. This is due to the presence of strong interactions between the PMMA homopolymer and the moieties present on the CNT surface.

4.3 Synthesis of CNTs decorated with magnetic nanoparticles

As a comparison to the magnetic CNTs (which are CNTs with magnetic nanoparticles embedded in the walls), the synthesis of CNTs decorated with magnetic nanoparticles on the outside was attempted.[25]

Oxidized MWCNTs were used in the decoration of MWCNTs with magnetic nanoparticles, where carboxylic acid moieties on the MWCNT backbone act as anchoring sites through which chemical functionalities can be attached.[20] Oxidation was performed in the same way as explained in section 4.2.1 above. In the 1st approach, separately prepared magnetic nanoparticles and CNTs were mixed, leading to CNTs with covalently attached magnetic nanoparticles (synthesis of *ex-situ* MWCNT-Fe_3O_4). In an attempt to simplify the synthesis a single-step method was also investigated – the 2nd and 3rd approach involved the *in-situ* precipitation of magnetic nanoparticles on the CNT surface (synthesis of *in-situ* MWCNT-$CoFe_2O_4$ and *in-situ* MWCNT-Fe_3O_4).

4.3.1 *Ex-situ* approach (synthesis of *ex-situ* MWCNT-Fe_3O_4)

The *ex-situ* approach for the synthesis of CNTs decorated with magnetic nanoparticles included two steps: (a) the synthesis of oleic acid capped iron oxide (Fe_3O_4) nanoparticles and (b) the covalent attachment of these nanoparticles to the CNT surface. The oleic acid capped Fe_3O_4 nanoparticle structure is presented in figure 4.9; where only one oleic acid molecule is shown on the Fe_3O_4 nanoparticle surface for clarity. Covalent attachment of the Fe_3O_4 nanoparticles to the

CNT surface takes place by the reaction of the oleic acid capping functionalities on the Fe_3O_4 nanoparticle and the carboxylic acid functionalities on the oxidized CNT surface, in order to form ex-situ MWCNT-Fe_3O_4.

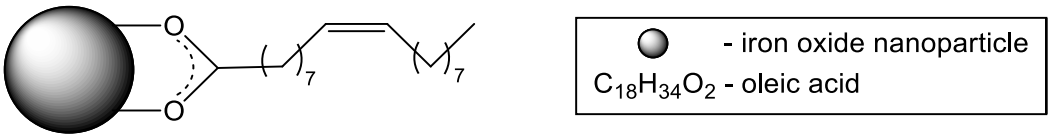

Figure 4.9: *Illustration of an oleic acid capped iron oxide nanoparticle.*[26,27]

(a) Oleic acid capped Fe_3O_4 nanoparticles

The magnetic character of the oleic acid capped Fe_3O_4 nanoparticles was confirmed using visual observations and a magnet. Upon the application of an external magnetic field by use of a magnet, an immediate response of the nanoparticles was observed. This is shown in figure 4.10 below.

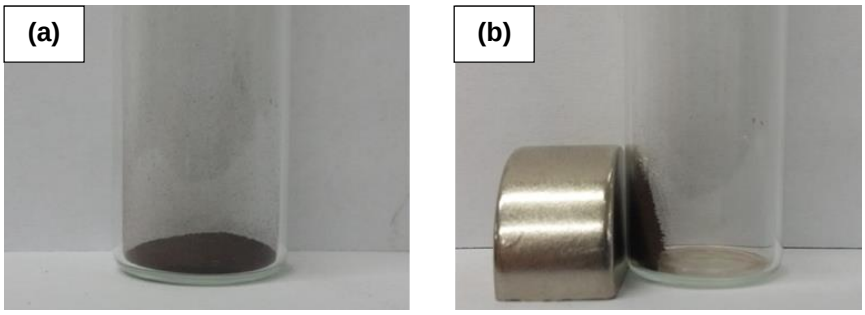

Figure 4.10: *Oleic acid capped Fe_3O_4 nanoparticles with (a) no magnet applied and (b) the application of an external magnetic field.*

The successful synthesis of oleic acid capped Fe_3O_4 nanoparticles (magnetic nanoparticles) was confirmed using ATR-FTIR and TEM. Figure 4.11 shows the ATR-FTIR results for the oleic acid capped Fe_3O_4 nanoparticles, which indicated a sp^3-hybridized C-H stretch signal at 2840-3000 cm^{-1} due to the long aliphatic chains of oleic acid. The signals observed at 1715-1740 cm^{-1} and 1050-1250 cm^{-1} were due to the C=O and C-O stretch of the carbonyl group of oleic acid. The carboxylate group, which forms when a carboxylic acid dissociates and coordinates to a metal atom surface, was indicated by the signal at 1400-1580 cm^{-1}.[27-29]

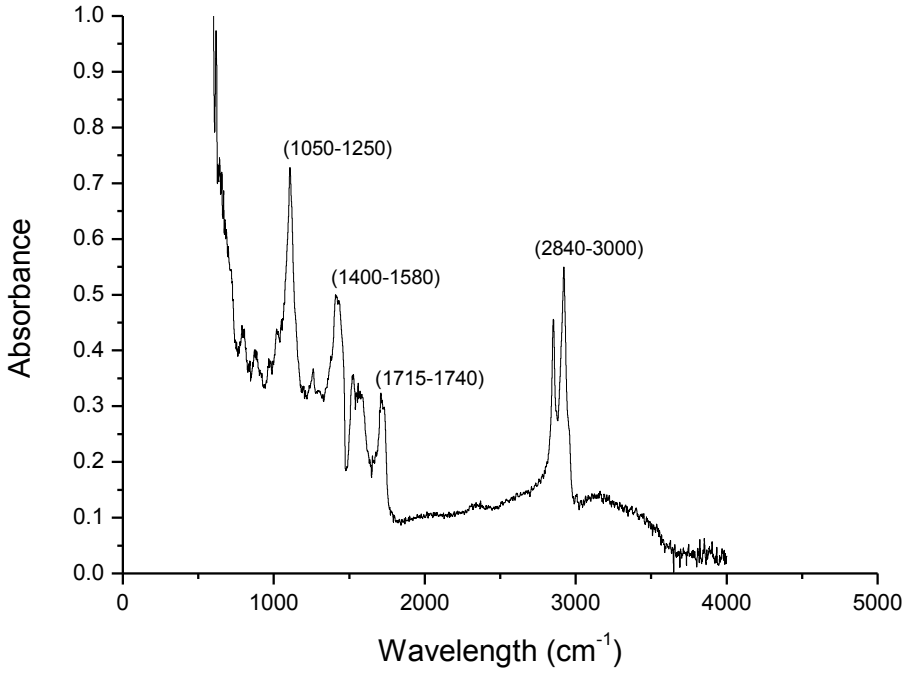

Figure 4.11: *ATR-FTIR spectrum of oleic acid capped magnetic Fe_3O_4 nanoparticles.*

Figure 4.12 displays the TEM images of the spherical oleic acid capped Fe_3O_4 nanoparticles with an average diameter of 14 nm and Đ of 1.82. The images were obtained by dispersion of the particles in ethanol, followed by sonication of the dispersion for 10 minutes prior to heating to 60 °C. A few drops of the dispersion were then dropped onto a TEM grid, where the grid was carbon coated to ensure the nanoscale sample does not 'fall through' the grid. Heating up of the dispersion ensured more rapid vaporization of the solvent (ethanol, b.p. = 78 °C) upon dropping. This was done in an attempt to minimize particle aggregation. Aggregation was significantly reduced in this manner, but could unfortunately still be observed in TEM images due to the high surface energies of the nanoparticles being minimized upon aggregation.[30] Unfortunately cryo-TEM was not available for this study, which would allow for the imaging of individual magnetic nanoparticles.

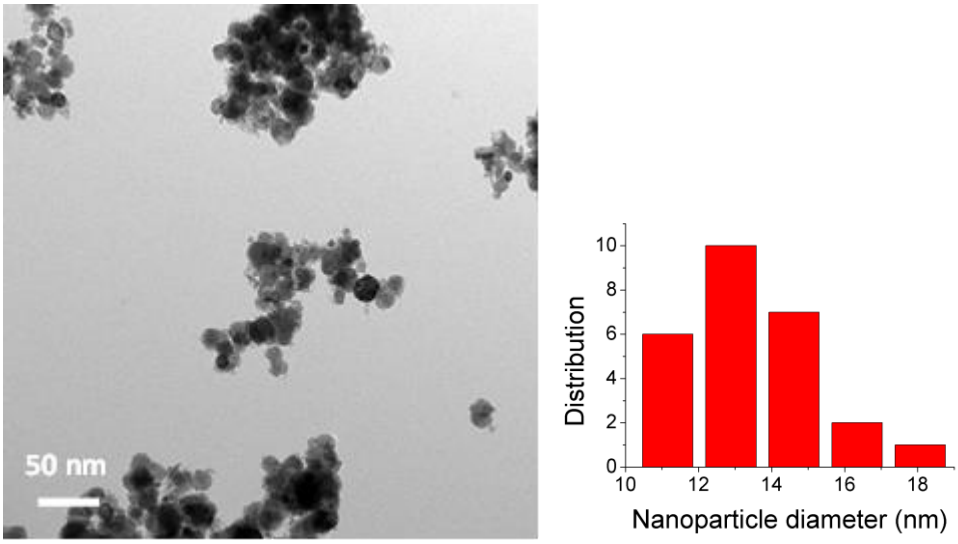

Figure 4.12: *TEM image of oleic acid capped magnetic Fe_3O_4 nanoparticles, with insert of size distribution values obtained.*

A Zetasizer Nano instrument was also used in an attempt to determine the average diameter of the nanoparticles. Attempts were, however, unsuccessful due to aggregation of the nanoparticles in the solution. This could readily be observed where particles dispersed in ethanol precipitated out as time passed. Results obtained indicated that as time increased with each consecutive run (each run is approximately 2.5 minutes apart), the average particle diameters as well as Đ values increased. These results, which are reported in table 4.2 below, thus confirmed that aggregation was apparent and becomes progressively worse over time.

Table 4.2: *Summary of average diameter and Đ results obtained for oleic acid capped magnetic nanoparticles in ethanol at 25 ℃ using a Zetasizer Nano instrument.*

	Average diameter (nm)	**Đ**
Run 1	766	0.23
Run 2	903	0.29
Run 3	1188	0.33
Run 4	1211	0.43

(b) Covalent attachment of nanoparticles on CNT surface

The oleic acid capped Fe_3O_4 nanoparticles were reacted with the oxidized MWCNTs in solution in order for the nanoparticles to covalently attach to the MWCNT surface and form *ex-situ* synthesized MWCNT-Fe_3O_4. The successful synthesis of *ex-situ* MWCNT-Fe_3O_4 was confirmed using visual observations and a magnet. The immediate response of the MWCNT-Fe_3O_4 toward an externally applied magnetic field by use of a magnet can be observed in figure 4.13 below. The magnetic sample was subjected to further tests for which results are reported below.

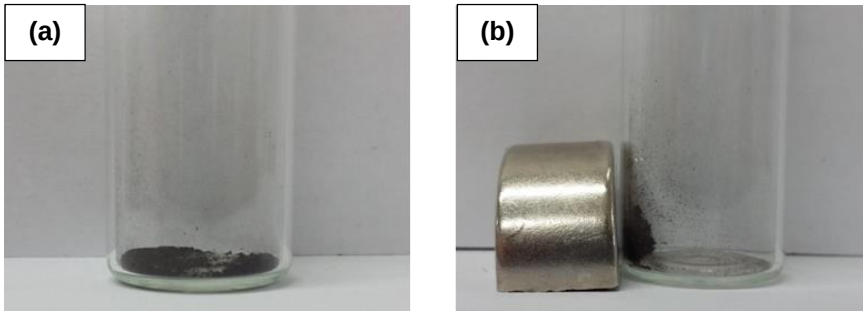

Figure 4.13: *Ex-situ synthesized MWCNT-Fe_3O_4 with (a) no magnet applied and (b) the application of an external magnetic field.*

In order to confirm the covalent attachment of the magnetic nanoparticles to the oxidized MWCNTs' surface was successful, TEM was used. Figure 4.14 (a-d) shows TEM images of the *ex-situ* MWCNT-Fe_3O_4, and it can clearly be seen that nanoparticles were attached to the MWCNT surface. Nanoparticles and MWCNTs with average diameters of 14 nm and 120 nm, respectively, were observed. Although some degree of aggregation of the magnetic Fe_3O_4 nanoparticles was observed, the nanoparticles are generally attached along the length of the MWCNTs.

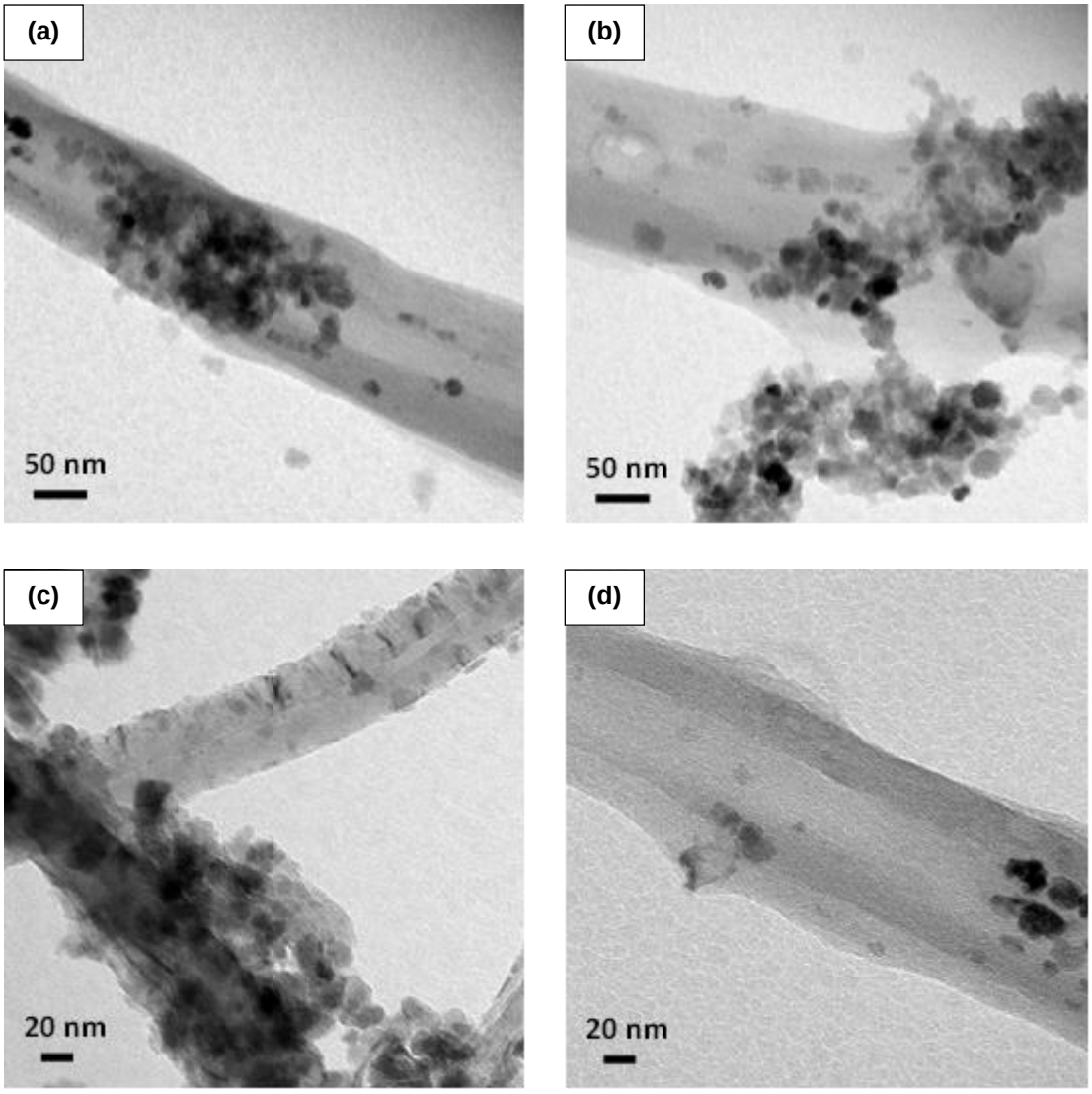

Figure 4.14: *TEM images (a) – (d) of MWCNTs decorated with magnetic nanoparticles in an ex-situ approach (ex-situ synthesized MWCNT-Fe_3O_4).*

The successful synthesis of the *ex-situ* MWCNT-Fe_3O_4 was analysed using TGA in order to determine the weight percentage of covalently attached oleic acid capped Fe_3O_4 nanoparticles. A conventional TGA cycle using nitrogen gas (as explained in the experimental section part 3.2) was implemented up to 600 °C, after which the program was set to keep the temperature constant at 600 °C under an oxygen atmosphere for 15 minutes. Figure 4.15 shows the TGA analysis of the oxidized MWCNTs (MWCNT-COOH), where a weight loss to zero at 600 °C was observed. This is due to the presence of oxygen at high temperatures resulting in the combustion of CNTs.[21]

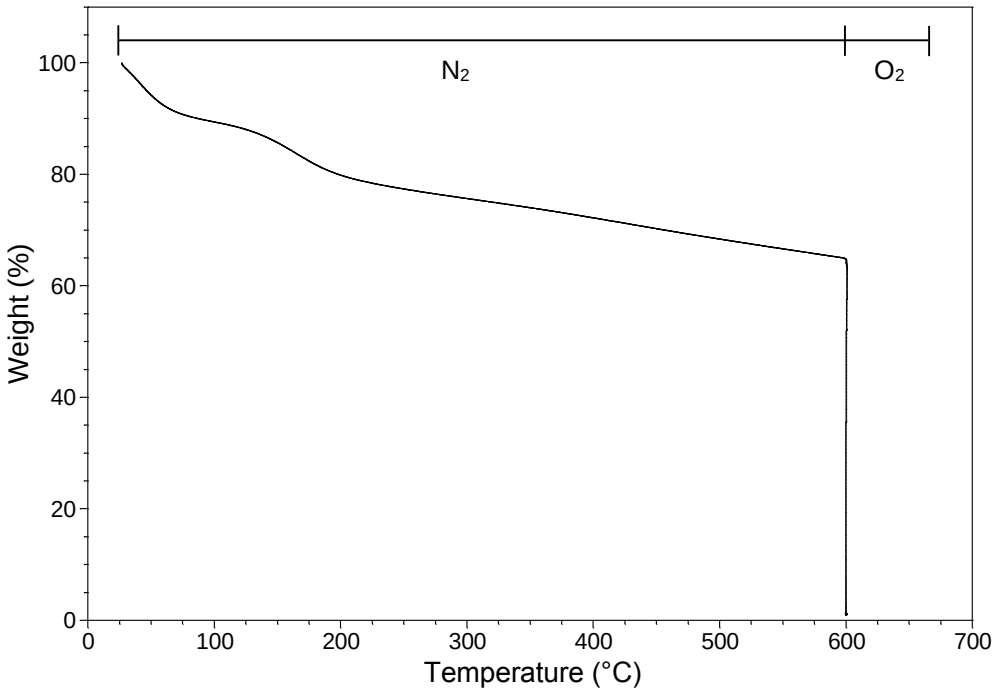

Figure 4.15: *TGA curve of oxidized MWCNTs (MWCNT-COOH) to zero after implementation of a nitrogen atmosphere followed by an oxygen atmosphere at 600 ℃.*

Figure 4.16 shows the TGA analysis of the *ex-situ* synthesized MWCNT-Fe_3O_4. When implementing an oxygen atmosphere at 600 °C for the MWCNT-Fe_3O_4, an isothermal weight loss was seen on the TGA curve. This can be attributed to the presence and degradation of the MWCNTs, and is thus a further indication that successful covalent functionalization of the MWCNTs took place. This could be concluded seeing as magnetic samples (as shown in figure 4.13) were used during TGA analysis which ensured that nanoparticles and MWCNTs were not simply mixed but were, in fact, attached to one another. An isothermal weight loss of 30 wt. % was noted for the MWCNTs. The weight loss observed before the isothermal cycle was implemented was as a result of oleic acid/carboxylic acid moieties. The residual iron nanoparticles remained stable, and the remaining weight percentage of 43 % can thus be ascribed to the nanoparticles.[31]

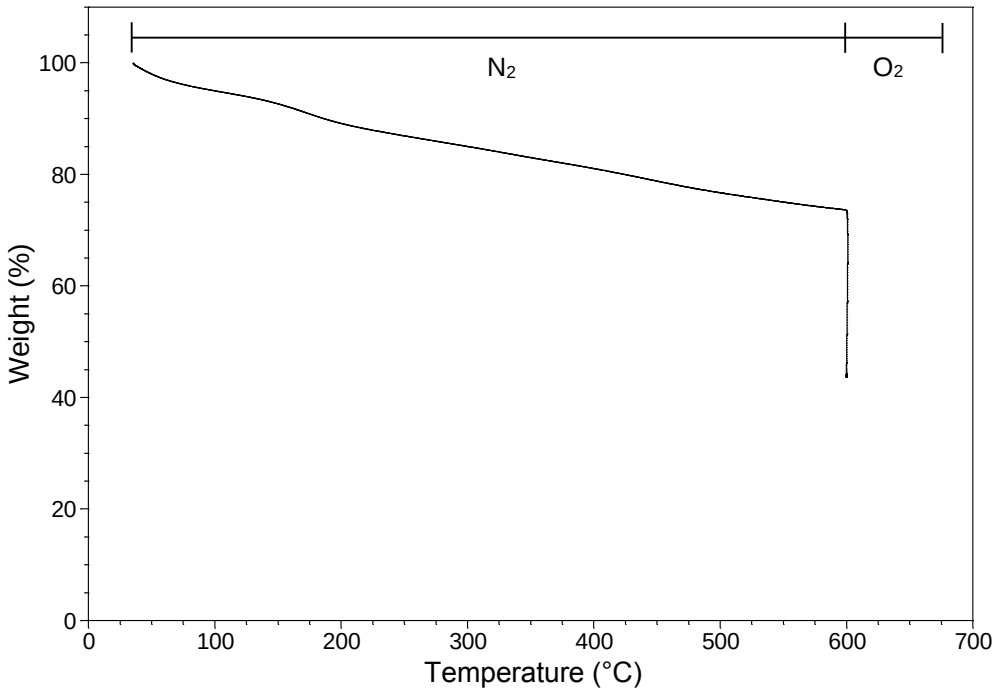

Figure 4.16: *TGA curve of ex-situ synthesized MWCNT-Fe_3O_4 under nitrogen atmosphere followed by the implementation of an oxygen atmosphere at 600 ℃.*

To characterize the presence of the Fe_3O_4 nanoparticles in the final composite material, XRD was used. Figure 4.17 shows the XRD analysis of the *ex-situ* synthesized MWCNT-Fe_3O_4 sample. The recorded pattern consisted of peaks characteristic of the Fe_3O_4 magnetic nanoparticles; where peaks were detected at 30, 35, 40-45, 53-58 and 63 degrees.[28] Significantly larger peaks were also observed at 10 and 20 degrees, which corresponds to the presence of MWCNTs.[31] These peaks were not included in the graph due to their large size leading to the insignificance of the smaller peaks observed for the Fe_3O_4 magnetic nanoparticles.

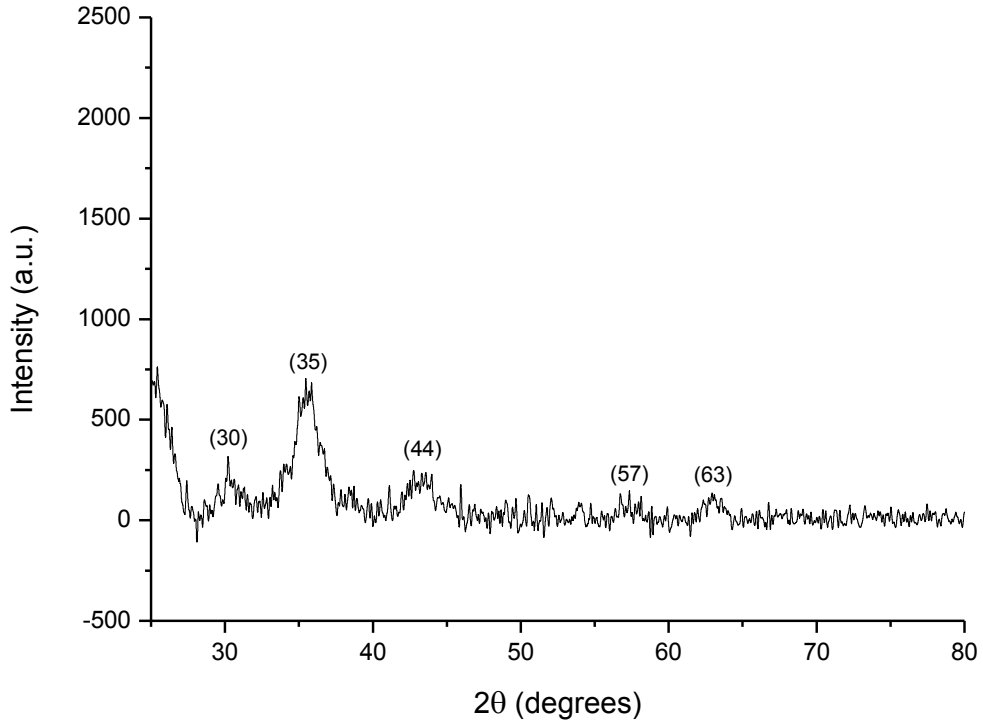

Figure 4.17: *XRD spectrum of ex-situ synthesized MWCNT-Fe_3O_4.*

ATR-FTIR was attempted in order to obtain greater clarity on the exact mechanism through which the magnetic nanoparticles covalently attached to the MWCNTs, in order to form MWCNT-Fe_3O_4. This was, unfortunately, unsuccessful due to the nature of MWCNTs; which leads to the absorption of too many frequencies of infrared radiation, causing a pattern with excessive noise. It is suggested by Georgakilas *et al.*[28] that the carboxylic acid moieties present on the MWCNT surface will link to the capped metal oxide nanoparticles through the oleic acid group present. On the contrary, Lamanna *et al.*[32] proposed that the decoration of MWCNTs with metal oxide nanoparticles takes place through the replacement of the oleic acid group (used as nanoparticle capping agent) with the carboxylic acid moieties present on the MWCNT surface. Further light could, however, not be shed on this topic due to the inconclusive ATR-FTIR results. However, regardless of the mechanism of attachment, it is clear that the magnetic nanoparticles were successfully attached to the MWCNT surface.

4.3.2 *In-situ* approach 1 (synthesis of *in-situ* MWCNT-$CoFe_2O_4$)

The *in-situ* decoration of iron/cobalt oxide ($CoFe_2O_4$) nanoparticles onto MWCNTs was carried out in an attempt to simplify the decoration process to a single step. By evasion of the conventional mixing step, the potential risk of nanoparticle agglomeration is avoided, and well distributed nanoparticles can be obtained. The process was based on a method by Galland *et al.*,[31] which entails the hydrolysis and precipitation of a metal precursor on the cellulose nanofibril surface, followed by the condensation of the precipitated precursors as magnetic $CoFe_2O_4$ nanoparticles. The precipitation and condensation of these $CoFe_2O_4$ nanoparticles were confined by the hydroxyl groups present on the nanofibril surface. By using MWCNT-COOH with carboxylic-rich surfaces (instead of cellulose nanofibrils) the same *in-situ* decoration is believed to be possible, and was attempted in this study. Visual observations using a magnet were used to display the magnetic characteristics of the product. The dried product was immediately attracted to an external magnetic field as observed in figure 4.18 below.

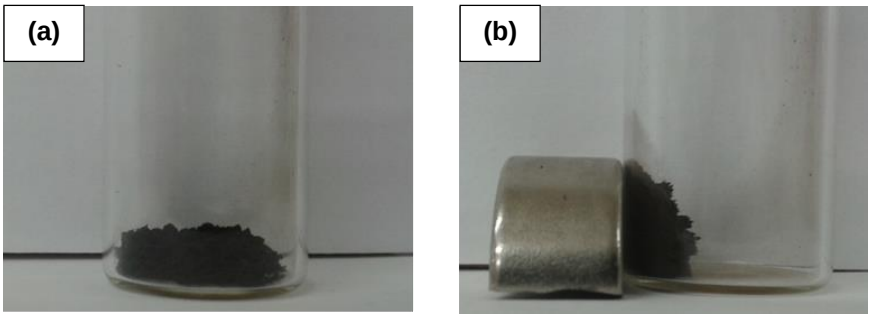

Figure 4.18: *In-situ synthesized MWCNT-$CoFe_2O_4$ with (a) no magnet applied and (b) the application of an external magnetic field.*

In order to confirm the *in-situ* decoration of the magnetic nanoparticles onto oxidized MWCNTs' surface was successful; the magnetic sample shown above (figure 4.18) was subjected to further testing using TEM, TGA and XRD. Figure 4.19 shows a TEM image of the MWCNT-$CoFe_2O_4$, which clearly indicates that nanoparticles are attached to the MWCNT surface. However, very large nanoparticles with an average diameter of 108 nm and Đ of 30.94 were observed. Similar large sized nanoparticles were also obtained by Galland *et al.*,[31] where these nanoparticles complimented the larger sized cellulose nanofibrils well.

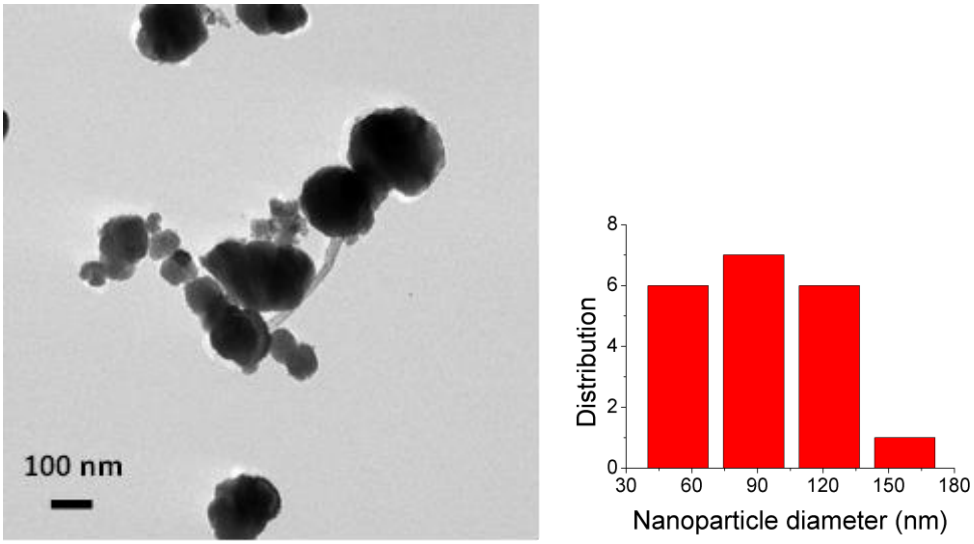

Figure 4.19: *TEM image of a MWCNT decorated with in-situ precipitated magnetic nanoparticles (in-situ synthesized MWCNT-$CoFe_2O_4$), with insert of size distribution values obtained.*

Figure 4.20 displays the TGA analysis of the *in-situ* synthesized MWCNT-$CoFe_2O_4$. The weight percentage of covalently attached nanoparticles was determined using TGA. A TGA cycle as explained in section 4.3.1 was implemented, where an oxygen atmosphere was introduced at 600 °C for 15 minutes before cooling. The presence of oxygen at high temperatures resulted in the combustion of CNTs, which was confirmed by the weight loss to zero at 600 °C for the oxidized MWCNTs (MWCNT-COOH) (refer to figure 4.15 above).[21] The isothermal weight loss at 600 °C could thus be attributed to the presence of 6 wt. % MWCNTs. The residual cobalt/iron nanoparticles remained stable, and the remaining weight percentage of 78 % was thus as a result of the nanoparticles. The TGA results proved suspicions that an excessive amount of nanoparticles relative to MWCNTs was present. This was also confirmed by the XRD analysis shown in figure 4.21 below. The main characteristic peaks for $CoFe_2O_4$ magnetic nanoparticles were noted at about 19, 30, 36, 37, 43, 57 and 63 degrees. Characteristic peaks for MWCNTs are present at 10 and 20 degrees, where the absence of the peak at 20 degrees is an indication of the insufficient quantity of the MWCNTs relative to the nanoparticles.[31]

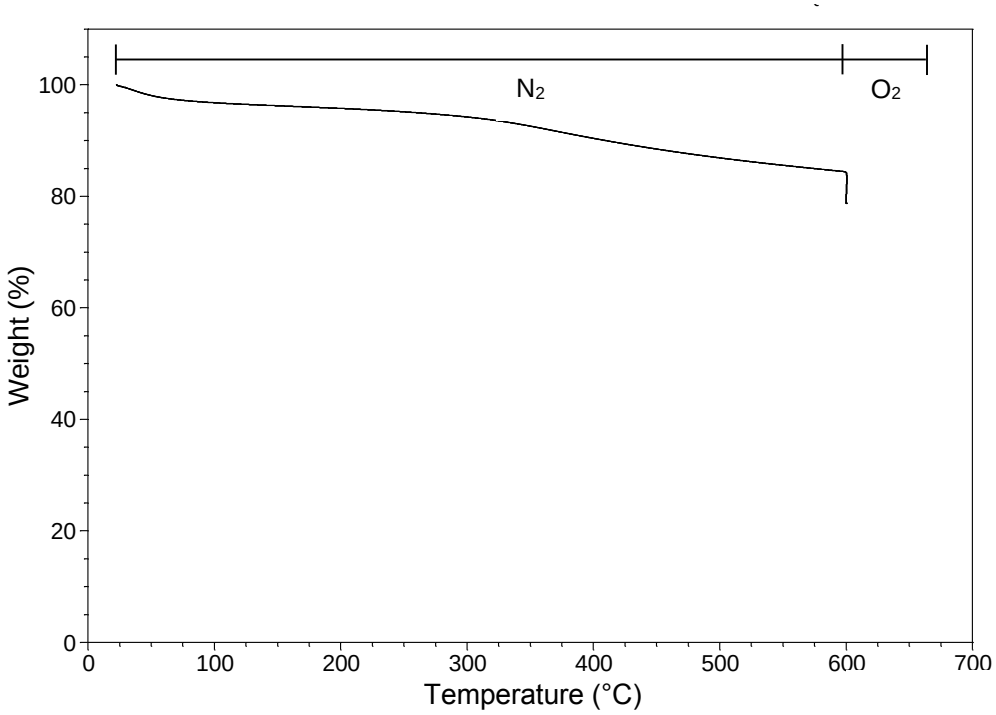

Figure 4.20: *TGA curve of in-situ synthesized MWCNT-$CoFe_2O_4$ under nitrogen atmosphere followed by the implementation of an oxygen atmosphere at 600 ℃.*

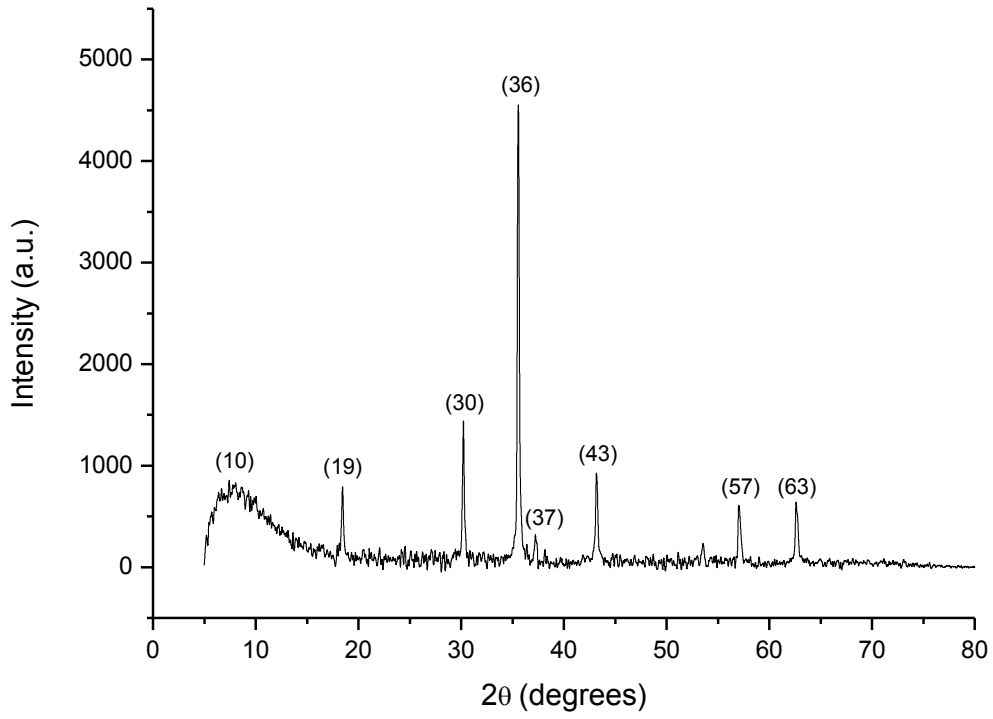

Figure 4.21: *XRD spectrum of in-situ synthesized MWCNT-$CoFe_2O_4$.*

Attempts to lower the magnetic nanoparticle loading as well as the nanoparticle size by varying the reaction conditions were carried out. Numerous reactions were carried out and are listed in table A.1 in appendix A. Reaction #7 in the table is the original reaction carried out and reported on above; and was used as a reference for the ratio adjustments.

Firstly, in an attempt to increase the wt. % of MWCNTs present, the amount of MWCNTs was increased from reaction #7-10, while the amounts of metal-salts and alkaline medium were decreased proportionally. The ratios used are set out in appendix A, table A.1. The reactions yielded magnetic products as observed with application of an external magnetic field. TGA data (refer to appendix B, figure B.1) indicated an increase in the wt. % MWCNTs present from reaction #7 to #10, as would be expected. TGA results obtained are tabulated below:

Table 4.3: *Summary of wt. % results obtained with TGA for reactions #7-10.*

	MWCNT (wt. %)	**Magnetic nanoparticles (wt. %)**
Reaction #7	6	78
Reaction #8	9	44
Reaction #9	14	27
Reaction #10	29	28

Due to the promising results obtained by TGA, further testing using TEM and XRD was carried out on products obtained in reaction #8-10. Inadequate attachment of magnetic nanoparticles onto MWCNTs could be observed in TEM images of all 3 samples (refer to appendix B, figure B.2). XRD results for reaction #8 (refer to appendix B, figure B.3 (a)) showed main characteristic peaks for $CoFe_2O_4$ at about 19, 30, 36, 43, 57 and 63 degrees. The broader peaks at 10 degrees and above 20 degrees correspond to the MWCNTs; however a larger peak above 20 degrees is expected for the MWCNTs loading to be considered sufficient. For reaction #9 and #10 (refer to appendix B, figure B.3 (b) and (c)) characteristic peaks for $CoFe_2O_4$ seem to disappear; while large peaks above 20 degrees can be observed for the MWCNTs, indicating that the quantity of MWCNTs present is too large.[31] TGA and XRD data thus concluded that reactions carried out with increased amounts of MWCNTs and decreased amounts of metal-salts and alkaline medium were unsuccessful.

Secondly, in an attempt to decrease the magnetic nanoparticle loading, the amounts of MWCNTs and alkaline medium were kept constant while the amount of metal-salts was decreased (refer to reactions #11-13). All products obtained did not respond to the application of an external magnetic field, and no further tests were therefore performed. Reactions were also carried out for longer periods (refer to reaction #14-16) in order to see if any change in the final product would occur, but no change was apparent. Reactions heated to 90 °C at a rate of 2 °C/min were also carried out in an attempt to control the magnetic nanoparticle growth and consequently reduce the nanoparticle size (refer to reactions #17-20); however no change in the nanoparticle size could be observed.

All attempts to lower the magnetic nanoparticle loading as well as the nanoparticle size were thus, regrettably, unsuccessful. Another approach for the synthesis of *in-situ* decorated MWCNTs was consequently pursued (refer to *in-situ* approach 2 below).

4.3.3 *In-situ* approach 2 (synthesis of *in-situ* MWCNT-Fe_3O_4)

The second *in-situ* method entails the decoration of MWCNTs with Fe_3O_4 nanoparticles by the hydrolysis of a coordinating metal precursor ($FeCl_3$) onto the MWCNT-COOH surface at high temperatures in order to produce MWCNT-Fe_3O_4. The method was followed as reported by He *et al.*[33] The successful synthesis of *in-situ* MWCNT-Fe_3O_4 was confirmed by displaying the magnetic characteristics of the product using visual observations and a magnet. The product immediately responded to the application of an external magnetic field; as can be observed in figure 4.22 below.

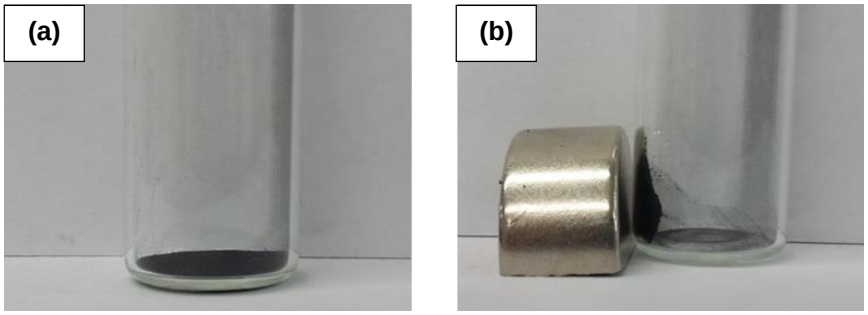

Figure 4.22: *In-situ synthesized MWCNT-Fe_3O_4 with (a) no magnet applied and (b) the application of an external magnetic field.*

Confirmation of the successful *in-situ* decoration of the magnetic nanoparticles onto the oxidized MWCNTs was accomplished by subjecting the magnetic sample shown above (figure 4.22) to

further testing using TEM, TGA and XRD. Figure 4.23 shows a TEM image of a Fe_3O_4 decorated MWCNT, where the image clearly indicates that nanoparticles were attached to the MWCNT surface. Very small nanoparticles with an average diameter of 2 nm and Đ of 0.18 were observed. The image also shows that the MWCNTs were extremely densely decorated.

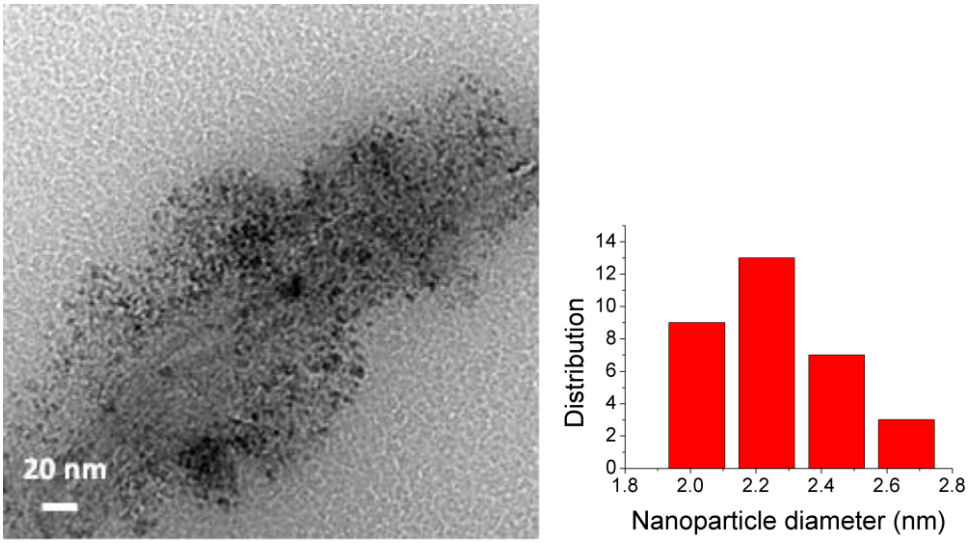

Figure 4.23: *TEM image of a MWCNT decorated with in-situ precipitated magnetic nanoparticles (in-situ synthesized MWCNT-Fe_3O_4), with insert of size distribution values obtained.*

TGA was used to determine the weight percentage of covalently attached nanoparticles. A TGA cycle as explained in section 4.3.1 was implemented, where an oxygen atmosphere was introduced at 600 °C for 15 minutes before cooling. The presence of oxygen at high temperatures resulted in the combustion of CNTs, which was confirmed by the weight loss to zero at 600 °C for the oxidized MWCNTs (MWCNT-COOH) (refer to figure 4.15 above).[21] Figure 4.24 displays the TGA analysis of the MWCNT-Fe_3O_4, where the isothermal weight loss at 600 °C can thus be attributed to the presence of 34 wt. % MWCNTs. The residual iron nanoparticles remained stable, and the remaining weight percentage of 37 % was thus as a result of the nanoparticles. Figure 4.25 shows the XRD analysis of the MWCNT-Fe_3O_4. XRD was used to characterize the presence of Fe_3O_4 nanoparticles in the final composite material. Peaks were recorded at 30, 35, 40-45, 53-58 and 63 degrees, where these peaks are characteristic of the Fe_3O_4 magnetic nanoparticles.[28] Significantly larger peaks were also observed at 10 and 20 degrees; which were as a result of MWCNTs' presence.[31] These peaks were not included in the graph due to their large size leading to the insignificance of the smaller peaks observed for the Fe_3O_4 magnetic

nanoparticles. The same results as for *ex-situ* synthesized MWCNT-Fe_3O_4 were thus obtained, indicating that a similar product was synthesized using a simpler single-step method.

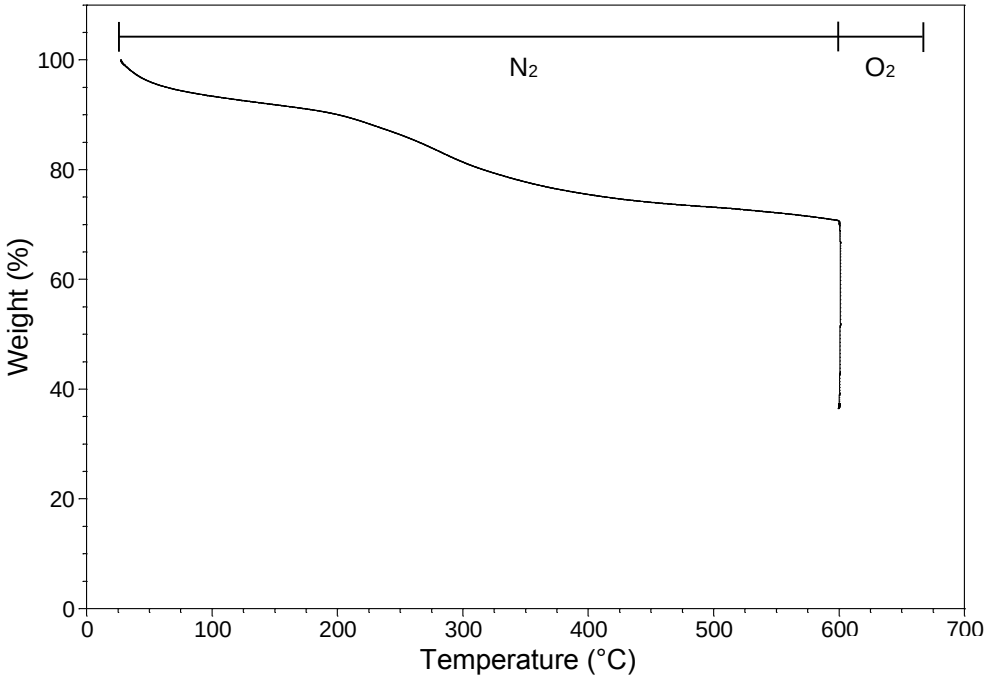

Figure 4.24: *TGA curve of in-situ synthesized MWCNT-Fe_3O_4 under nitrogen atmosphere followed by the implementation of an oxygen atmosphere at 600 ℃.*

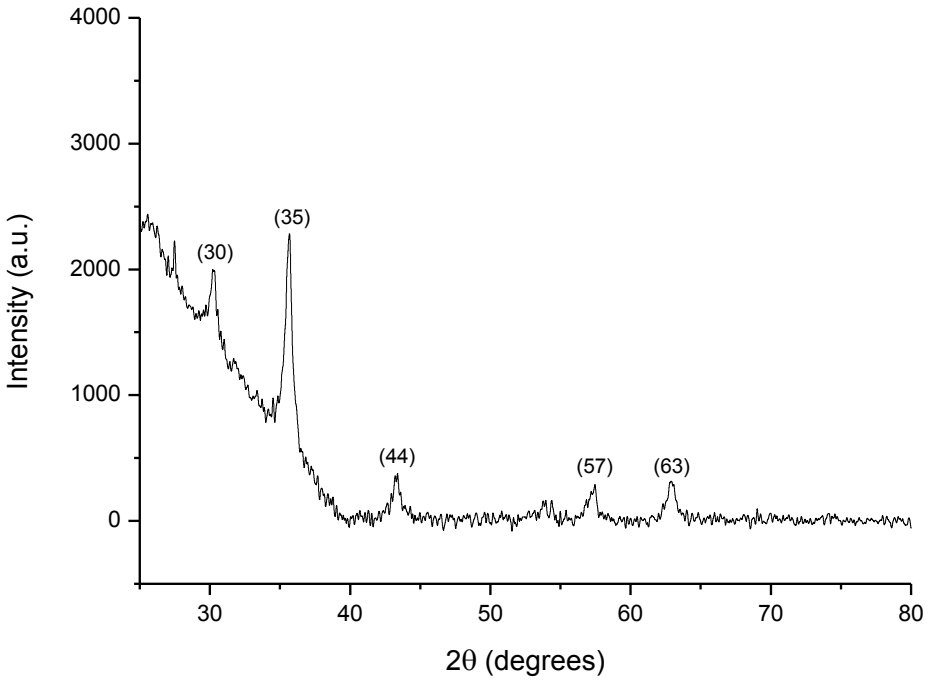

Figure 4.25: *XRD spectrum of in-situ synthesized MWCNT-Fe_3O_4.*

4.3.4 Dispersion tests

Figure 4.26 displays images of the dispersion tests performed on all the CNTs decorated with magnetic nanoparticles. For these tests, 1.5 mg of sample was dispersed in 0.5 mL of solvent (DMF). The mixture was sonicated for 20 minutes prior to dispersion observations at room temperature. Immediately after sonication (0 h), samples which were well dispersed in the polar solvent were observed. For sample b (*in-situ* synthesized MWCNT-$CoFe_2O_4$), interaction with the solvent significantly decreased as time progressed, which was observed where the sample started to accumulate at the bottom of the vial as time increased. For sample a and c (*ex-situ* synthesized MWCNT-Fe_3O_4 and *in-situ* synthesized MWCNT-Fe_3O_4, respectively), interactions were seen to remain stable after 24 hours. The interaction of the *ex-situ* synthesized MWCNT-Fe_3O_4 and *in-situ* synthesized MWCNT-Fe_3O_4 with the solvent was observed to be stable even after one month; which is presented in figure 4.27.

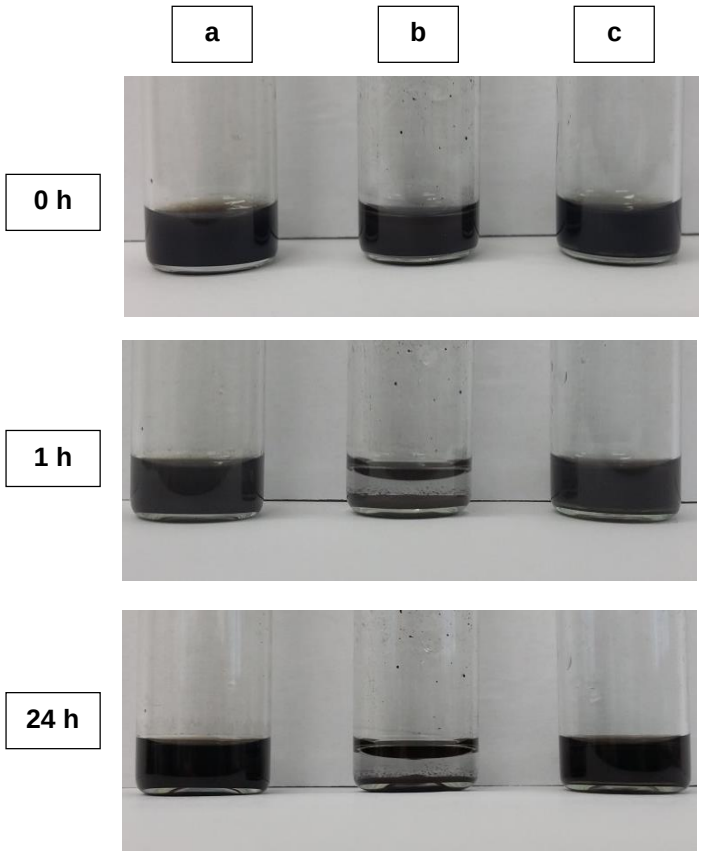

Figure 4.26: *Dispersion test observations, in DMF after 20 minutes of sonication, of (a) ex-situ synthesized MWCNT-Fe_3O_4, (b) in-situ synthesized MWCNT-$CoFe_2O_4$ and (c) in-situ synthesized MWCNT-Fe_3O_4.*

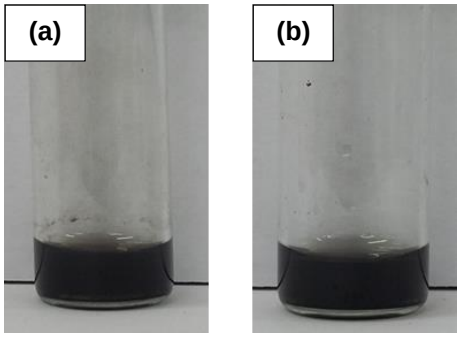

Figure 4.27: *Dispersion test observations, in DMF after 20 minutes of sonication and standing for one month, of (a) ex-situ synthesized MWCNT-Fe_3O_4 and (b) in-situ synthesized MWCNT-Fe_3O_4.*

For sample b (*in-situ* synthesized MWCNT-$CoFe_2O_4$), inadequate dispersion can be attributed to the presence of an excess of the chemically inert magnetic nanoparticles. This was proven by TGA results (refer to figure 4.20 above); where only 6 wt. % MWCNTs were noted in the presence of 78 wt. % magnetic nanoparticles. For sample a and c (*ex-situ* synthesized MWCNT-Fe_3O_4 and *in-situ* synthesized MWCNT-Fe_3O_4, respectively), good dispersion of the samples in the solvent can be attributed to the carboxylic acid groups present on the CNT surface as a result of oxidation. Magnetic nanoparticles are attached to the CNT surface through the carboxylic acid groups present; where not all carboxylic acid moieties are utilized. This was proven by TGA results (refer to figure 4.16 and 4.24), where the weight loss of more than 20 wt. % observed before implementation of the isothermal cycle was as a result of carboxylic acid moieties. Good dispersion can be attributed to the polar carboxylic acid groups present on the CNT surface, which facilitates dissolution in polar solvents such as DMF. For electrospinning, the interactions between the solvent molecules and carboxylic acid moieties were replaced with interactions between the functional groups of the PMMA polymer used as matrix and carboxylic acid moieties. This interaction allowed for good dispersion of samples a and c in the PMMA polymer matrix.

4.4 Electrospun PMMA nanofibres

Electrospinning is an uncomplicated yet versatile method in which continuous polymer nanofibres are produced. By the incorporation of reinforcing nanomaterials, the end product can be enhanced. CNTs are popular for use as reinforcing nanomaterials, where the inclusion of CNTs into a polymer matrix leads to increased tensile strength and modulus.[11,12,34] In this study, PMMA electrospun nanofibres constituted the polymer matrix, with the addition of the various CNTs previously functionalized and decorated with magnetic nanoparticles as reinforcing nanomaterials. The

optimal electrospinning parameters for the PMMA homopolymer were found to be 15 wt. % PMMA with an applied voltage of 15 kV, a distance between the capillary and target of 15 cm, as well as a flow rate of 0.039 mL/min.

4.4.1 Effect of wt. %

The amounts as well as type of CNTs [oxidized MWCNTs (MWCNT-COOH), oxidized magnetic CNTs (magnetic CNT-COOH), PMMA grafted MWCNTs (MWCNT-PMMA), PMMA grafted magnetic CNTs (magnetic CNT-PMMA), MWCNTs decorated *ex-situ* with magnetic nanoparticles (*ex-situ* MWCNT-Fe_3O_4), MWCNTs decorated *in-situ* with magnetic nanoparticles in approach 1 (*in-situ* MWCNT-$CoFe_2O_4$), and MWCNTs decorated *in-situ* with magnetic nanoparticles in approach 2 (*in-situ* MWCNT-Fe_3O_4)] were varied; where 0.5 wt. %, 1.5 wt. % and 3.0 wt. % of every type of CNT were added to the electrospinning polymer solution. However; by adding CNTs the viscosity of the electrospinning solution increases, which prevents efficient electrospinning. The polymer concentration was, therefore, varied depending on the amount of CNTs incorporated; where ratios were adjusted according to an article by Bayley *et al*.[35] The various polymer solution ratios used for electrospinning are set out in the experimental section 3.7, in table 3.1. After electrospinning fibres in the nanometer range were obtained, as observed in the SEM images presented in figure 4.28 and 4.29 below.

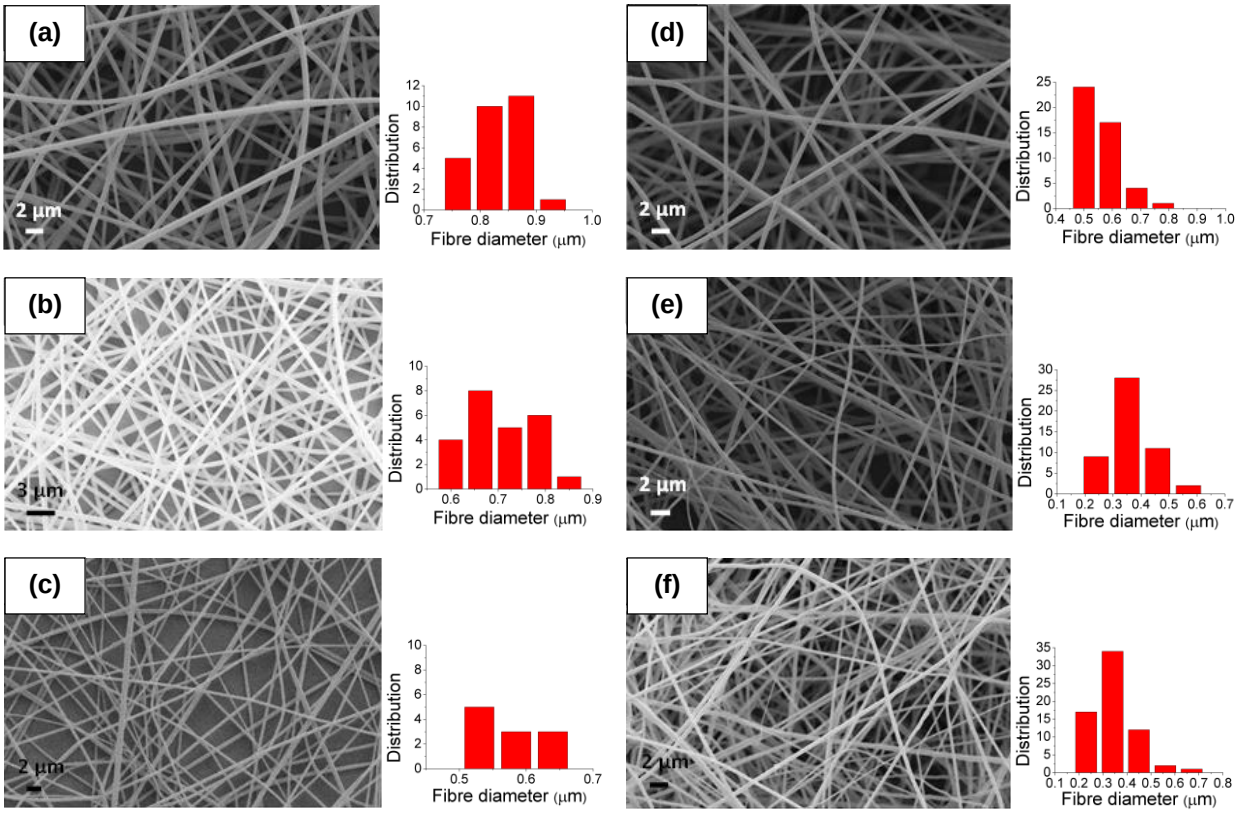

a, b, c: MWCNT-COOH d, e, f: magnetic CNT-COOH

Figure 4.28: *SEM images of electrospun nanofibres with (a, d) 0.5 wt. % CNTs, (b, e) 1.5 wt. % CNTs, and (c, f) 3.0 wt. % CNTs incorporated.*

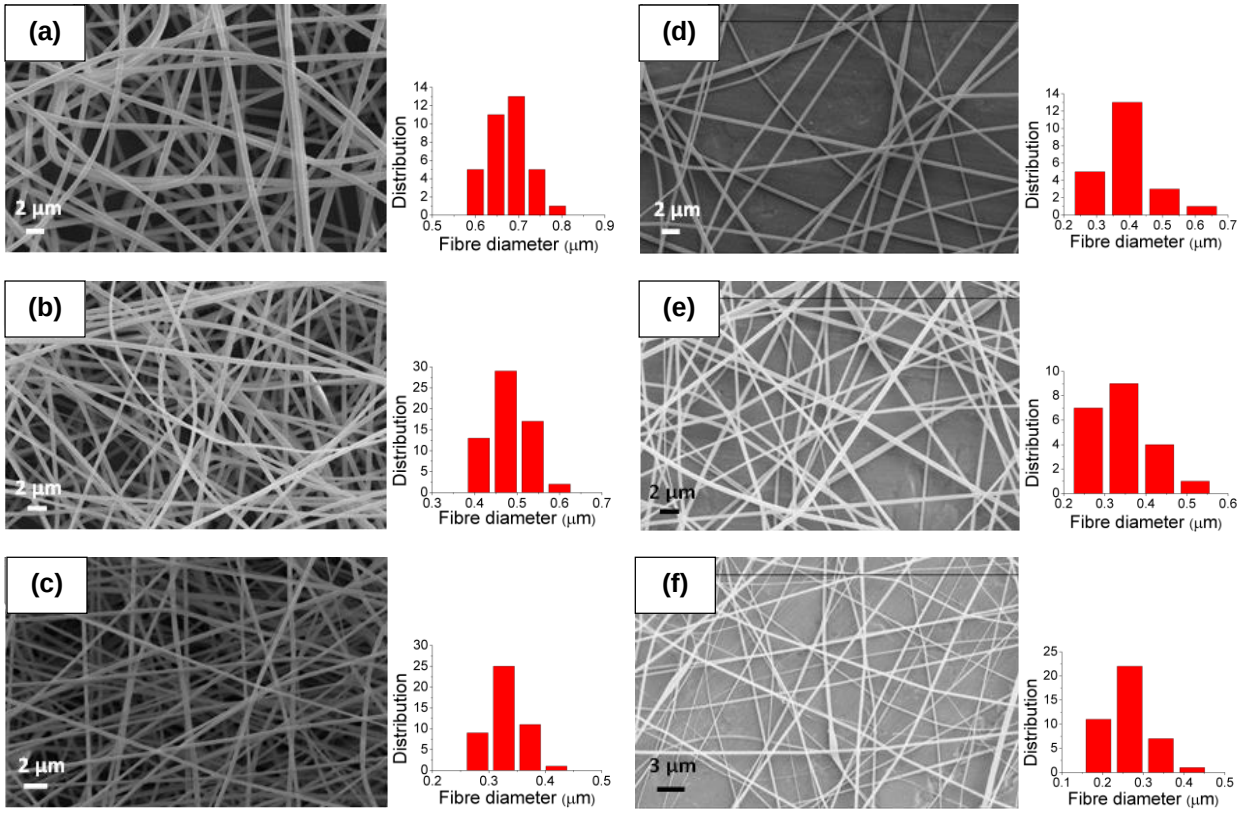

a, b, c: MWCNT-PMMA d, e, f: magnetic CNT-PMMA

Figure 4.29: *SEM images of electrospun nanofibres with (a, d) 0.5 wt. % CNTs, (b, e) 1.5 wt. % CNTs, and (c, f) 3.0 wt. % CNTs incorporated.*

Overall results obtained indicated that the fibre diameter decreased and fibres became more uneven (more beading and irregularities were observed) as the amount of CNTs incorporated were increased. The decreasing fibre diameter can be attributed to the conductive properties of CNTs, which results in an increase of the electrical conductivity of the electrospinning solution. This leads to an increase in the electrostatic repulsive forces within the solution, allowing for more whipping and stretching of the electrospinning jet. Another factor influencing the fibre diameter is the CNT to polymer ratio. As the amount of CNTs in the electrospinning solution is increased, the viscosity of the solution increases. The concentration of the polymer in the solution then has to be reduced in order to decrease the solution viscosity, in compensation for the increase caused by the added CNTs. The reduced polymer concentration results in less polymer chain entanglements being present for the same volume of electrospinning solution, which consequently cause decreased fibre diameters.

When comparing the fibre diameter results obtained for oxidized MWCNTs and PMMA grafted MWCNTs it was noted that where PMMA grafted MWCNTs were incorporated, decreased fibre

diameters and narrower standard deviations were obtained. The same trend was seen when comparing fibre diameters for oxidized magnetic CNTs and PMMA grafted magnetic CNTs. All the magnetic samples had overall lower average fibre diameters, while higher standard deviation values were prominent. This is due to the incorporation of magnetic nanoparticles resulting in electrospinning solutions with increased conductivity.[36] As a result of increased conductivity more whipping and stretching of the electrospinning jet occurs, leading to fibres with decreased diameters (as explained in section 2.4). Figure 4.30 below outlines the fibre diameter results, as measured from SEM images.

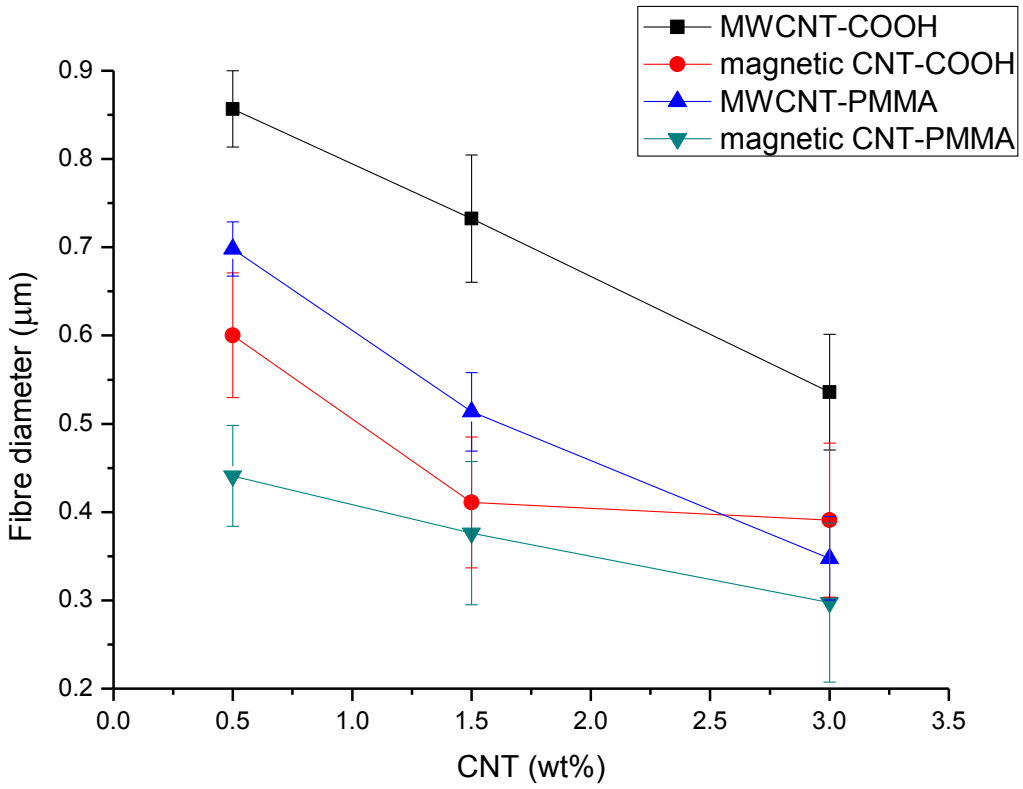

Figure 4.30: *Fibre diameter (µm) as a function of CNT weight incorporation (wt. %).*

Similar trends to that of magnetic CNTs (above) arose for magnetic samples produced by decorating MWCNTs with magnetic nanoparticles. Overall the average fibre diameters were lower than that of non-magnetic MWCNT samples, while higher standard deviation values were obtained. SEM images of the electrospun nanofibres containing magnetic nanoparticle decorated MWCNTs are presented in figure 4.31 below:

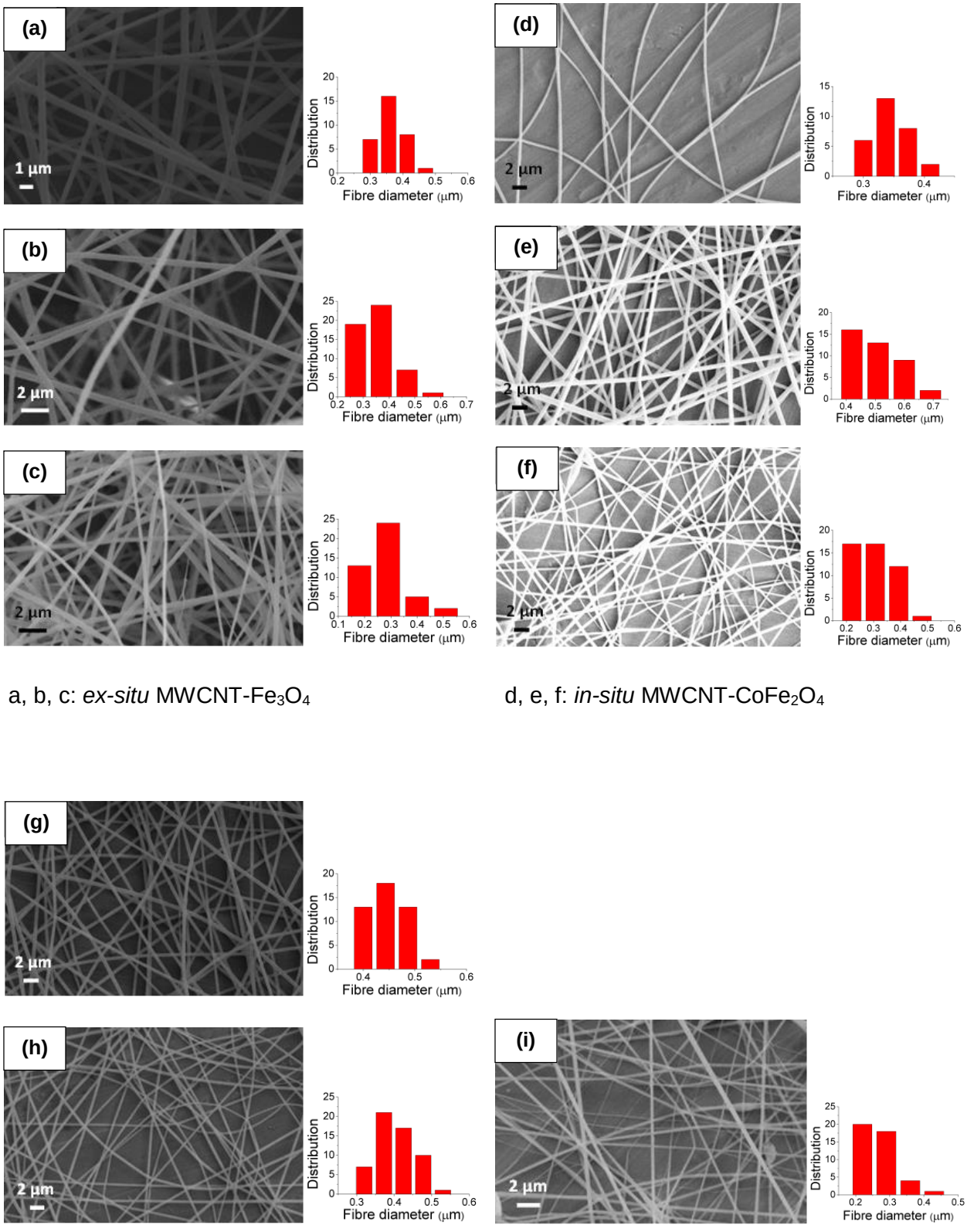

a, b, c: *ex-situ* MWCNT-Fe_3O_4

d, e, f: *in-situ* MWCNT-$CoFe_2O_4$

g, h, i: *in-situ* MWCNT-Fe_3O_4

Figure 4.31: *SEM images of electrospun nanofibres with (a, d, g) 0.5 wt. % CNTs, (b, e, h) 1.5 wt % CNTs, and (c, f, i) 3.0 wt. % CNTs incorporated.*

Figure 4.32 shows the results for fibre diameter versus MWCNT wt. % incorporation. The samples containing the *in-situ* MWCNT-$CoFe_2O_4$ resulted in the highest standard deviations. This is due to the inadequate dispersion of the sample in the electrospinning solution as a result of the presence of an excess chemically inert magnetic nanoparticles (as proven by dispersion test results in section 4.3.4).

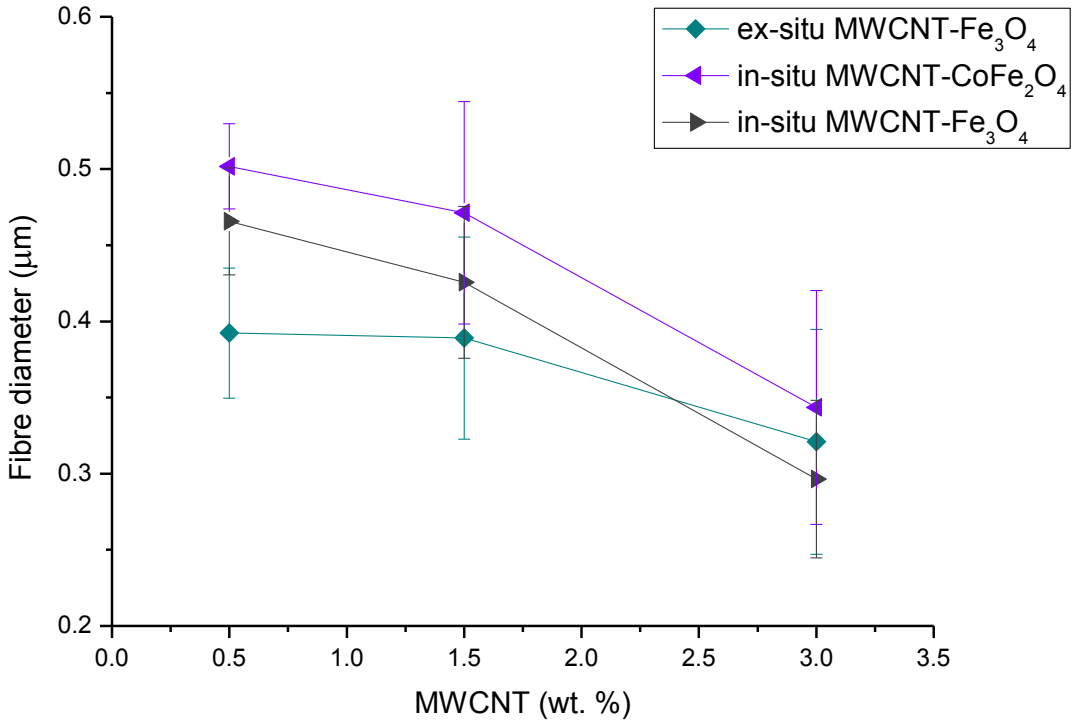

Figure 4.32: *Fibre diameter (µm) as a function of MWCNT weight incorporation (wt. %).*

Figure 4.33 displays a TEM image of magnetic CNT-PMMA containing electrospun nanofibres, which confirms the successful incorporation, and thus interaction of the CNTs with the electrospun polymer matrix. This is observed where incorporated CNTs which align along the fibre axis can be seen. Samples of the electrospun nanofibres were embedded in agar resin prior to microtoming in order to visualize the inside of fibres. The wt. % of CNTs incorporated was upscaled to 12 wt. % in order to increase the observation probability. Due to the timely and challenging procedure associated with TEM imaging of incorporated CNTs (fibres first have to be embedded in resin and then the perfect microtomed 'slice' along the fibre length has to be obtained), STEM was investigated as an alternate means to directly observe the CNTs inside the polymer nanofibres. Figures 4.34 and 4.35 show STEM images of electrospun nanofibres containing various CNTs, where the alignment of the various CNTs inside the nanofibres could be observed by simply

imaging a mat of electrospun nanofibres placed on a grid. In the case of magnetic samples, CNTs decorated with magnetic nanoparticles could clearly be seen. In the case of fibres containing *in-situ* MWCNT-$CoFe_2O_4$, the large nanoparticles present in excess were apparent (refer to figure 4.35 (b)). Efficient interaction of the various CNTs with the polymer matrix is confirmed by TEM and STEM images where well distributed CNTs with no agglomeration are apparent. The CNTs align along the electrospun polymer fibres (refer to the arrows in figure 4.33-4.35) due to the stretching of the fibres during electrospinning.[35]

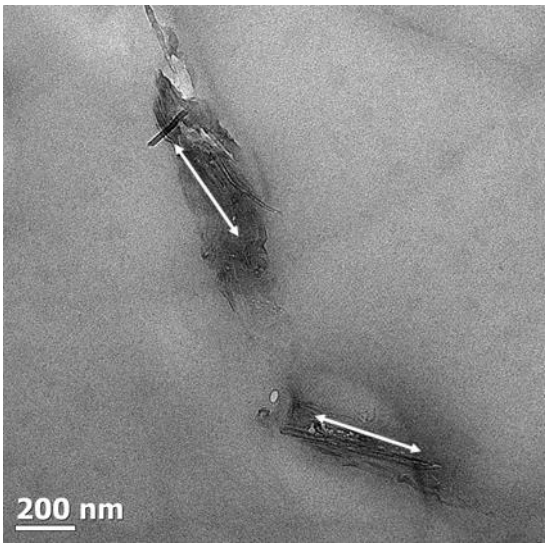

Figure 4.33: *TEM image obtained from magnetic CNT-PMMA containing electrospun nanofibres (12 wt. %) embedded in agar resin prior to microtoming.*

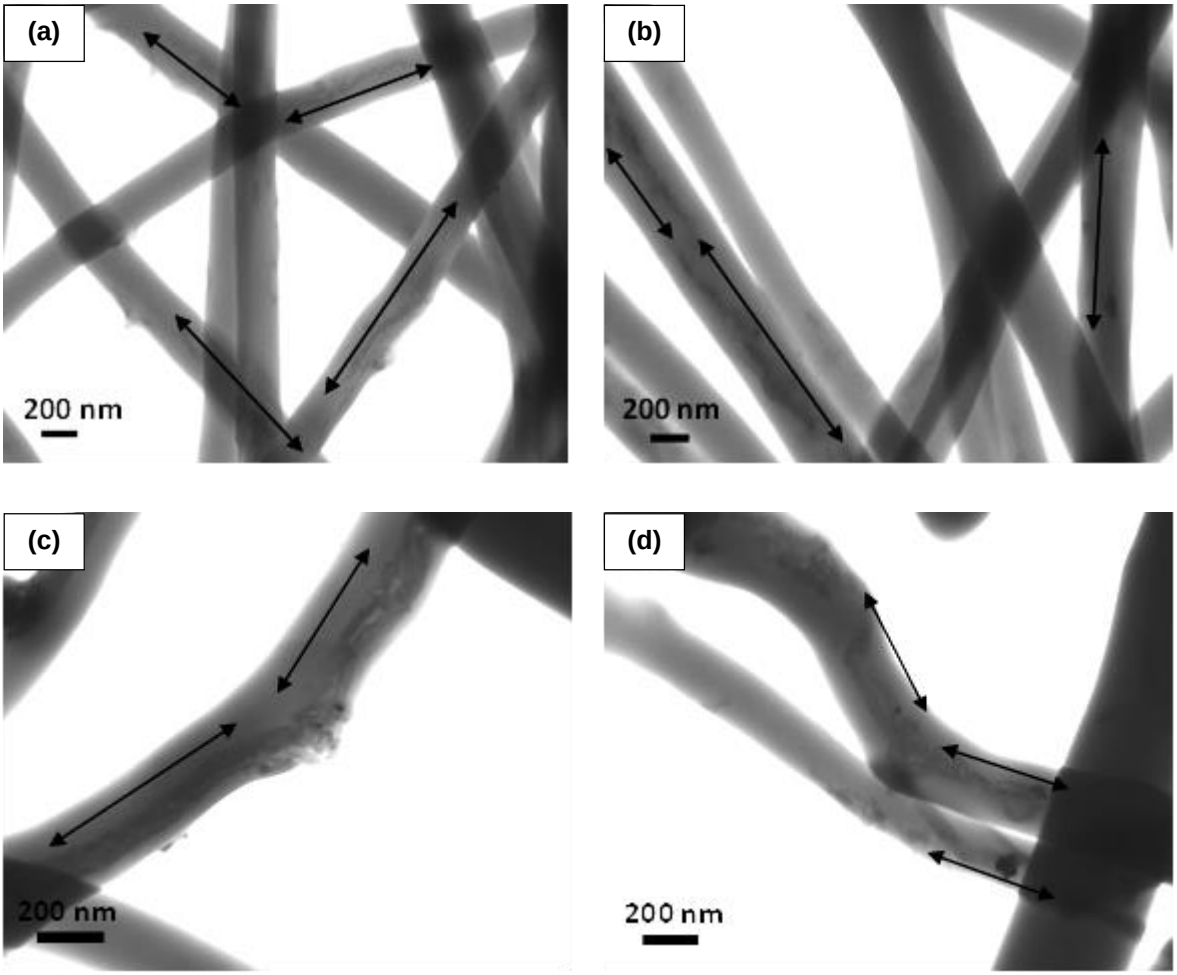

Figure 4.34: *STEM images obtained from 3.0 wt. % (a) MWCNT-COOH, (b) MWCNT-PMMA, (c) magnetic CNT-COOH and (d) magnetic CNT-PMMA containing electrospun nanofibres clearly indicating successful incorporation and alignment of the various CNTs along the fibre length.*

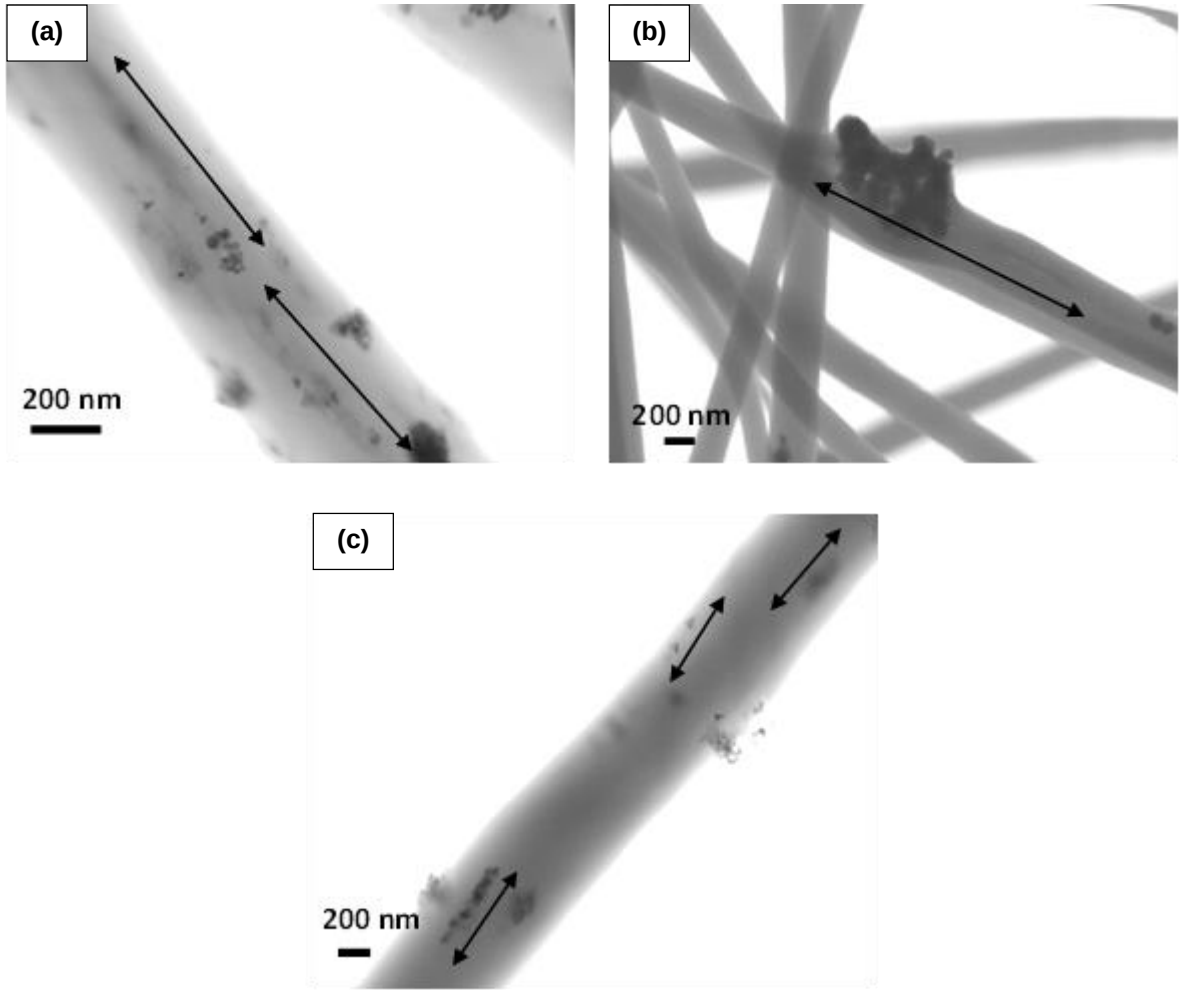

Figure 4.35: *STEM images obtained from 3.0 wt. % (a) ex-situ MWCNT-Fe_3O_4, (b) in-situ MWCNT-$CoFe_2O_4$ and (c) in-situ MWCNT-Fe_3O_4 containing electrospun nanofibres clearly indicating successful incorporation and alignment of the various CNTs along the fibre length.*

Illustrated in figure 4.36 are the nanofibrous mats of electropsun nanofibres obtained when various CNTs were incorporated. Successful CNT incorporation was again confirmed by these visual observations, where the nanofibrous mat of electrospun nanofibres became darker as the concentration (wt. %) of various black CNTs incorporated were increased. This trend was observed for all other samples.

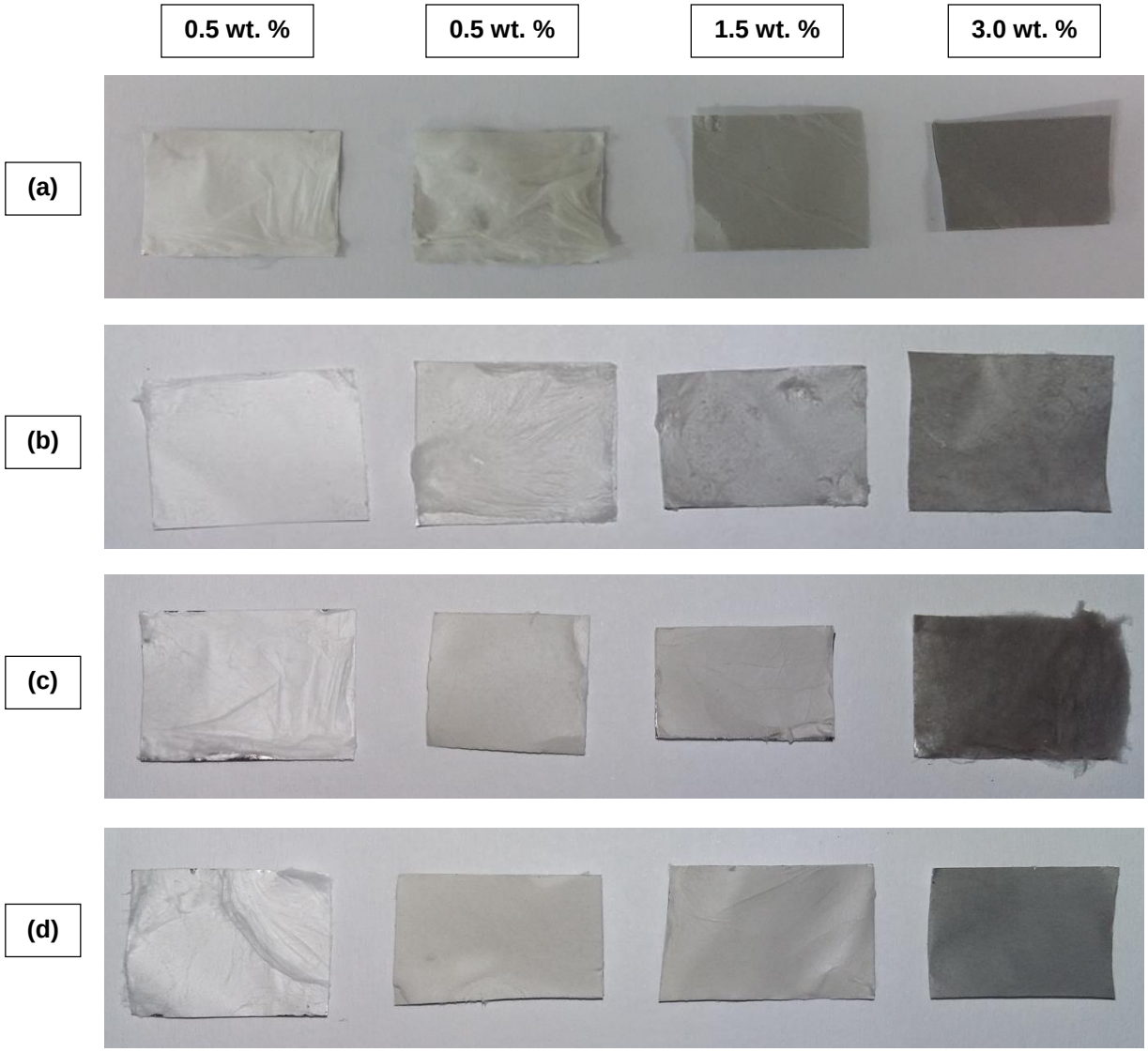

Figure 4.36: *Nanofibrous mat of electrospun nanofibres incorporated with (a) MWCNT-PMMA, (b) magnetic CNT-PMMA, (c) ex-situ MWCNT-Fe_3O_4 and (d) in-situ MWCNT-Fe_3O_4.*

4.4.2 Effect of voltage on fibres containing magnetic CNTs

In order to investigate the effect the magnetic properties of magnetic CNT samples have on the fibre morphology, the electrospinning voltage was varied. A 1.5 wt. % CNT and 14 wt. % PMMA electrospinning solution were used for this experiment, while voltages were varied from 5-30 kV. Samples of magnetic CNT-COOH, *ex-situ* MWCNT-Fe_3O_4, *in-situ* MWCNT-$CoFe_2O_4$ and *in-situ* MWCNT-Fe_3O_4 were incorporated. Figure 4.37 shows SEM images of the nanofibres obtained. SEM images and distribution graphs for the various nanofibres obtained by the electrospinning process when varying the voltage can be seen in appendix C, figure C.1- C.3.

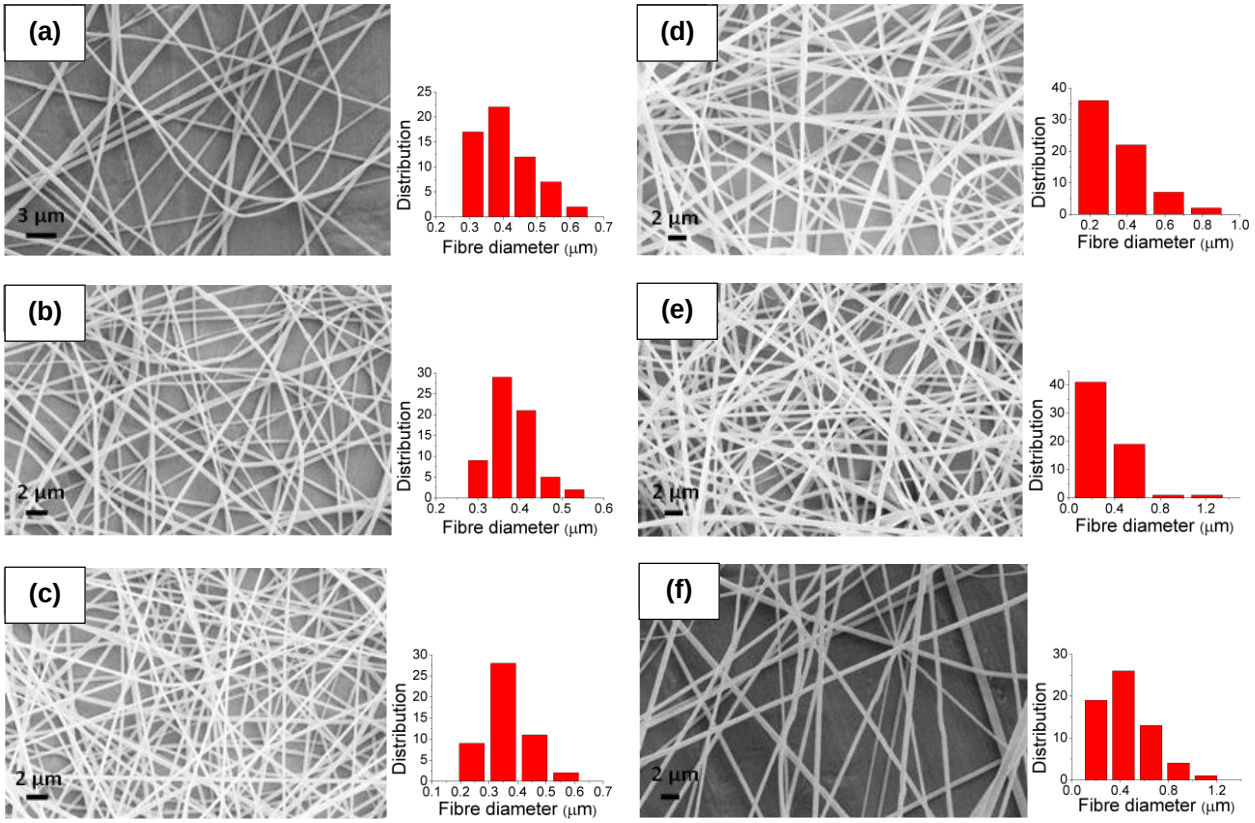

Figure 4.37: *SEM images of electrospun fibres with 1.5 wt. % magnetic CNT-COOH & 14 wt. % PMMA incorporated, and a voltage of (a) 5 kV, (b) 10 kV, (c) 15 kV, (d) 20 kV, (e) 25 kV and (f) 30 kV.*

Figure 4.38 displays the results obtained for fibre diameter versus applied voltage. At a voltage of 5 kV dripping was occasionally observed. This was as a result of the voltage being too low, and there consequently not being enough electrical charge present to carry the electrospinning jet towards the collector plate. Overall the results showed a decrease in the fibre diameter from 5 kV to 15 kV. The lower applied voltage of 5 and 10 kV resulted in the electrostatic repulsive forces within the electrospinning solution caused by the induced charges being less; leading to less whipping and stretching of the jet, and thus increased fibre diameters. No definite trend in the fibre diameter could be observed for voltages above 15 kV. More beading and larger standard deviations were, however, observed. This was as a result of the higher voltage affecting the shape and stability of the Taylor cone, which in turn influences the fibre morphology.[1,37,38] During electrospinning at voltages above 15 kV, spraying of the solution was also readily observed, which indicated that the applied voltage was too high. At 15 kV the lowest amount of beads was observed and the lowest values for standard deviation were obtained – 15 kV was thus found to be the optimal voltage for electrospinning.

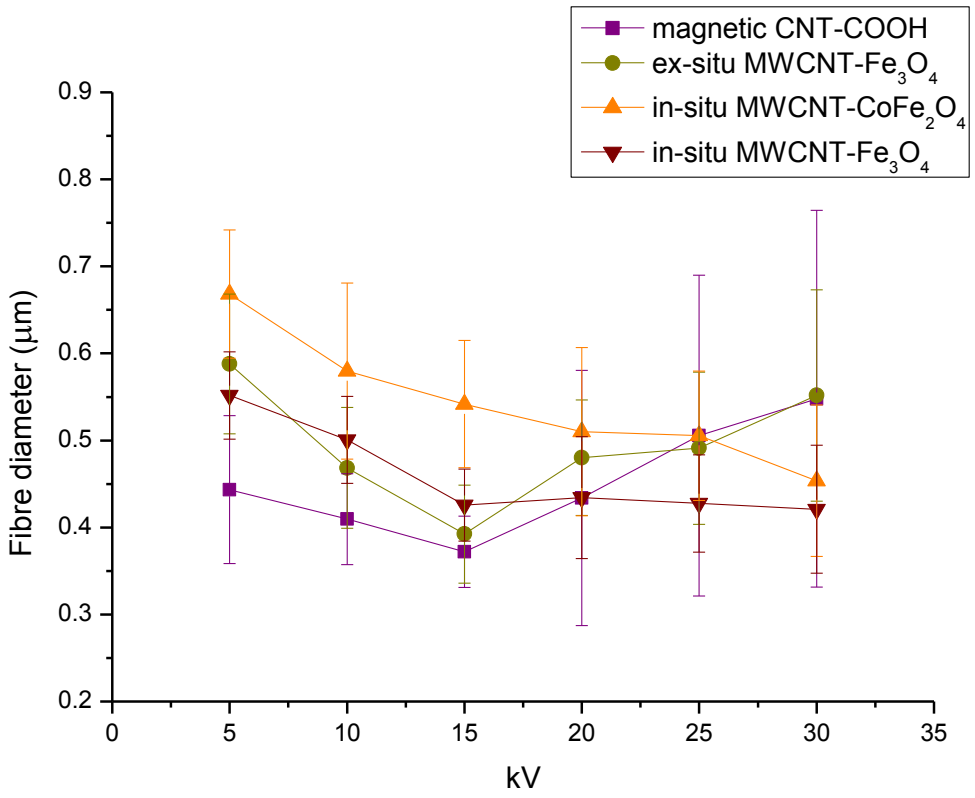

Figure 4.38: *Fibre diameter (µm) as a function of voltage used during the electrospinning process (kV).*

4.5 Magnetic characterization

The magnetic response of various magnetic samples synthesized was analysed using a superconducting quantum interference device (SQUID). By using results obtained with SQUID magnetometry, curves for applied magnetic field (Oe) versus magnetization (emu/g) (M-H curves) can be drawn. The magnetic properties of oleic acid capped Fe_3O_4 nanoparticles, various magnetic CNTs (embedded with magnetic nanoparticles in the walls as well as decorated with nanoparticles), and electrospun PMMA nanofibres containing various magnetic CNTs were characterized using SQUID magnetometry.

Superparamagnetism (SPM) is a type of magnetism which occurs in small size nanoparticles which exhibit ferromagnetic behaviour. When nanoparticles are below a critical size, a sample of these nanoparticles exhibits a uniform magnetization resulting in a superparamagnetic response.[39,40] Figure 4.39 shows the magnetic response curve of the magnetic CNT-PMMA. The sample did not show ideal superparamagnetic behaviour; where an open M-H curve (called a hysteresis loop) with the characteristic sigmoidal shape indicating ferromagnetic characteristic was obtained. This is as

a result of the larger size nanoparticles (average diameter of 26 nm) found in the magnetic CNTs, which is larger than the critical size. Magnetic CNT-PMMA containing electrospun nanofibres did not display the sigmoidal shape, indicating that ideal magnetic characteristics were not present in the sample. This is as a result of the lower magnetic nanoparticle loading, where nanoparticles are not as regularly observed inside the CNTs (refer to TEM images in figure 4.6 *c* and *d*) when compared to samples decorated with nanoparticles in an *ex-* and *in-situ* approach (refer to TEM images in figure 4.14 and 4.23). Figures 4.40 and 4.41 show the magnetic response curves of the various *ex-situ* and *in-situ* synthesized MWCNT-Fe_3O_4 samples. These samples exhibited ideal superparamagnetic behaviour, where curves with the characteristic sigmoidal shape showing zero coercivity, zero remanence and no hysteresis loops were obtained. The appearance of SPM is as a result of the small sized nanoparticles (average diameter of 14 nm and 2 nm respectively) present in high quantities in the *ex-situ* MWCNT-Fe_3O_4 and *in-situ* MWCNT-Fe_3O_4.[39,41]

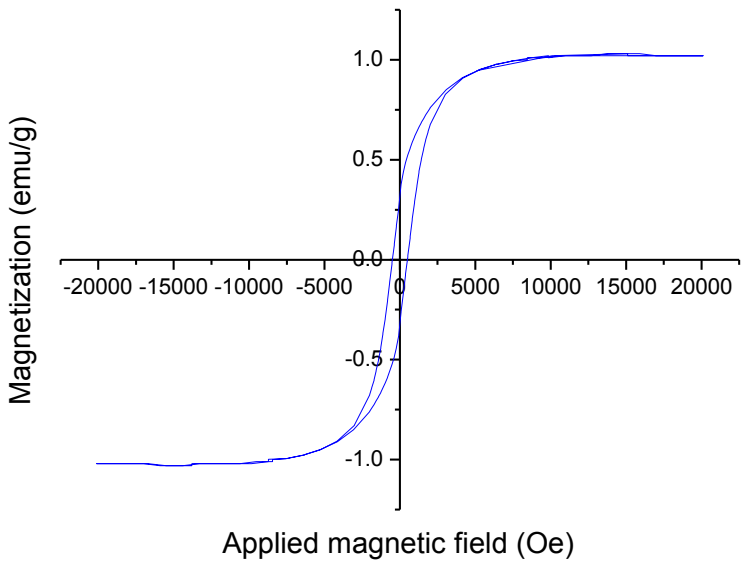

Figure 4.39: *Magnetic response of magnetic CNT-PMMA demonstrating ferromagnetic behaviour.*

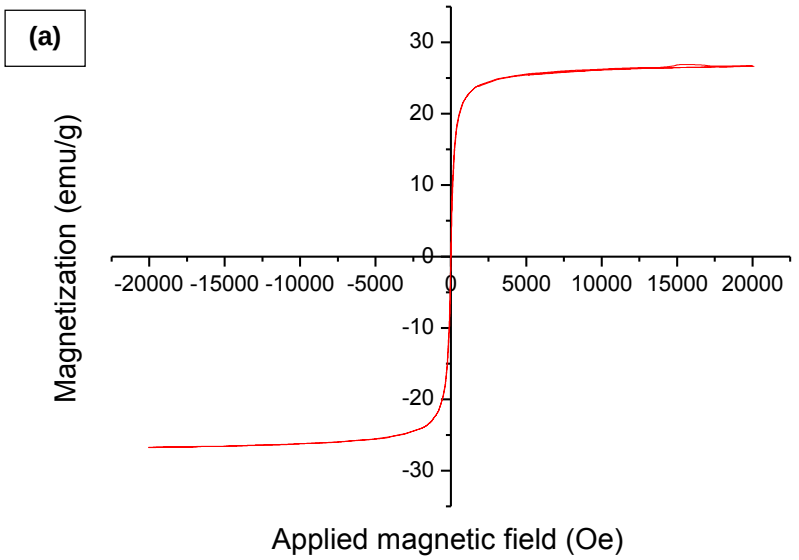

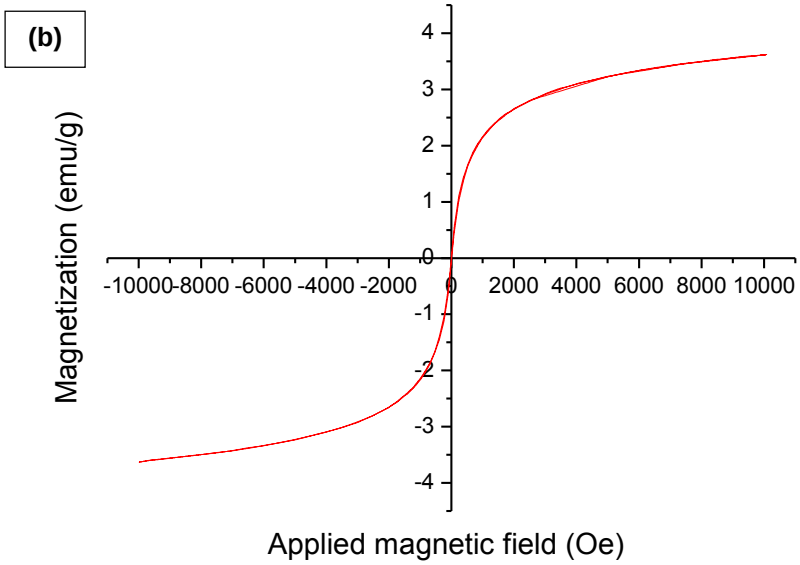

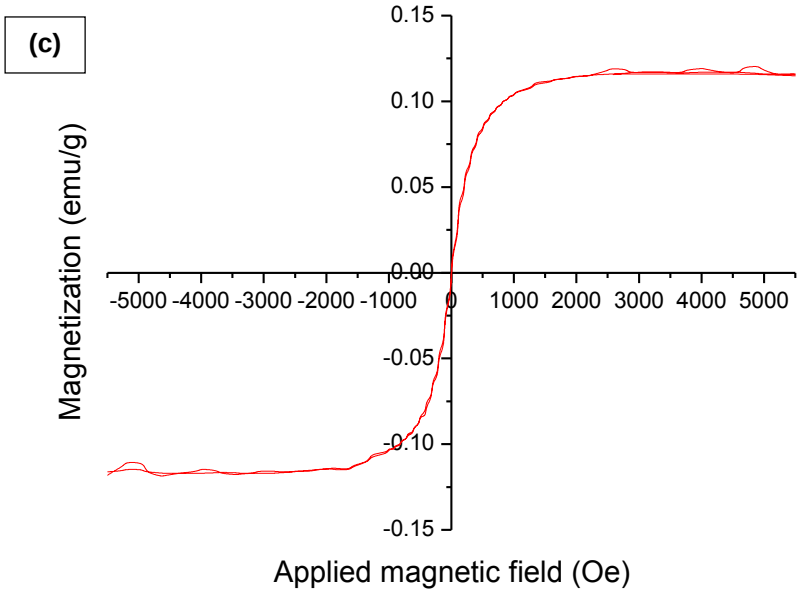

Figure 4.40: *Magnetic response of (a) oleic acid capped Fe_3O_4 nanoparticles, (b) ex-situ MWCNT-Fe_3O_4 and (c) 8 wt. % ex-situ MWCNT-Fe_3O_4 containing electrospun nanofibres demonstrating superparamagnetic behaviour.*

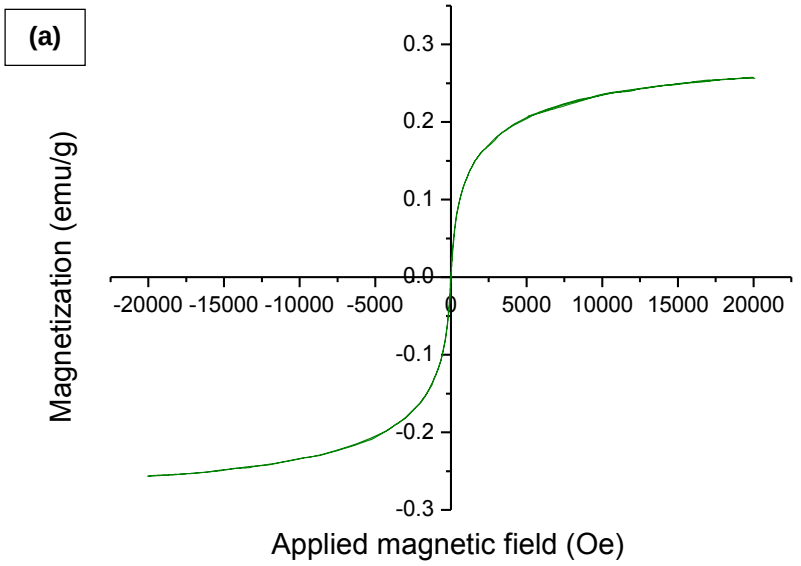

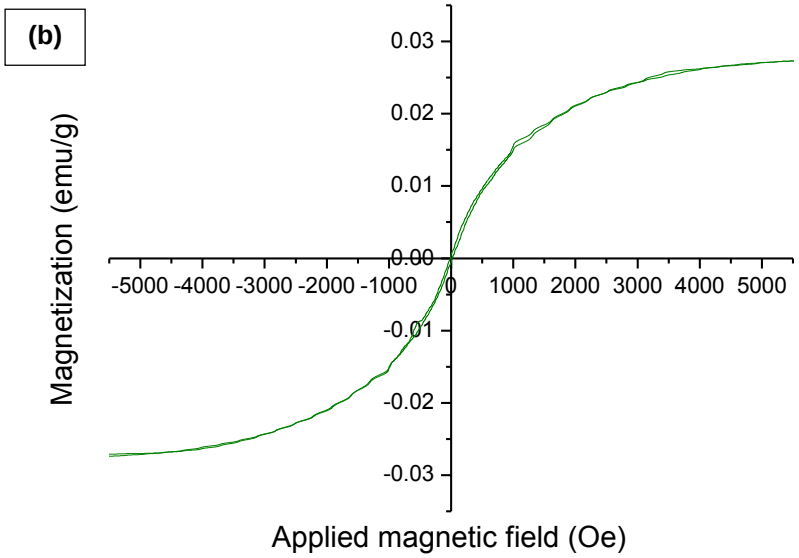

Figure 4.41: *Magnetic response of (a) in-situ MWCNT-Fe_3O_4 and (b) 8 wt. % in-situ MWCNT-Fe_3O_4 containing electrospun nanofibres demonstrating superparamagnetic behaviour.*

Samples of *in-situ* MWCNT-$CoFe_2O_4$ were not submitted for magnetic characterization due to the nature of the sample exhibiting poor dispersion (as reported in section 4.3.4) and SQUID magnetometry being an expensive and unreadily available analysis technique.

When comparing *ex-situ* and *in-situ* synthesized MWCNT-Fe_3O_4, saturation was reached at 3.620 emu/g and 0.258 emu/g respectively (refer to figure 4.40 (b) and figure 4.41 (a)). In the case of electrospun nanofibres containing these decorated MWCNTs, saturation was reached at 0.116 emu/g and 0.026 emu/g respectively (refer to figure 4.40 (c) and 4.41 (b)). Samples of *ex-situ* synthesized MWCNT-Fe_3O_4 thus show overall higher values of magnetization (emu/g) when saturation is reached. This is due to the larger sized small nanoparticles present in the *ex-situ* MWCNT-Fe_3O_4 (average diameter of 14 nm) when compared to the *in-situ* MWCNT-Fe_3O_4 (average diameter of 2 nm). The higher magnetic nanoparticle loading of 43 wt. % present for the *ex-situ* MWCNT-Fe_3O_4 (when compared to 34 wt. % for *in-situ* MWCNT-Fe_3O_4; as confirmed with TGA analysis in section 4.3) also has an effect on the higher final magnetization value obtained. This indicated that electrospun composite nanofibres containing *ex-situ* MWCNT-Fe_3O_4 showed the higher superparamagnetic response; and can thus be classified as the more magnetic composite.[41]

4.6 References

1. L. Cronje and B. Klumperman, *Eur. Polym. J.,* 2013, **49**, 3814-3824.

2. M. K. Georges, R. P. Veregin, P. M. Kazmaier and G. K. Hamer, *Macromolecules,* 1993, **26**, 2987-2988.

3. Y. Qian, Y. Su, X. Li, H. Wang and C. He, *Iran. Polym. J.,* 2010, **19**, 23-129.

4. J. Vonch, A. Yarin and C. Megaridis, *Am. J. Undergrad. Res.,* 2007, **1**, 1-6.

5. S. Sarabi-Maneji, J. Scott and D. J. Pagé, *Proceedings of the International Conference on New Trends in Transport Phenomena,* Avestia Publishing, Ottawa, 2014, pp. 1-8.

6. G. M. Bayley and P. E. Mallon, *Polymer,* 2012, **53**, 5523-5539.

7. X. Wang, Y. Kim, C. Drew, B. Ku, J. Kumar and L. A. Samuelson, *Nano Lett.,* 2004, **4**, 331-334.

8. Y. Liu, V. Klep, B. Zdyrko and I. Luzinov, *Langmuir,* 2004, **20**, 6710-6718.

9. E. Malmström and A. Carlmark, *Polym. Chem.,* 2012, **3**, 1702-1713.

10. S. Anandhan and S. Bandyopadhyay, *Nanocomposites and Polymers with Analytical Methods,* ed. J. Cuppoletti, InTech, Croatia, 2011, ch. 1, pp. 3-28.

11. V. N. Popov, *Mater. Sci. Eng.,R,* 2004, **43**, 61-102.

12. H. Hou, J. J. Ge, J. Zeng, Q. Li, D. H. Reneker, A. Greiner and S. Z. D. Cheng, *Chem. Mater.,* 2005, **17**, 967-973.

13. V. Choudhary and A. Gupta, *Carbon Nanotubes - Polymer Nanocomposites*, ed. S. Yellampalli, InTech, Croatia, 2011, ch. 4, pp. 65-90.

14. M. Biercuk, M. C. Llaguno, M. Radosavljevic, J. Hyun, A. T. Johnson and J. E. Fischer, *Appl. Phys. Lett.,* 2002, **80**, 2767-2769.

15. Z. Ounaies, C. Park, K. Wise, E. Siochi and J. Harrison, *Compos. Sci. Technol.,* 2003, **63**, 1637-1646.

16. M. Weisenberger, E. Grulke, D. Jacques, A. T. Rantell and R. Andrewsa, *J.Nanosci. Nanotechno.,* 2003, **3**, 535-539.

17. P. Liu, *Eur. Polym. J.,* 2005, **41**, 2693-2703.

18. H. Wu, R. Tong, X. Qiu, H. Yang, Y. Lin, R. Cai and S. Qian, *Carbon,* 2007, **45**, 152-159.

19. M. A. Hamon, J. Chen, H. Hu, Y. Chen, M. E. Itkis, A. M. Rao, P. C. Eklund and R. C. Haddon, *Adv. Mater.,* 1999, **11**, 834-840.

20. L. Meng, C. Fu and Q. Lu, *Prog. Nat. Sci.,* 2009, **19**, 801-810.

21. A. Mahajan, A. Kingon, A. Kukovecz, Z. Konya and P. M. Vilarinho, *Mater. Lett.,* 2013, **90**, 165-168.

22. K. Matyjaszewski and J. Xia, *Chem. Rev.,* 2001, **101**, 2921-2990.

23. K. Matyjaszewski, *Macromolecules,* 2012, **45**, 4015-4039.

24. H. Kong, C. Gao and D. Yan, *J. Am. Chem. Soc.,* 2004, **126**, 412-413.

25. D. Mattia, G. Korneva, A. Sabur, G. Friedman and Y. Gogotsi, *Nanotechnology,* 2007, **18**, DOI: 10.1088/0957-4484/18/15/155305.

26. D. Wilson and M. Langell, *Appl. Surf. Sci.,* 2014, **303**, 6-13.

27. L. Bronstein, X. Huang, J. Retrum, A. Schmucker, M. Pink, B. Stein and B. Dragnea, *Chem. Mater.,* 2007, **19**, 3624-3632.

28. V. Georgakilas, V. Tzitzios, D. Gournis and D. Petridis, *Chem. Mater.,* 2005, **17**, 1613-1617.

29. G. Lampman, D. Pavia, G. Kriz, J. Vyvyan, *Spectroscopy*, Brooks/Cole, US, 4th edn., 2010, ch. 2-3, pp. 15-176.

30. W. Wu, Q. He and C. Jiang, *Nanoscale Res. Lett.*, 2008, **3**, 397–415.

31. S. Galland, R. L. Andersson, M. Salajková, V. Ström, R. T. Olsson and L. A. Berglund, *J. Mater. Chem. C,* 2013, **1**, 7963-7972.

32. G. Lamanna, A. Garofalo, G. Popa, C. Wilhelm, S. Bégin-Colin, D. Felder-Flesch, A. Bianco, F. Gazeau and C. Ménard-Moyon, *Nanoscale,* 2013, **5**, 4412-4421.

33. H. He and C. Gao, *J. Nanomater.,* 2011, **2011**, DOI: 10.1155/2011/193510.

34. J. H. Koo, *Polymer nanocomposites*, McGraw-Hill, New York, 2006, 9.

35. G. M. Bayley and P. E. Mallon, *Polymer,* 2012, **53**, 5523-5539.

36. M. Wang, H. Singh, T. Hatton and G. Rutledge, *Polymer,* 2004, **45**, 5505-5514.

37. T. Subbiah, G. Bhat, R. Tock, S. Parameswaran and S. Ramkumar, *J. Appl. Polym. Sci.,* 2005, **96**, 557-569.

38. G. Bayley, PhD Dissertation, University of Stellenbosch, 2011.

39. Q. A. Pankhurst, J. Connolly, S. Jones and J. Dobson, *J. Phys. D,* 2003, **36**, R167-R181.

40. S. Bedanta and W. Kleemann, *J. Phys. D,* 2009, **42**, DOI: 10.1088/0022-3727/42/1/013001.

41. Y. Xiong, J. Ye, X. Gu and Q. Chen, *J. Magn. Magn. Mater.,* 2008, **320**, 107-112.

Chapter 5: Conclusions and Recommendations

5.1 Conclusions

The first objective of the study entailed the synthesis of PMMA using a FRP technique, where ^{1}H NMR was used to confirm successful synthesis. Chromatographic (SEC) results proved an adequately high molar mass (M_n) suitable for electrospinning was reached, whilst a narrow dispersity (Đ) for FRP of 1.55 was achieved. PMMA was used as polymer matrix for the formation of nanofibres by means of the electrospinning technique; where optimal parameters for fibre formation were found to be 15 wt. % PMMA with an applied voltage of 15 kV, a distance between capillary and target of 15 cm as well as a flow rate of 0.039 mL/min.

The second objective of the study involved the chemical modification of the surface of MWCNTs and magnetic CNTs (where controlled amounts of magnetic iron oxide nanoparticles are embedded in the walls of the CNTs) by means of oxidation and subsequent polymer grafting via *in-situ* ATRP. TGA and TEM results confirmed a weight percentage of 33 % PMMA and an average thickness of 4 nm enwrapped grafted polymer layer present for the PMMA grafted MWCNTs, which correlate well to the attempted values. For the PMMA grafted magnetic CNTs an average thickness of 4 nm enwrapped grafted polymer layer was also observed, however, a weight percentage of only 12 % PMMA was found to be present. This low weight percentage was ascribed to the irregularity and fundamental fusion of the magnetic CNTs, as was observed in TEM images. Chromatographic (SEC) results of cleaved polymer indicated that a M_n of 2361 g.mol^{-1} and Đ of 1.02 for PMMA grafted MWCNTs, and a M_n of 2193 g.mol^{-1} and Đ of 1.13 for PMMA grafted magnetic CNTs were present. These Đ values fall well within the range expected for ATRP.

As a comparison to the magnetic CNTs mentioned above, magnetic CNTs were synthesized by decorating the surface of oxidized MWCNTs with magnetic nanoparticles. Decoration was made possible by carboxylic acid moieties present on the oxidized MWCNT backbone, which acted as anchoring sites through which chemical functionalities could be attached. Synthesis was attempted by three different methods: In the 1st approach, separately prepared magnetic nanoparticles and oxidized MWCNTs were mixed, leading to CNTs with covalently attached magnetic nanoparticles (synthesis of *ex-situ* MWCNT-Fe_3O_4). A simpler single-step method was also investigated; where the 2nd and 3rd approaches involved the *in-situ* precipitation of magnetic nanoparticles on the surface of oxidized MWCNTs (synthesis of *in-situ* MWCNT-$CoFe_2O_4$ and *in-situ* MWCNT-Fe_3O_4). Products obtained were subjected to external magnetic field application, TEM, TGA and XRD tests in order to establish if magnetic CNTs were developed. MWCNTs decorated with nanoparticles could clearly be observed in TEM images. The most favourable magnetic products were obtained by the synthesis of *ex-situ* MWCNT-Fe_3O_4 and *in-situ* MWCNT-Fe_3O_4. TGA confirmed the presence of 30 wt. % MWCNTs and 43 wt. % iron oxide nanoparticles for the *ex-situ* synthesized MWCNT-Fe_3O_4; while 34 wt. % MWCNTs and 37 wt. % iron oxide nanoparticles were present

for the *in-situ* synthesized MWCNT-Fe_3O_4. Products obtained by the synthesis of *in-situ* MWCNT-$CoFe_2O_4$ resulted in MWCNTs decorated with excess large sized iron/cobalt oxide nanoparticles. Attempts to lower the magnetic nanoparticle loading and size were, regrettably, unsuccessful.

The last section of the study focused on the incorporation of the various CNTs into electrospun nanofibres as reinforcing nanomaterials; and thus the formation of PCNs. Chemical modification of MWCNTs and magnetic CNTs by means of oxidation and polymer grafting were carried out in order to compatibilize the reinforcing nanomaterials with the polymer matrix, for production of PCNs with a well dispersed and exfoliated structure. In the case of the *ex-situ* synthesized MWCNT-Fe_3O_4 and *in-situ* synthesized MWCNT-Fe_3O_4 samples, compatibilization was achieved via the remaining carboxylic acid functionalities present as a result of initial oxidation. Dispersion tests confirmed the interaction of the various CNTs with the solvent used for electrospinning (DMF); where good dispersion can be attributed to the polar carboxylic acid groups present on the CNT surface, which fascilitates dissolution in polar solvents such as DMF. The interactions were also greatly enhanced where CNTs were grafted with PMMA.

In each case 0.5 wt. %, 1.5 wt. % and 3.0 wt. % of the various CNTs were added to the electrospinning polymer solution. By the addition of CNTs the viscosity of the electrospinning solution increased, which prevented efficient electrospinning. The polymer concentration was, therefore, varied in specific ratios depending on the amount of CNTs incorporated. After electrospinning, fibres in the nanometer range were obtained, as observed in SEM images. Nanofibres obtained where CNTs were incorporated as reinforcing nanomaterial possessed lower fibre diameters when compared to nanofibres without reinforcement. This is as a result of the electrically conductive properties of CNTs which increase the solution conductivity; leading to more whipping and stretching and thus decreased fibre diameters. When comparing the fibre diameter results obtained for oxidized MWCNTs and PMMA grafted MWCNTs, it was noted that where PMMA grafted MWCNTs were incorporated, decreased fibre diameters and narrower standard deviations were obtained. The same trend was seen when comparing fibre diameters for oxidized magnetic CNTs and PMMA grafted magnetic CNTs. All magnetic samples had overall lower average fibre diameters than that of non-magnetic samples, while higher standard deviation values were prominent. This was due to the incorporation of magnetic nanoparticles resulting in electrospinning solutions with increased conductivity. As a result of increased conductivity more whipping and stretching of the electrospinning jet occurs, leading to fibres with decreased diameters. Successful incorporation (and thus interaction of the CNTs with the electrospun polymer matrix) was confirmed using TEM and STEM; where images verified the presence of well distributed CNTs which align along the electrospun polymer nanofibres due to the stretching of the fibres during electrospinning. The effect the electrospinning voltage has on the fibre morphology

where magnetic CNTs were incorporated was also investigated; where 15 kV was, once again, found to be the optimal voltage.

Magnetic tests were performed on samples of PMMA grafted magnetic CNTs, *ex-situ* synthesized MWCNT-Fe_3O_4 and *in-situ* synthesized MWCNT-Fe_3O_4. Electrospun composite nanofibres containing PMMA grafted magnetic CNTs did not show a magnetic response, where a curve with the characteristic sigmodial shape was not obtained. The PMMA grafted magnetic CNTs by itself resulted in a curve characteristic of ferromagnetic behaviour, where hysteresis loops could be observed. The magnetic response of the various *ex-situ* and *in-situ* synthesized MWCNT-Fe_3O_4 samples exhibited ideal superparamagnetic behaviour, where curves with the characteristic sigmoidal shape showing zero coercivity, zero remanence and no hysteresis loops were obtained. The *ex-situ* MWCNT-Fe_3O_4 samples by itself reached saturation at 3.620 emu/g while electrospun composite nanofibres containing these decorated MWCNTs reached saturation at 0.116 emu/g. In comparison, the *in-situ* MWCNT-Fe_3O_4 samples by itself reached saturation at 0.258 emu/g while electrospun composite nanofibres conataining these decorated MWCNTs reached saturation at 0.026 emu/g.

In summation, the production of electrospun composite nanofibres incorporated with magnetic CNTs was successfully achieved. Electrospun composite nanofibres containing *ex-situ* synthesized MWCNT-Fe_3O_4 and *in-situ* synthesized MWCNT-Fe_3O_4 yielded the most promising end-products; where superparamagnetic behaviour was exhibited. Electrospun composite nanofibres containing *ex-situ* MWCNT-Fe_3O_4 showed the highest superparamagnetic response of all the composite samples; and can thus be classified as the most magnetic composite.

5.2 Recommendations for future work prospects

An alternative method for the production of nanofibres with a higher output rate should be investigated. A needleless electrospinning process, which produces nanofibres up to 20 times faster than the basic single needle electrospinning technique, is a promising alternative.[1] The use of different polymer matrix materials, where the matrix utilized depends on the specific end-use of the product, should also be investigated.

Certain aspects of this study open the door to additional investigations suitable for future projects. In this study, property enhancement of electrospun polymer nanofibres was achieved by the incorporation of CNTs decorated with magnetic nanoparticles; where two different types of reinforcing nanomaterials (CNTs and magnetic nanoparticles) were thus incorporated. The magnetic properties induced by the reinforcing materials can potentially be used for SMART polymer applications. By variation of the nanoparticles decorating the CNTs, numerous

end-products are imaginable. The work done in this study is thus very versatile; where numerous end-products are possible by only varying the nanoparticles in question.

In this study, PMMA was grafted onto the CNT surface. These grafted CNTs were subjected to decoration with magnetic nanoparticles in an *ex*- and *in-situ* approach, where attempts did not result in successfully decorated CNTs. By the grafting of poly(methyl methacrylate)/poly(methacrylic acid) copolymer (PMMA-co-PMAA) onto the CNT surface, more active sites for grafting will be present. This may allow for better decoration of CNTs with magnetic nanoparticles where the surface is grafted with PMMA-co-PMAA, and is recommended for future investigation.[2]

In the case where nanometer-thick layers of clay are used as reinforcing nanomaterial, increases in the tensile strength, modulus, thermal stability and fire retardancy are observed. A much lower fraction of clay incorporation is necessary in order to show dramatic improvement in properties as opposed to conventional reinforcing nanomaterials; which is a major advantage.[3,4] The reinforcing potential and magnetic rendering of these nanomaterials should thus be investigated.

5.3 References

1. H. Niu, X. Wang and T. Lin, *J. Text. I.,* 2012, **103**, 787-794.

2. S. Petr, S. Petr, R. Pavel, B. Roman and S. Petr, *JSEMAT,* 2012, **2**, 221-226.

3. A. Olad and A. Rashidzadeh, *Prog. Org. Coat.,* 2008, **62**, 293-298.

4. A. Usuki, N. Hasegawa, M. Kato and S. Kobayashi, *Adv. Polym. Sci.*, Springer, Berlin, 2005, vol. 179, ch. 4, pp. 135-195.

Appendix

Appendix A

Table A.1: *Various reactions carried out in an attempt to synthesize magnetic nanoparticle decorated MWCNTs.*

Reaction #	Magnetic nanoparticle type		Approach			Solvent	Ratio		Time (h)	Temp (°C)	Success
	$CoFe_2O_4$	Fe_3O_4	In-situ	Ex-situ	Oleic acid		MWCNTs	Magnetic nanoparticles			
1		x		x	y	Ethanol/chloroform	1	5	48	rt	y
2		x		x	y	Ethanol/chloroform	1	4	48	rt	y
3		x		x	y	Ethanol/chloroform	1	3	48	rt	y
4		x		x	y	Ethanol/chloroform	1	2	48	rt	y
5		x		x	y	Ethanol/chloroform	1	1	48	rt	y
6		x		x	y	Ethanol/chloroform	2	1	48	rt	n
7	x		x		n	Water	6	94	6	90	y
8	x		x		n	Water	1	4	6	90	n
9	x		x		n	Water	7	13	6	90	n
10	x		x		n	Water	1	1	6	90	n
11	x		x		n	Water	6	47	6	90	n
12	x		x		n	Water	12	47	6	90	n

13	x		x		n	Water	24	47	6	90	n
14	x		x		n	Water	3	47	24	90	n
15	x		x		n	Water	6	70.5	24	90	n
16	x		x		n	Water	1	4	24	90	n
17	x		x		n	Water	3	47	6	90 @ 2°C/min	n
18	x		x		n	Water	6	70.5	6	90 @ 2°C/min	n
19	x		x		n	Water	1	4	6	90 @ 2°C/min	n
20	x		x		n	Water	6	47	6	90 @ 2°C/min	n
21		x	x		y	Water	1	1	0.5	80	n
22		x	x		n	Water	1	1	0.5	80	n
23		x	x		y	Water	1	4	0.5	80	n
24		x	x		n	Water	1	4	0.5	80	n
25		x	x		y	Ethanol/chloroform	1	1	0.5	80	n
26		x	x		n	Ethanol/chloroform	1	1	0.5	80	n
27	x		x		n	Water (w/o CNTs)	3	47	6	90	y
28	x		x		y	Water (w/o CNTs)	3	47	6	90	n
29		x (in solution)		x	y	Ethanol/chloroform	1	3	48	rt	n
30		x (in		x	y	Ethanol	1	3	48	rt	n

	solution)									
31	x (in solution)		x	y	Ethanol/chloroform	1	4	48	rt	n
32	x	x		n	Diethylene glycol	1	2	1	220	y
33	x	x		n	Diethylene glycol	1	1	1	220	n
34	x		x	y	Ethanol/chloroform	1 (MWCNT-PMMA)	1	48	rt	n
35	x	x		n	Water	1 (MWCNT-PMMA)	1	0.5	80	n

Ex-situ MWCNT-Fe_3O_4 was synthesised in reactions #1-6; where with increasing reaction number the magnetic nanoparticle loading was decreased. All reactions were successful and reaction #4 was chosen for use as reinforcing nanomaterial in electrospun composite nanofibres due to the favourable wt. % of MWCNTs and magnetic nanoparticles present (as proven by TGA). The reaction was also attempted in-situ with and without oleic acid in different solvents (reaction #21-26); however products obtained did not respond to the application of an external magnetic field. Similar *ex-situ* and *in-situ* reactions were carried out using MWCNT-PMMA instead of MWCNT-COOH (reaction #34-35); however magnetic products were once again not obtained. In an attempt to skip the drying step of the magnetic nanoparticles reactions #29-31 were attempted, where magnetic nanoparticles in solution were used; however problems with quantifying the amounts of magnetic nanoparticles added were encountered.

The synthesis of *in-situ* MWCNT-$CoFe_2O_4$ was attempted in reactions #7-20; where the different attempts are elaborated on in section 4.3.2. Reaction #27 was carried out in order to confirm that large nanoparticles (average diameter of 108 nm) are obtained even when CNTs are not

present. Oleic acid was also added (reaction #28) in an attempt to obtain smaller size nanoparticles. A non-magnetic product was, however, obtained.

In-situ MWCNT-Fe_3O_4 was synthesized in reaction #32. In an attempt to lower the magnetic nanoparticle loading reaction #33 was carried out; however the product obtained did not respond to the application of an external magnetic field.

Products obtained from reaction #4, #7 and #32 were identified for use as reinforcing nanomaterials in electrospun PMMA nanofibres. Analysis of these products, as well as results obtained when they are incorporated as reinforcement, are set-out in section 4.3.

Appendix B

Reaction numbers used as per table A.1, appendix A.

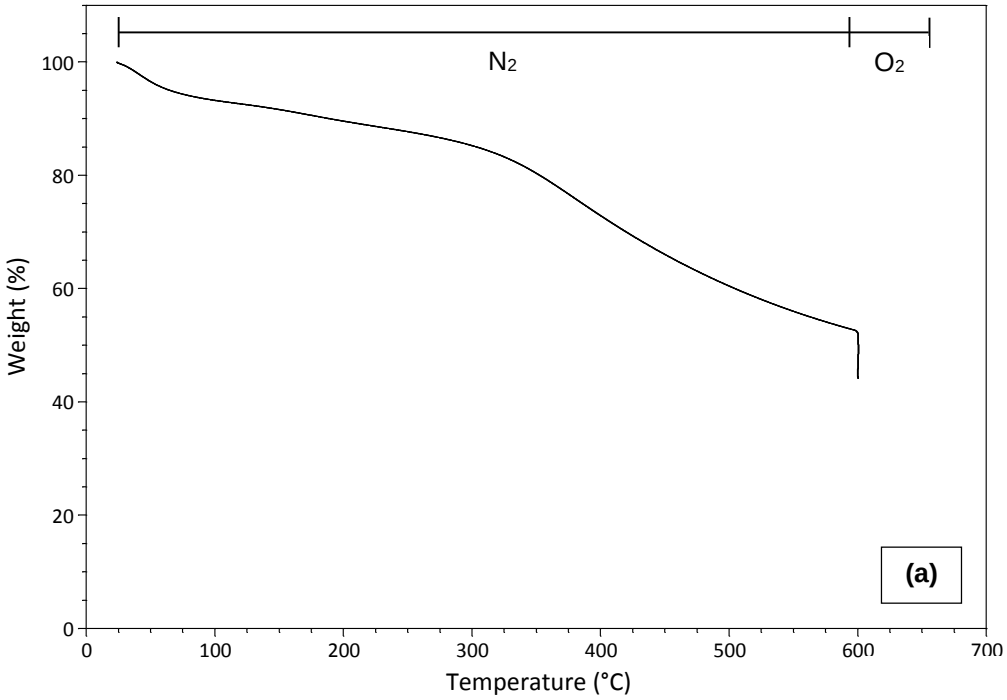

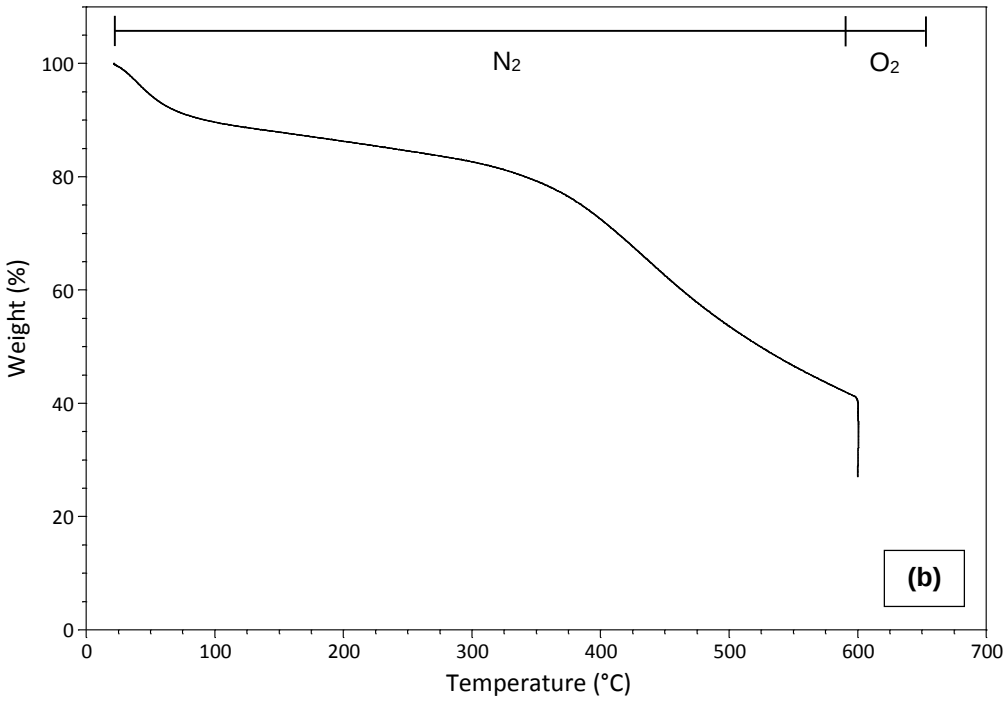

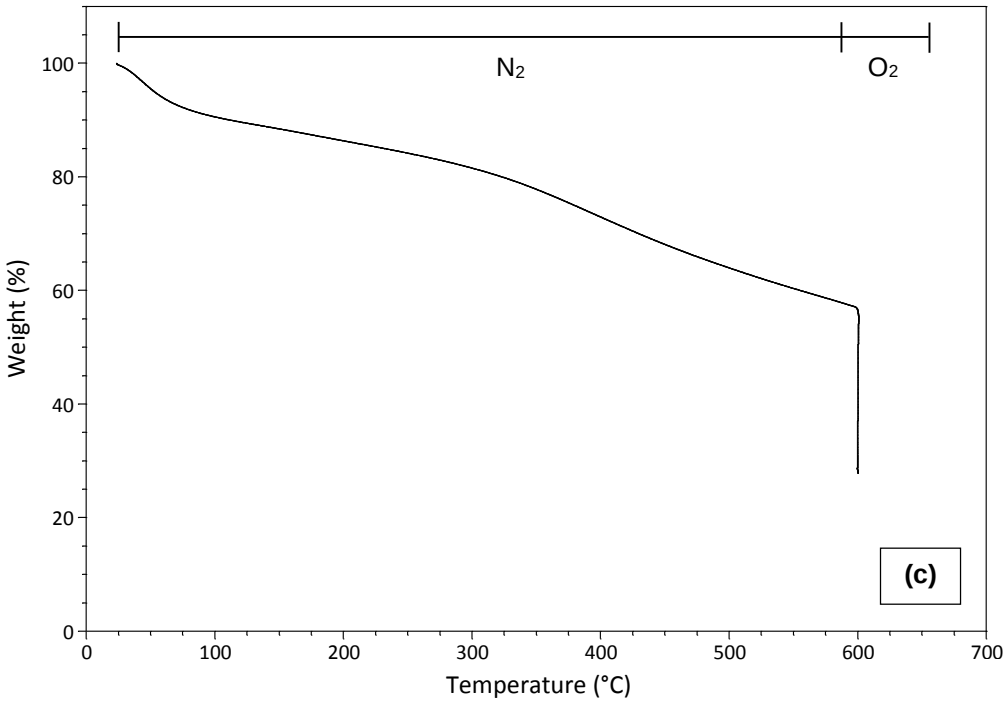

Figure B.1: *TGA curves of in-situ synthesized MWCNT-$CoFe_2O_4$ for reaction (a) #8, (b) #9, and (c) #10 correlating to a weight percentage of (a) 9 %, (b) 14 %, and (c) 29 % MWCNTs present.*

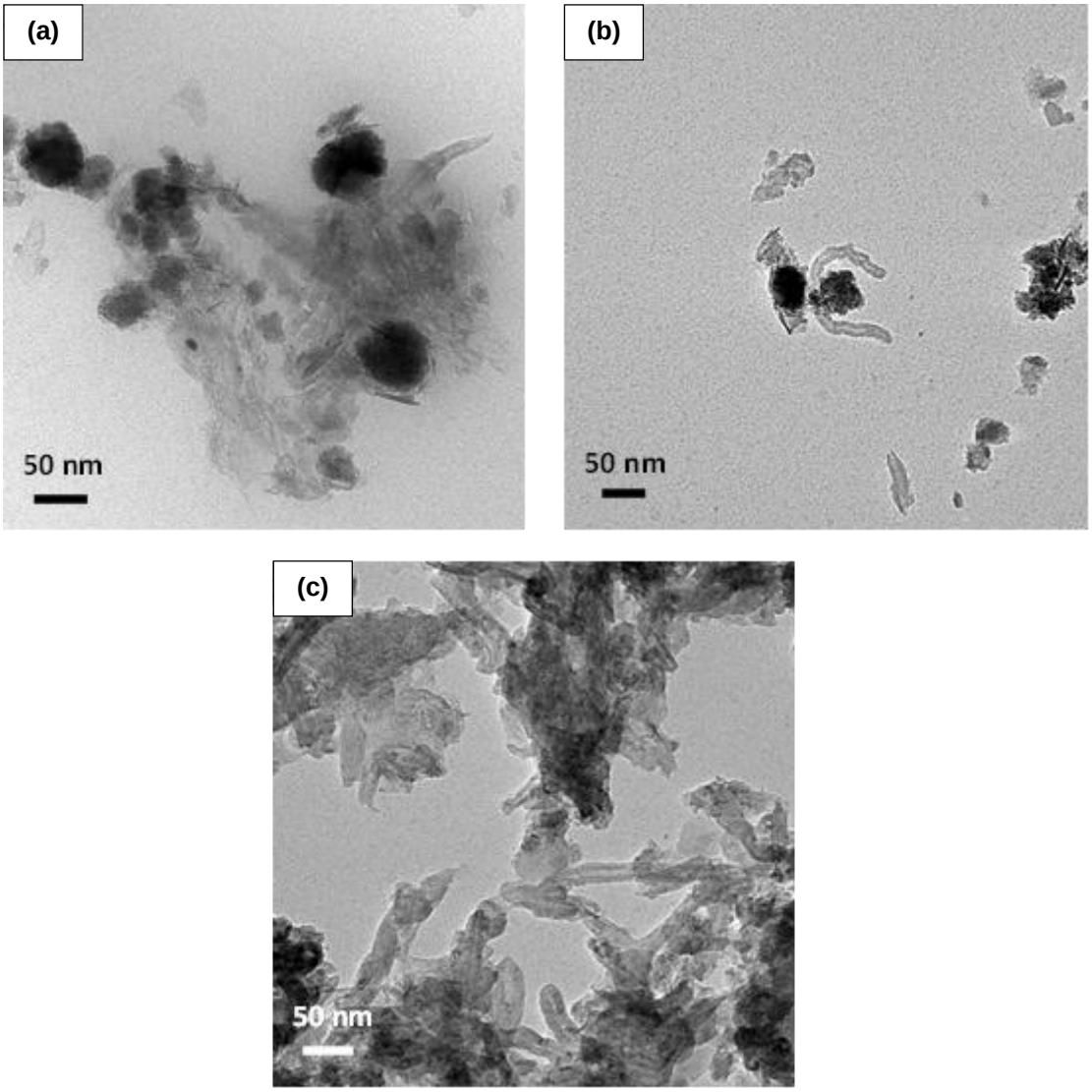

Figure B.2: *TEM images of in-situ synthesized MWCNT-$CoFe_2O_4$ for reaction (a) #8, (b) #9, and (c) #10.*

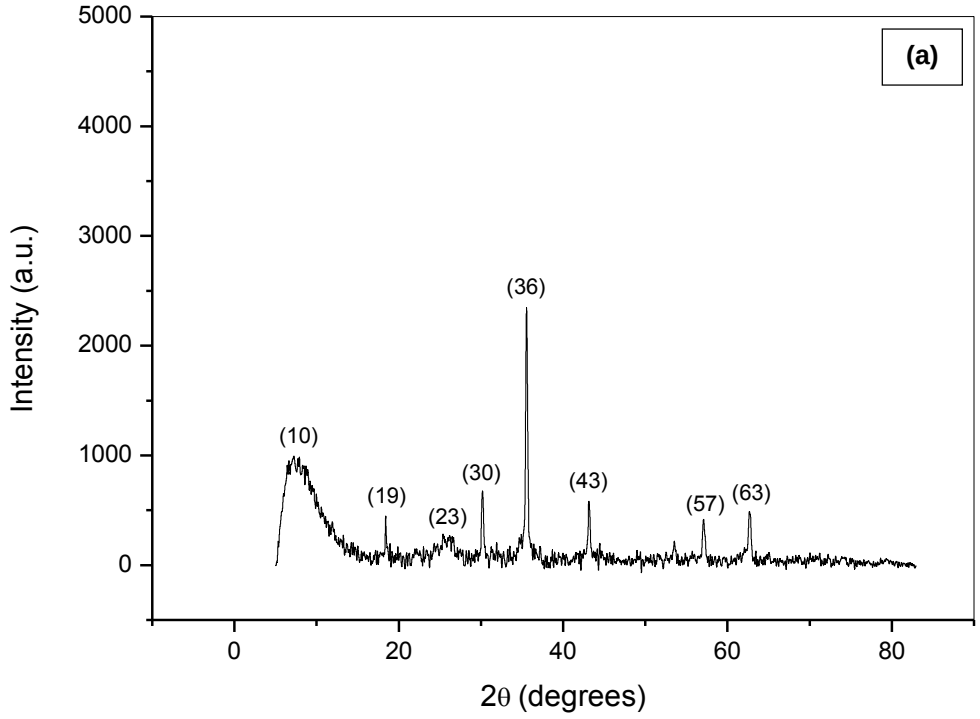

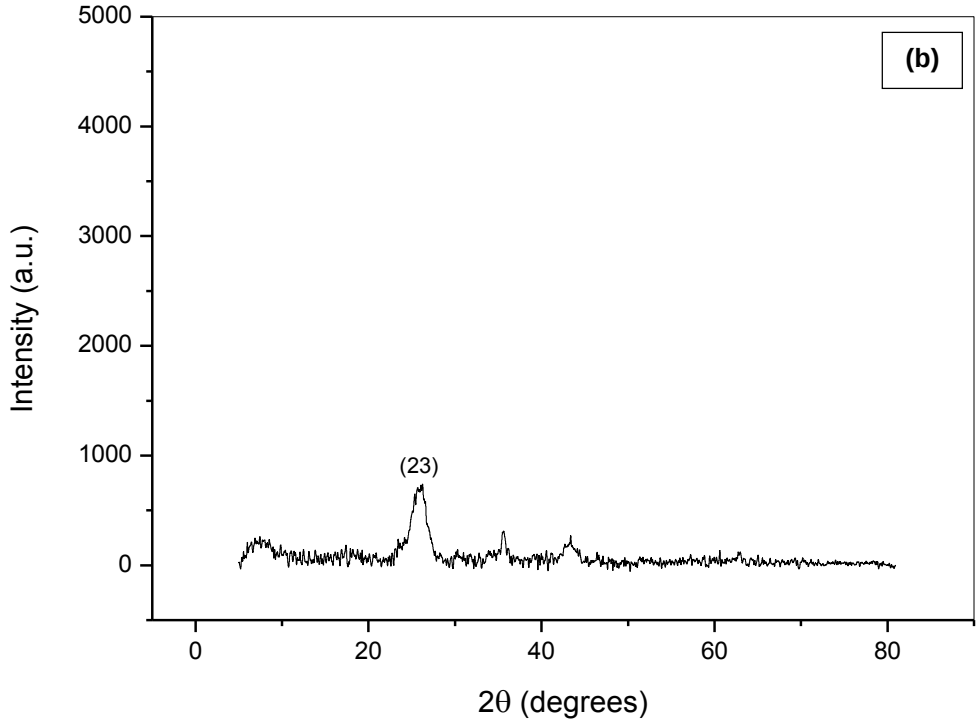

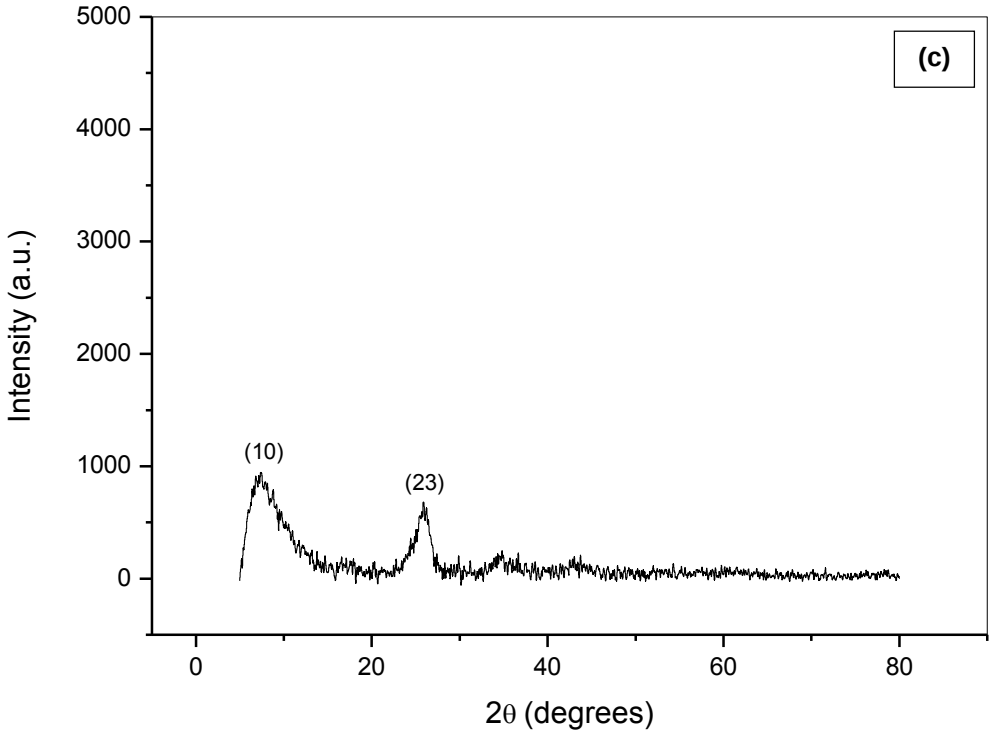

Figure B.3: *XRD spectrum of in-situ synthesized MWCNT-$CoFe_2O_4$ for reaction (a) #8, (b) #9, and (c) #10.*

Appendix C

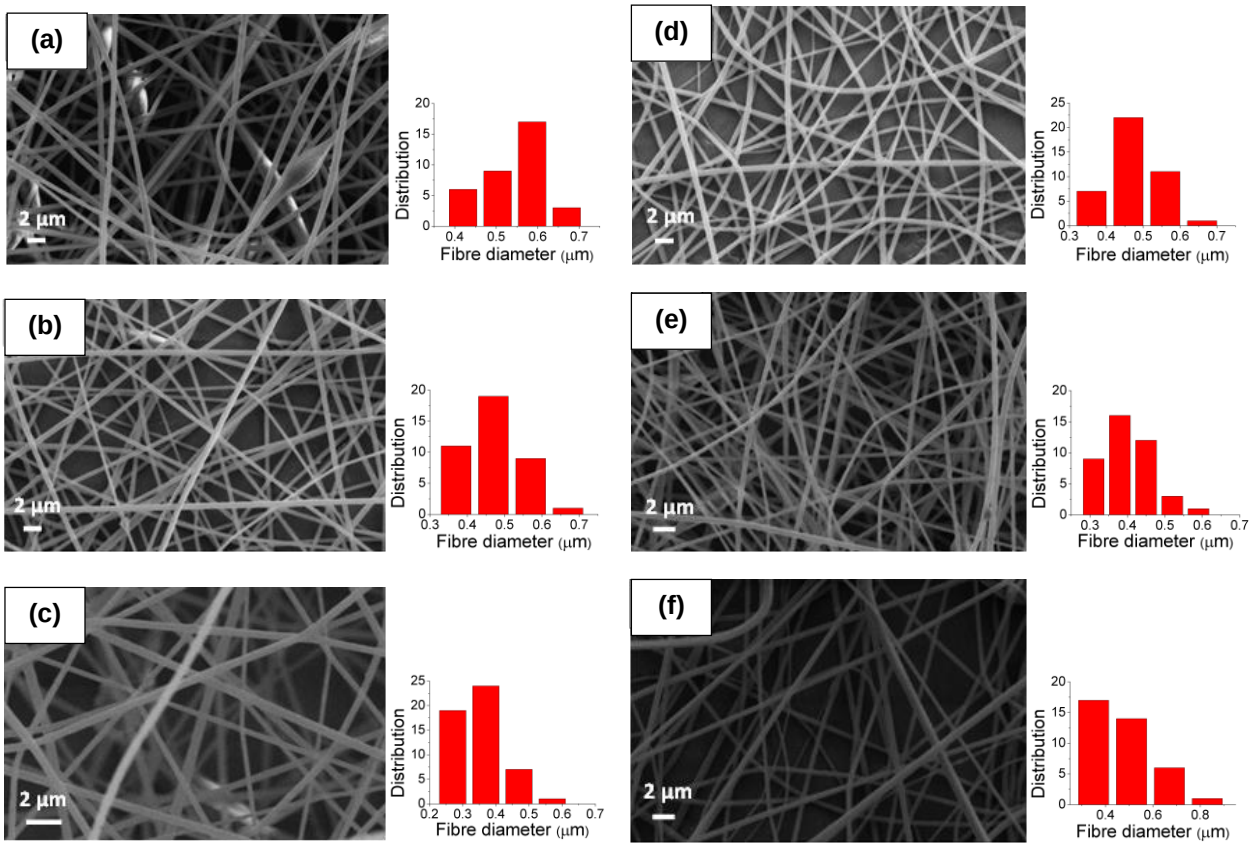

Figure C.1: *SEM images of electrospun fibres with 1.5 wt. % ex-situ MWCNT-Fe_3O_4 & 14 wt. % PMMA incorporated, and a voltage of (a) 5 kV, (b) 10 kV, (c) 15 kV, (d) 20 kV, (e) 25 kV and (f) 30 kV.*

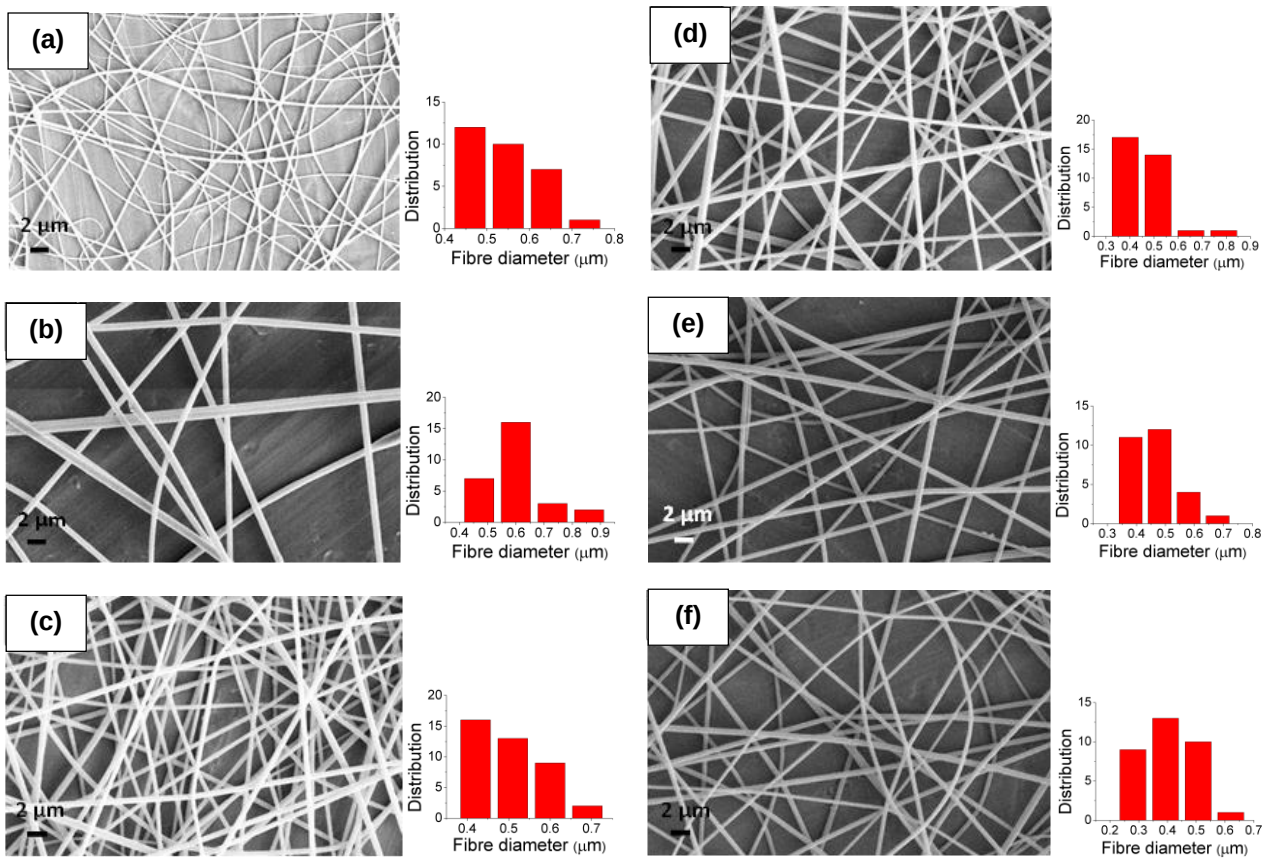

Figure C.2: *SEM images of electrospun fibres with 1.5 wt. % in-situ MWCNT-$CoFe_2O_4$ & 14 wt. % PMMA incorporated, and a voltage of (a) 5 kV, (b) 10 kV, (c) 15 kV, (d) 20 kV, (e) 25 kV and (f) 30 kV.*

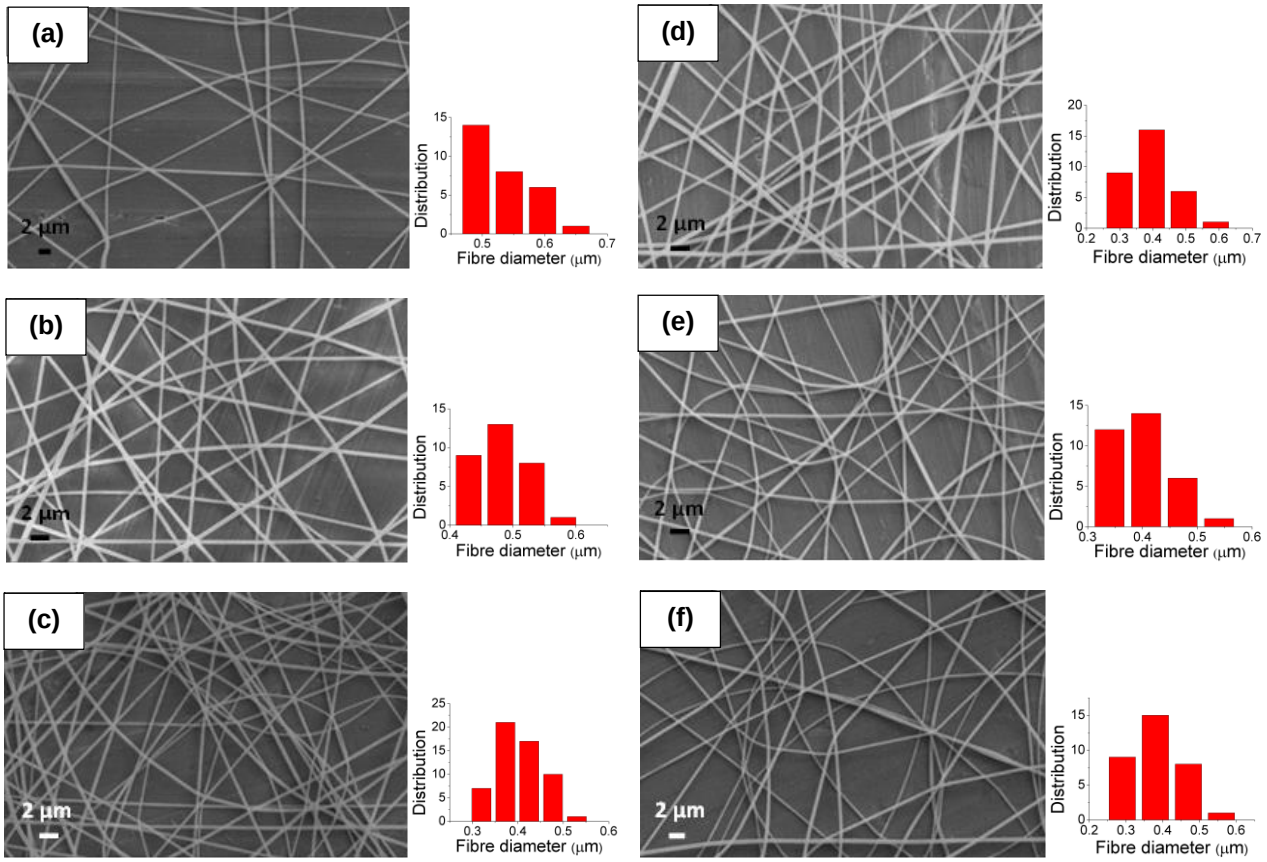

Figure C.3: *SEM images of electrospun fibres with 1.5 wt. % in-situ MWCNT-Fe_3O_4 & 14 wt. % PMMA incorporated, and a voltage of (a) 5 kV, (b) 10 kV, (c) 15 kV, (d) 20 kV, (e) 25 kV and (f) 30 kV.*